UNIVERSITY OF CALIFORNIA,
IRVINE

Where do trees die?
Climate change impacts and biological feedbacks in California forests

DISSERTATION

submitted in partial satisfaction of the requirements
for the degree of

DOCTOR OF PHILOSOPHY

in Biological Sciences

by

Carl August Norlen

Dissertation Committee:
Professor Michael L Goulden, Chair
Professor James T Randerson
Professor Travis E Huxman

2023

DEDICATION

To

All the people I grew up with who haven't gotten the same opportunities I have. May we build a society where everyone can contribute their full talents to making a more sustainable and just society.

TABLE OF CONTENTS

LIST OF FIGURES

LIST OF TABLES

ACKNOWLEDGEMENTS

I would like to express the deepest thanks to my committee chair, Professor Michael L. Goulden, for taking me on as a PhD student in 2018. His broad knowledge and guidance helped me convert my questions and ideas about forests, disturbances, and climate change into tangible research results. Without his guidance, this dissertation would not have been possible.

I would like to thank my committee members, Professor James T. Randerson, and Professor Travis H. Huxman for their invaluable insights and guidance. Their insights on ecology, remote sensing, physiology, land management, climate change and so much more have made this research possible.

I also acknowledge my presence on the unceded territories of the Acjachemen and Tongva peoples, the original inhabitants and stewards of present-day Irvine, many of whom maintain strong ties to this area. I strongly advocate for the inclusion of Native perspectives and traditional knowledge in addition to the Western scientific knowledge presented in this dissertation, particularly regarding the protection and stewardship of ecosystems.

Thank you to my amazing partner Chioma, my family, and my friends, the work in this dissertation would not have been possible without your love and support.

Thank you to the camaraderie and collaboration of many undergraduate, graduate, and postdoctoral colleagues in EEB and ESS Departments, and the Ridge to Reef (R2R) NSF Research Traineeship I wouldn't have made it here without you. Outside of research I have benefited greatly from my involved with CLEAN Education, SCANAS, GPS STEM, and the EEB Anti-Racism Diversity, Equity, and Inclusion (ARDEI) Council, and by serving as a Leadership Coach with the Grad Division DECADE PLUS Program.

In addition, a thank you to Professor Steven D. Allison and Courtney Hunt, for their dedication to preparing the next generation of scholars for climate action R2R. The many enriching training, networking, and collaboration opportunities through R2R have shaped me as a scientist and a person.

Financial support was provided by the University of California, Irvine, NSF Grant DGE-1735040, Lab Fees Grant LFR-18-542511, and California Strategic Growth Council Grant CCR20021.

Chapter 1 of this dissertation is a reprint of the material as it appears in Norlen, C. A., & Goulden, M. L. Recent Tree Mortality Dampens Semi-Arid Forest Die-Off During Subsequent Drought. AGU Advances, 4(3), e2022AV000810 (2023), used with permission from the American Geophysical Union. The co-author listed in this publication is Michael L. Goulden.

Chapters 2 and 3 of this dissertation are currently unpublished material used with the permission of co-authors Kyle S. Hemes, Jonathan A. Wang, Michael L. Goulden, James T. Randerson, and Ved N. Bhoot.

VITA

Carl August Norlen

EDUCATION

2010 B.A. in Biology, Pomona College

2022 M.S. in Biological Sciences, University of California, Irvine

2023 Ph.D. in Biological Sciences, University of California, Irvine

RESEARCH INTERESTS

Impacts of climate change on ecology, biogeochemistry and human systems; Ecological theory; Land management to achieve ecological, biogeochemical, and societal goals; Remote sensing of ecosystem properties; Socio-ecological systems; Science education

PUBLICATIONS

Madakumbura, G. D., Goulden, M. L., Hall, A., Fu, R., Moritz, M. A., Koven, C. D., Norlen, C.A. & Randerson, J. T. (2020). Recent California tree mortality portends future increase in drought-driven forest die-off. Environmental Research Letters, 15(12), 124040.

Hemes, K. S., Norlen, C. A., Wang, J. A., Goulden, M. L., & Field, C. B. (2023). The magnitude and pace of photosynthetic recovery after wildfire in California ecosystems. Proceedings of the National Academy of Sciences, 120(15), e2201954120.

Norlen, C. A., & Goulden, M. L. (2023). Recent Tree Mortality Dampens Semi-Arid Forest Die-Off During Subsequent Drought. AGU Advances, 4(3), e2022AV000810.

POLICY WRITING

Norlen CA, Aravindan A, Cutie S (2023) “One Small Step: Anticipatory Diplomacy in Outer Space” Day One Project

PRESENTATIONS

Hill R, Norlen CA (2022) “Environmental STEAM: Collaboration in Practice” NSF Research Traineeship Conference

Norlen, CA (2022) "Understanding interactions between multiple forest disturbances" Ecology and Evolutionary Biology Graduate Student Seminar

Bhoot V, Goulden ML, Heme KS, Norlen CA, Wang JA (2021) "Can Machine Learning Predict Post-Fire Vegetation Recovery?" American Geophysical Union, Fall Meeting

Johnson KR, Bandy AM, Coffield S, Druffel ERM, Kim JE, Norlen CA (2021) "Commitment to JEDI principles and Anti-Racism at a Minority Serving R1 University: Progress, Opportunities, and Challenges at UC Irvine Department of Earth System Science" American Geophysical Union, Fall Meeting

Norlen CA, Hemes KS, Wang JA, Randerson JT, Goulden ML (2020) "How does past wildfire impact vulnerability to forest die-off?" American Geophysical Union, Fall Meeting

Thayer MR, Norlen CA, Hinojo Hinojo C, Goulden ML (2020) "Changes in vegetation associated with recent climate trends in Southern California: A remote sensing approach" American Geophysical Union, Fall Meeting

Norlen CA (2020) "How do fires change how many trees are killed by less rain?" American Geophysical Union, Fall Meeting (Science Communication, Up-Goer Challenge)

Norlen, CA, Goulden, ML (2019) "Biological feedbacks decrease subsequent forest dieback" American Geophysical Union, Fall Meeting

FELLOWSHIPS

2018 UCI Diversity Recruitment Fellowship

2018 UCI School of Biological Sciences Dean's Fellowship

2019-2020 UCI DECADE PLUS Fellowship (*Mentorship*)

2020-2021 UCI DECADE PLUS Fellowship (*Mentorship*)

2021 NSF Research Traineeship (Ridge 2 Reef) Fellowship (12-month)

2022 NSF Research Traineeship (Ridge 2 Reef) Fellowship (2-month)

RESEARCH EXPERIENCE

Doctoral Researcher 2018–2023
Department of Earth System Science – University of California, Irvine

Noxious Weeds Specialist May–November 2012
Noxious Weeds Control Program – King County, Seattle, Washington

Wetlands Technician April–September 2011
Aviation Division – Port of Seattle, SeaTac, Washington

Conservation and Land Management Intern, June–November 2010
Anchorage Field Office – Bureau of Land Management, Anchorage, Alaska

Research Assistant 2007–2010
Department of Biology, Pomona College

Land Management Intern February–August 2009
Asociación Ribera Norte, Buenos Aires, Argentina

TEACHING EXPERIENCE

Teaching Assistant – Molecular Biology & Microbiology Spring 2023
Department of Molecular Biology and Biochemistry

Teaching Assistant – Limnology & Freshwater Ecology Winter 2022
Department of Ecology and Evolutionary Biology, University of California, Irvine

Head Teaching Assistant – Organisms to Ecosystems Winter 2020, 2021
Department of Ecology and Evolutionary Biology, University of California, Irvine

Teaching Assistant – Organisms to Ecosystems Winter 2019
Department of Ecology and Evolutionary Biology, University of California, Irvine

Academic Specialist – Tutorial Teaching, Community Outreach Spring 2017
School of Education – University of California, Riverside

Academic Specialist – 9th to 12th Grade, Academic Preparation Programs 2016–2018
Upward Bound Programs – University of California, Riverside

Teacher – 6th to 8th Grade Science 2013–2016
Louise Radloff Middle School – Gwinnett County Public Schools, Duluth, Georgia

Teacher – 9th to 12th Grade, "Pursuing Urban Sustainability at Home" Summer 2014
Georgia Institute of Technology, Atlanta, Georgia

Teaching Fellow – 8th Grade Physical Science Summer 2013
Paul D. West Middle School – Fulton County Public Schools, Atlanta, Georgia

SERVICE

Volunteer Pen Pal, Letters to Pre-Scientists 2022–2023

Planning Committee, "What Can I Do With My PhD?" Workshop 2022
Department of Ecology and Evolutionary Biology, University of California, Irvine

Council Member, Anti-Racism, Diversity, Equity and Inclusion (ARDEI) Council 2020–2022
Department of Ecology and Evolutionary Biology, University of California, Irvine

Pod Member, Unlearning Racism in the Geosciences (URGE) 2020–2022
Department of Earth System Science, University of California, Irvine

Leadership Coach, UC Irvine, DECADE PLUS 2019–2021
Graduate Division, University of California, Irvine

Presenter, Climate, Literacy, Empowerment and iNquiry (CLEAN) Education 2018–2022
Board Member 2020–2022
Department of Earth System Science, University of California, Irvine

Mentorship Coordinator, Climate Solutions Conference Fall 2019–Winter 2020
Department of Earth System Science, University of California, Irvine

Volunteer, Master Gardener Program 2017–present
University of California, Agricultural and Natural Resources (UCANR)

ABSTRACT OF THE DISSERTATION

Where do trees die?

Climate change impacts and biological feedbacks in California forests

by

Carl August Norlen
Doctor of Philosophy in Biological Sciences
University of California, Irvine, 2023
Professor Michael L. Goulden, Chair

Climate change is impacting forests in multiple interacting ways such as changing fire regimes and hotter droughts linked to drought induced forest die-off. These first order climate change impacts can interact with subsequent disturbances by producing amplifying feedbacks that make subsequent disturbances more severe or dampening feedbacks that make subsequent disturbances less severe.

In Chapter 1 we tested the common assumption that that recent tree mortality will not alter die-off severity during subsequent droughts. by comparing die-off in semi-arid conifer forest stands in California that were exposed to a single drought and two sequential droughts. We found that recent tree morality reduces die-off severity in semi-arid conifer forests exposed to subsequent drought.

In Chapter 2 we tested how a history of prescribed fire and wildfire with varying severities changes forest cover and water use and forest drought vulnerability. Forests with recent fire history had reduced tree cover, increased shrub cover, and decreased water use (ET), with the greatest changes due to wildfires and high severity fires. These

decreases in tree cover and ET led to decreased forest die-off severity compared to similar forests that had not recently experienced fire.

In Chapter 3, we compared the importance of potential forest drought vulnerability risk factors and modeled how forest die-off risk is changing using a simple statistical approach. We found that drought exposure, proximity to the climate water limit, and forest density were generally the most important predictors of drought vulnerability. Forests without recent disturbance, especially those at moderate elevations with relatively high tree cover and where water use and annual precipitation are similar in magnitude currently have the highest drought vulnerability.

As forests continue to experience disturbances linked to climate change, dampening effects will impose a transient, and perhaps long-term, constraint on the impact of drought. Human actions such as prescribed fire and perhaps other management actions, can produce decreases in tree cover and water that in turn increase forest resistance to drought. Implementing natural climate solutions that consider both climate change amplified risks and dampening feedbacks, will improve the likelihood that climate mitigation projects provide long-term climate mitigation.

INTRODUCTION

Global Importance of Forests

Climate change is often framed as an existential threat to planet Earth and all life. However, this misses the more pressing threat of climate change for human civilization as we know it. Humans both rely on stable ecosystems such as forests for survival through ecosystem services such as access to water, controls on climate, and controls on wildfire. The value of ecosystems to humans is often framed through important, but less essential services such as recreation and improved mental health. Unfortunately, humans are also the drivers of changes to ecosystem, which in turn, threatens human survival.

In this era of rapid climate change, forests are of particular interest and importance for climate change impacts because they have large carbon stocks and play an important role in the global carbon cycle (Pan et al., 2011). Climate change is making drivers of forest disturbance such as droughts and fire weather more common and more extreme (Anderegg et al., 2020). This means that carbon currently stored in living forests is more likely to be quickly released during wildfires or slowly released as live trees become dead trees and begin to decompose.

Forest Ecosystem Services and Natural Climate Solutions

Forests provide ecosystem services including water, climate regulation, reduced wildfire risk, forest products, recreation, carbon storage, and more (Ninan & Inoue, 2013). Impacts from climate change amplified disturbances such as wildfires and drought induced mortality are changing forest structure and therefore the services that forest provide. The pace and scale of these changes to forest structure and their implications for ecosystems

services remain relatively uncertain. Whether forests will continue to provide the services that our current human civilization relies on is an open question. If forests and other ecosystems that humans rely on change more rapidly than human society adapts to and mitigates the effects of climate change it is an open question whether humans can survive in a world with drastically altered ecosystems. Improved forest management, reforestation, and avoided deforestation are promising potential natural climate solution to store additional carbon (Anderegg et al., 2020; Fargione et al., 2018; Griscom et al., 2017). That highlights the importance of understanding how these proposed management actions and risks to forests under climate change (Aponte et al., 2016; Field et al., 2020).

Climate Change Impacts on Forests

Climate change has large impacts on forests such as drought induced mortality, wildfires and increased windthrow all of which can lead to releases of stored carbon and therefore accelerate climate change instead of mitigating it (McDowell et al., 2020). Models often predict large future tree mortality events (Jiang et al., 2013; McDowell et al., 2016). However, climate change induced self-limiting feedbacks or dampening effects can also play a role in reducing the long term effects of climate change amplified disturbances on forests (Lloret et al., 2012; Seidl et al., 2017).

Where do Trees Die?

Large episodic tree death events have been of high interest to scientists for at least the last several four decades, which is unsurprising due to the essential links been trees, forests, and human society (Breshears et al., 2005; Mueller-Dombois, 1987). Increased stress from climate change provides the opportunity and necessity to better understand

forests, trees, and tree mortality. Due to the importance of forests to the global carbon cycle and regional human societies better understanding of how forests are currently responding to climate change and will respond in the future is of both high interest and benefit to the public at large, policy makers, and land managers.

California as a Study System

California provides an ideal study system to better understand forests under climate change because of its diverse forests and record of climate change amplified disturbances due to drought and wildfire over the last several decades. In addition to experiencing a series of severe droughts, and increasing burned area over the last several decades, there are a wide variety of forest habitats and a wealth of forest inventory, remote sensing, and other geospatial data. This ideal study system allows for exciting investigations into understanding the climate change amplified of wildfires and droughts on forests.

References

Anderegg, W. R. L., Trugman, A. T., Badgley, G., Anderson, C. M., Bartuska, A., Ciais, P., Cullenward, D., Field, C. B., Freeman, J., Goetz, S. J., Hicke, J. A., Huntzinger, D., Jackson, R. B., Nickerson, J., Pacala, S., & Randerson, J. T. (2020). Climate-driven risks to the climate mitigation potential of forests. *Science*, *368*(6497). https://doi.org/10.1126/science.aaz7005

Aponte, C., de Groot, W. J., & Mike Wotton, B. (2016). Forest fires and climate change: causes, consequences and management options. *International Journal of Wildland Fire*, *25*(8), i–ii.

Breshears, D. D., Cobb, N. S., Rich, P. M., Price, K. P., Allen, C. D., Balice, R. G., Romme, W. H., Kastens, J. H., Floyd, M. L., Belnap, J., Anderson, J. J., Myers, O. B., & Meyer, C. W. (2005). Regional vegetation die-off in response to global-change-type drought. *Proceedings of the National Academy of Sciences of the United States of America*, *102*(42), 15144–15148.

Fargione, J. E., Bassett, S., Boucher, T., Bridgham, S. D., Conant, R. T., Cook-Patton, S. C., Ellis, P. W., Falcucci, A., Fourqurean, J. W., Gopalakrishna, T., Gu, H., Henderson, B., Hurteau, M. D., Kroeger, K. D., Kroeger, T., Lark, T. J., Leavitt, S. M., Lomax, G., McDonald, R. I., … Griscom, B. W. (2018). Natural climate solutions for the United States. *Science Advances*, *4*(11), eaat1869.

Field, J. P., Breshears, D. D., Bradford, J. B., Law, D. J., Feng, X., & Allen, C. D. (2020). Forest Management Under Megadrought: Urgent Needs at Finer Scale and Higher Intensity. *Frontiers in Forests and Global Change*, *3*. https://doi.org/10.3389/ffgc.2020.502669

Griscom, B. W., Adams, J., Ellis, P. W., Houghton, R. A., Lomax, G., Miteva, D. A., Schlesinger, W. H., Shoch, D., Siikamäki, J. V., Smith, P., Woodbury, P., Zganjar, C., Blackman, A., Campari, J., Conant, R. T., Delgado, C., Elias, P., Gopalakrishna, T., Hamsik, M. R., … Fargione, J. (2017). Natural climate solutions. *Proceedings of the National Academy of Sciences of the United States of America*, *114*(44), 11645–11650.

Jiang, X., Rauscher, S. A., Ringler, T. D., Lawrence, D. M., Park Williams, A., Allen, C. D., Steiner, A. L., Michael Cai, D., & McDowell, N. G. (2013). Projected Future Changes in Vegetation in Western North America in the Twenty-First Century. *Journal of Climate*, *26*(11), 3671–3687.

Lloret, F., Escudero, A., Iriondo, J. M., Martínez-Vilalta, J., & Valladares, F. (2012). Extreme climatic events and vegetation: the role of stabilizing processes. *Global Change Biology*, *18*(3), 797–805.

McDowell, N. G., Allen, C. D., & Anderson-Teixeira, K. (2020). Pervasive shifts in forest dynamics in a changing world. *Science*. https://www.science.org/doi/abs/10.1126/science.aaz9463?casa_token=BN2Jpf5tT9sAAAAA:q9l0O7UJXg4Xk8YB4YlURsrt11d8nAznGOprLfang9uH-vLkqg7II94W7bd2pEUDl59lmsaVhB2wKIQ

McDowell, N. G., Williams, A. P., Xu, C., Pockman, W. T., Dickman, L. T., Sevanto, S., Pangle, R., Limousin, J., Plaut, J., Mackay, D. S., Ogee, J., Domec, J. C., Allen, C. D., Fisher, R. A., Jiang, X., Muss, J. D., Breshears, D. D., Rauscher, S. A., & Koven, C. (2016). Multi-scale predictions of massive conifer mortality due to chronic temperature rise. *Nature Climate Change*, *6*(3), 295–300.

Mueller-Dombois, D. (1987). Natural Dieback in Forests. *Bioscience*, *37*(8), 575–583.

Ninan, K. N., & Inoue, M. (2013). Valuing forest ecosystem services: What we know and what we don't. *Ecological Economics: The Journal of the International Society for Ecological Economics*, *93*, 137–149.

Pan, Y., Birdsey, R. A., Fang, J., Houghton, R., Kauppi, P. E., Kurz, W. A., Phillips, O. L., Shvidenko, A., Lewis, S. L., Canadell, J. G., Ciais, P., Jackson, R. B., Pacala, S. W., McGuire, A. D., Piao, S., Rautiainen, A., Sitch, S., & Hayes, D. (2011). A large and persistent carbon sink in the world's forests. *Science*, *333*(6045), 988–993.

Seidl, R., Thom, D., Kautz, M., Martin-Benito, D., Peltoniemi, M., Vacchiano, G., Wild, J., Ascoli, D., Petr, M., Honkaniemi, J., Lexer, M. J., Trotsiuk, V., Mairota, P., Svoboda, M., Fabrika, M., Nagel, T. A., & Reyer, C. P. O. (2017). Forest disturbances under climate change. *Nature Climate Change*, *7*(6), 395–402.

CHAPTER 1

Recent tree mortality dampens semi-arid forest die-off during subsequent drought

Reprint of:
Norlen, C. A., & Goulden, M. L. (2023). Recent Tree Mortality Dampens Semi-Arid Forest Die-Off During Subsequent Drought. AGU Advances, 4(3), e2022AV000810.

1.1 Introduction

Climate change is expected to increase drought frequency and intensity (Pachauri et al., 2014), which are commonly predicted will increase forest stress and disturbance over the coming century (Allen et al., 2015; Anderegg et al., 2020a). Ecological models project 50% or greater needleleaf evergreen conifer tree loss by 2100 in the Northern Hemisphere (Jiang et al., 2013; McDowell et al., 2016). The effects of 21st century droughts on forests are well documented, with drought and hotter temperatures combining to increase forest die-off severity (Allen et al., 2015; Breshears et al., 2005; Goulden & Bales, 2019; McDowell et al., 2011). Forest die-off threatens ecosystem services (Thom & Seidl, 2016) such as carbon sequestration (Pan et al., 2011), water quality, habitat, and controls on wildfire risk (Miura et al., 2015).

The interactions between disturbance agents – drought, wind, wildfire, and pathogens – remain uncertain (Anderegg et al., 2020a; Kleinman et al., 2019; Seidl et al., 2017). An increase in die-off frequency and severity will inevitably increase the occurrence of repeated or co-occurring disturbances (i.e., multiple disturbances). These sequential or simultaneous disturbances may be independent from, amplify, or dampen each other (Seidl et al., 2017). Model projections often assume that forest die-off severity in response to drought is constant and independent from past disturbance (Adams et al., 2013; Jiang et al., 2013; McDowell et al., 2016). Much of our understanding of drought-induced tree mortality is based on observations of die-off thresholds over the last 20 to 30 years (Allen et al., 2015; Hartmann et al., 2018; McDowell et al., 2008). These observations demonstrate predisposing factors for die-off such as high forest water use, high leaf area (Goulden & Bales, 2019; Jump et al., 2017), high forest density (Mueller-Dombois, 1987; Savage, 1994,

1997; Young et al., 2017), and the presence of trees with physiological drought vulnerabilities (McDowell et al., 2002, 2008; Ryan et al., 2006; Ryan & Yoder, 1997) such as needleleaf conifers (Brodrick & Asner, 2017; Fellows & Goulden, 2012; Fettig et al., 2019) and large individuals (Fellows & Goulden, 2012; Fettig et al., 2019; Stovall et al., 2019). However, recent die-off episodes that dampen future disturbance severity would reduce the impact of subsequent drought on forests by mitigating these pre-disposing factors (Mueller-Dombois, 1987; Waring, 1987). Changes in drought stress or dampening effects from prior die-off provide potential mechanisms to explain spatial and temporal patterns of semi-arid conifer forest die-off (Goulden & Bales, 2019; Madakumbura et al., 2020; Young et al., 2017). Reduced forest leaf area or density can increase resource availability (e.g., water (Goulden & Bales, 2019; Young et al., 2017)). The death of vulnerable trees can decrease the density of physiologically vulnerable (Waring, 1987) or pathogen-susceptible trees (Franklin et al., 1987; Waring, 1987). Drought exposure can produce physiological acclimation in surviving trees (Anderegg et al., 2020a; McDowell et al., 2019; Seidl et al., 2017). However, observational studies have rarely considered these possible feedbacks (but see (Anderegg et al.,2020b; DeSoto et al., 2020; McDowell et al., 2019))

Semi-arid forests in the western United States have experienced a series of droughts over recent decades, with recent extreme episodes in 1999-2002 and 2012-2015. Forests in the Southwestern United States (i.e., Arizona, California, Colorado, Utah, New Mexico) experienced die-off due to a 1999-2002 drought (Breshears et al., 2005). Forests in California's Sierra Nevada experienced die-off due to a widespread 2012-2015 drought (Asner et al., 2016; Byer & Jin, 2017; Goulden & Bales, 2019); this second drought also impacted many of the same areas in inland Southern California Mountains that had

experienced die-off during the 1999-2002 drought (Fellows & Goulden, 2012; Kelly & Goulden, 2008; Minnich, 2007). This created a regional mosaic (Fig. 1.1a), with semi-arid conifer forest stands that have been exposed to either one (1999-2002 or 2012-2015) or both (1999-2002 and 2012-2015) droughts.

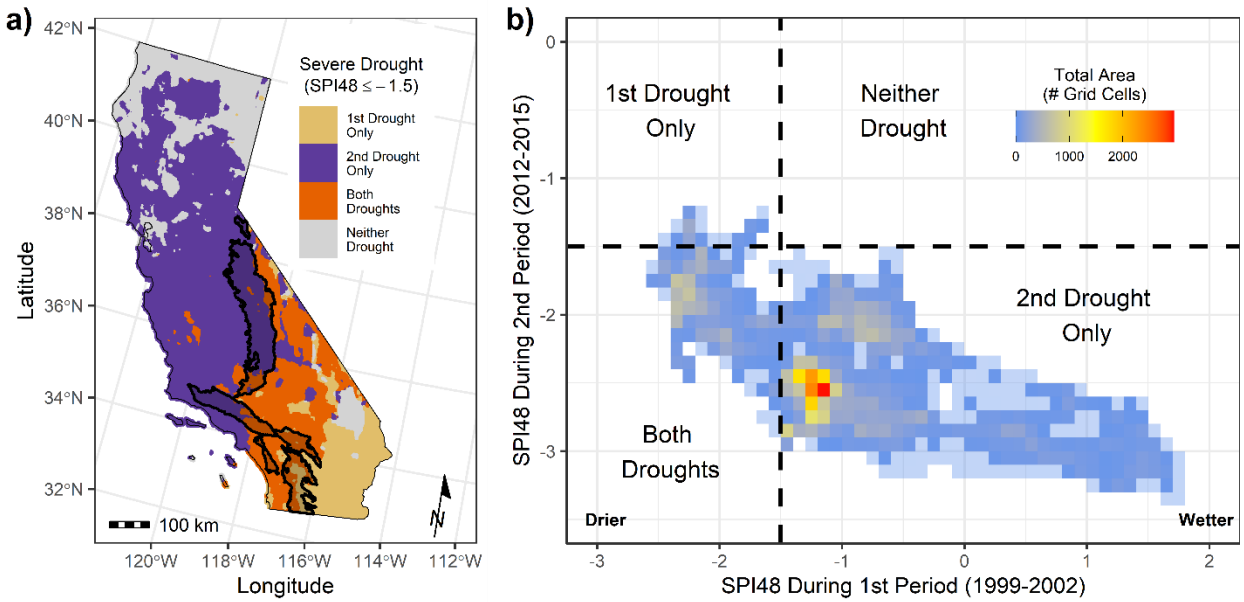

Figure 1.1. The distribution of drought exposure sequences across California. (a) The spatial overlap between drought exposure, defined as forty-eight month Standardized Precipitation Index (SPI48) ≤ -1.5, in *1st Period* (1999-2002) and *2nd Period* (2012-2015). Yellow locations were exposed in 1999-2002 only (*1st Drought Only*), purple locations were exposed in 2012-2015 only (*2nd Drought Only*), orange locations were exposed to drought in both 1999-2002 and 2012-2015 (*Both Droughts*), and gray locations were exposed to drought in neither 1999-2002 nor 2012-2015 (*Neither Droughts*). The black polygons outline the study region in the Sierra Nevada and Southern California Mountains. (b) The distribution of grid cells by SPI48 exposure in the *1st Period* and *2nd Period*. In the color bar, blue represents fewer grid cells, yellow represents an intermediate number of grid cells, and red represents a greater number of grid cells. The partially opaque blue squares represent SPI48 exposure combinations with less than 20 grid cell observations. The sample size for both panels is N = 62,887.

We used geospatial and forest inventory data and analyses to compare semi-arid conifer forest stands in California that were exposed to a single drought during 2012-2015 (we refer to this sample as *2nd Drought Only*) with stands that were exposed to droughts in both 1999-2002 and 2012-2015 (we refer to this sample as *Both Droughts*; Fig. 1.1). We

first evaluated whether die-off during 2012-2015, which we call the *2nd Period*, was independent from, amplified by or dampened by die-off during 1999-2002, which we call the *1st Period*. We then explored whether changes in cumulative moisture deficit, a measure of water availability that we defined as the difference between water use and water input, or changes in susceptibility to cumulative moisture deficit were the underlying mechanism(s) that explain changes to die-off severity.

1.2 Materials and Methods

1.2.1 Experimental Design

Semi-arid conifer forests in the study region spanned 62,887 grid cells (each grid cell is nine hectares or 100 Landsat pixels) or approximately 566,000 hectares (Figure 1.1). We quantified extreme drought exposure as forty-eight-month Standardized Precipitation Index (SPI48) ≤ -1.5. SPI48 is a measure of precipitation anomalies over four water years, with SPI48 ≤ -1.5 indicating a precipitation shortfall 1.5 standard deviations below the climate normal. SPI48 ≤ -1.5, occurred in 13,580 of 62,887 grid cells (~22%) during the *1st Period* (1999-2002) and 61,898 of 62,887 grid cells (~98%) during the *2nd Period* (2012-2015; Figure 1.1b).

We separated grid cells into four drought exposure sequences: *Neither Drought*, *Both Droughts*, *1st Drought Only*, and *2nd Drought Only*. We quantified the difference between SPI48 in 1999-2002 and 2012-2015 (dSPI48) to compare four-year precipitation between the two time periods. To identify forests in the *Neither Drought* sample we filtered for locations with 1999-2002 and 2012-2015 SPI48 >-1.5. To identify forest in the *Both Droughts* sample we filtered for locations with 1999-2002 and 2012-2015 SPI48 ≤-1.5 and dSPI48 ≤ 0.5. To identify forests in the *2nd Drought Only* sample we filtered for forests

where drought was extreme in only 2012-2015 by identifying grid cells with 2012-2015 SPI48 ≤ -1.5, 1999-2002 SPI48 >-1.5, and dSPI48 > 0.5. To identify forests in the *1st Drought Only* sample we filtered for forests where drought was extreme in only 1999-2002 by identifying grid cells with 1999-2002 SPI48 ≤ -1.5, 2012-2015 SPI48 > -1.5 and dSPI48 > 0.5. In practice, the dSPI48 threshold removed a total of 3,966 grid cells either were in the *Both Droughts* sample and had different levels of SPI48 drought exposure were in the *2nd Drought Only* sample and had similar levels of SPI48 drought exposure (Fig. A.3).

We excluded the *1st Drought Only* and *Neither Drought* exposure sequences from further analysis due to low or non-existent sample sizes within our study region (773 *1st Drought Only* and 0 *Neither Drought* grid cells). We continued our analysis with 8,923 grid cells exposed to *Both Droughts*, and 49,222 grid cells exposed to drought in *2nd Drought Only* (Fig. A.1). In the *Both Droughts* sample, 64% of grid cells were in the Southern California Mountains versus 36% in the Sierra Nevada (Fig. A.2). In the *2nd Drought Only* sample, 92% of grid cells were in the Sierra Nevada versus 8% in the Southern California Mountains (Fig. A.2).

We used SPI48 (Abatzoglou et al., 2017) calculated on a per-pixel basis to track drought exposure because it incorporates only water inputs from precipitation (Pr) and uses a four-year timescale that reflects long-term forest access to soil moisture (Goulden & Bales, 2019; Madakumbura et al., 2020). We retrieved 4-km resolution SPI48 data from https://wrcc.dri.edu/wwdt/archive.php. We down-sampled the SPI48 layers for 1999-2002 and 2012-2015 to 30-m resolution with bilinear interpolation.

1.2.2 General Geospatial Data Processing

We retrieved California-wide geospatial observations to supplement the Landsat vegetation indices. We used a California state perimeter with an added 500-m buffer to filter geospatial observations. The California state perimeter was retrieved from https://developers.google.com/earth-engine/datasets/catalog/TIGER_2016_States. We used the arcpy python package form ArcGIS Pro and Earth Engine to reproject and rasterize vector data to 30-m resolution. We first converted and co-registered all geospatial datasets to 30-m spatial resolution in the Albers Equal Area (EPSG 5070) projection using Earth Engine.

1.2.2.1 Landsat Data Processing

We used Landsat observations to calculate a proxy for forest die-off and Evapotranspiration (ET). We retrieved Landsat observations for the state of California, filtered for clouds, snow, and shadows and calculated annual composites for three vegetation indices using Earth Engine (Gorelick et al., 2017). The steps we used to retrieve, process, and composite Landsat data are listed below.

(1) We retrieved all collection 1, level 1 Landsat 5, 7, and 8 (L5, L7, L8) surface reflectance scenes observed between March 1, 1984 and December 31, 2019 that intersected a state of California perimeter with a 500-meter (m) buffer.

(2) We used the United States Geological Survey (USGS) provided pixel_qa layer based on FMask to remove snow, clouds with high confidence, and cloud shadows from each Landsat image. For Landsat 8 we also removed clouds with high cirrus confidence with FMask (Z. Zhu et al., 2015).

(3) We renamed Landsat 7 and Landsat 8 bands to follow Landsat 5 naming conventions.

(4) We homogenized Landsat 5 equivalents of B1 (Blue), B2 (Green), B3 (Red), B4 (Near Infrared), B5 (Shortwave Infrared 1), B7 (Shortwave Infrared 2) for Landsat 7 and Landsat 8 using the ordinary least squares regression lines derived for the Continental United States (Roy et al., 2016).

(5) We calculated Tasseled Cap Brightness (Crist & Cicone, 1984; Healey et al., 2005), NDVI and NDMI for each Landsat image.

a. $Tasseled\ Cap\ Brightness = B1 * 0.3037 + B2 * 0.2793 + B3 * 0.4743 + B4 * 0.5585 + B5 * 0.5082 + B7 * 0.1863$

b. $NDVI = \frac{B4 - B3}{B4 + B3}$

c. $NDMI = \frac{B4 - B5}{B4 + B5}$

(6) We calculated the mean and standard deviation of Tasseled Cap Brightness for the full time series stack. We removed Landsat pixels that were anomalously (two standard deviations) brighter (snow or clouds) or darker (cloud shadows) than the mean time series brightness for each pixel.

(7) ***NDMI and NDVI.*** We calculated the mean water year NDVI (Oct 1 – Sep 30) and mean late season NDMI (Aug 1 – Oct 31) for each year in the full Landsat time series.

1.2.2.2 Geospatial Data Masking and Regridding

We applied masks using Earth Engine to exclude pixels that had burned, were not identified as needleleaf conifer forests, and that occurred outside our study region in the Sierra Nevada and Southern California Mountains. We excluded burned pixels to avoid confusing remote sensing observations of wildfire for forest die-off. We included only needleleaf conifer forests because they are the most susceptible to die-off in our study region. We excluded geospatial data outside our study region United States Forest Service

(USFS) Ecological Subsections to allow for landscape level comparisons between geospatial and forest inventory observations.

We next regridded all data, including Landsat observations, to 300-m spatial resolution using Earth Engine. We assigned each 300-m grid cell the mean value of intersecting 30-m pixels except for vegetation type where we assigned the mode value of the intersecting 30-m pixels. We excluded grid cells calculated based on less than 20 pixels.

We used wildfire history data to remove grid cells that had burned from 1980 to 2019 from our analysis. We reprojected and rasterized each year of fire data.

We used the fire history dataset from California's Fire and Resource Assessment Program (FRAP) retrieved from https://frap.fire.ca.gov/mapping/gis-data/.

We identified grid cells dominated by needleleaf conifer forest types using Landscape Fire and Resource Management Planning Tools Existing Vegetation type (LANDFIRE EVT) data for 2001. We retrieved the LANDFIRE EVT layer for 2001 (EVT us_105) from https://www.landfire.gov/viewer/.We included pixels where LANDFIRE EVT was one of the following: Redwood (EVT code #2015), Juniper-Pinyon Woodland (2016, 2025, 2019, 2059, 2119, 2115), Grand Fir (2018, 2047, 2232), Bristlecone Pine (2020, 2057), Knobcone Pine (2022, 2034, 2170, 2177), Sierra Nevada Mixed Conifer (2027, 2231), Jeffrey Pine (2031), Red Fir (2032), Interior Douglas-Fir (2045, 2051, 2227, 2166), Limber Pine (2049), White Fir (2052, 2172, 2208, 2028), Interior Ponderosa Pine (2053, 2054, 2060, 2117, 2179), Lodgepole Pine (2058, 2167, 2173, 2050), or Pacific Douglas-Fir (2200, 2206).

We excluded geospatial observations outside of our study region using USFS Ecological Subsections. We retrieved the geodatabase of USFS Ecological Subsections from https://data.fs.usda.gov/geodata/edw/datasets.php?xmlKeyword=ecomap+subsection. We included the following subsections: San Rafael-Topatopa Mountains (M262Ba), Northern Transverse Ranges (M262Bb), Sierra Pelona-Mint Canyon (M262Bc), San Gabriel Mountains (M262Bd), Upper San Gabriel Mountains (M262Be), Santa Ana Mountains (M262Bf), San Gorgonio Mountains (M262Bg), Upper San Gorgonio Mountains (M262Bh), Little San Bernardino-Bighorn Mountains (M262Bi), San Jacinto Foothills-Cahuilla Mountains (M262Bl), San Jacinto Mountains (M262Bm), Palomar-Cuyamaca Peak (M262Bo), Desert Slopes (M262Bp), Lower Batholith (M261Ep), Upper Batholith (M261Eq), Eastern Slopes (M261Er), Tehachapi-Piute Mountains (M261Es), and Kern Plateau (M261Eu).

1.2.3 Observations of Forest Die-off

We used the following geospatial proxies for forest die-off: change in NDMI (dNDMI) for die-off intensity, and the USFS Aerial Detection Surveys (ADS) for die-off extent (Goulden & Bales, 2019; Madakumbura et al., 2020). We used Forest Inventory and Analysis (FIA) data as an alternative measurement of forest mortality. We did not differentiate between forest die-off caused by physical drought stress, bark beetle and other insect attack, or a combination of both.

1.2.3.1 dNDMI

NDMI is related to the amount of moisture per ground area and as such is sensitive to both the LAI and hydration of individual leaves (Goodwin et al., 2008; Hardisky et al., 1983). dNDMI is particularly sensitive to changes in live leaf area, with negative values providing a

proxy for decreased live leaf area and die-off, and positive values providing a proxy for increased live leaf area and canopy growth (Goodwin et al., 2008; Goulden & Bales, 2019). We calculated dNDMI for 2004 to capture die-off in 1999-2002 by subtracting the mean NDMI for 1997, 1998, and 1999 (three years before the drought) from the mean NDMI for 2003 and 2004 (the two years after the end of the drought). We calculated dNDMI for 1991 to 2005 similarly to dNDMI for 2004. For example, we calculated dNDMI for 1991 by subtracting mean NDMI for 1984, 1985, and 1986 from mean NDMI for 1990 and 1991. We calculated dNDMI for 2017 to capture die-off in 2012-2015 by subtracting the pre-drought mean NDMI (mean of 2009, 2010, and 2011) from post-drought NDMI (mean of 2016 and 2017). We calculated dNDMI for 2006 to 2019 similarly to dNDMI for 2017.

1.2.3.2 USFS ADS (Aerial Detection Surveys)

We used ADS observations as an independent measure of the presence or absence of mortality in our study region. We retrieved the ADS mortality surveys for USFS Region 5 for the years 1978 to 2019 from https://www.fs.usda.gov/detail/r5/forest-grasslandhealth/?cid=fsbdev3_046696. The ADS data is measured in units of dead trees acre^{-1} (TPA1). In addition to mortality, ADS polygons with total flown area are recorded. We added a TPA1 field with a value of zero to the flown area polygons. We rasterized the TPA1 field for both the ADS survey and flown area polygons. We created an annual raster layer of die-off by taking the maximum of TPA1 for the rasterized mortality survey and flown area layers for each year.

We used ADS to compare landscape scale die-off extent between the 1999-2002 and 2012-2015 time periods at 300-meters. Observations from ADS are more reliable for comparing die-off extent than die-off intensity measured with TPA1 (Hicke et al., 2020),

partially due to a shift to digital from analog sketch mapping starting in the early 2000s and a change from TPA1 to broad die-off intensity categories in 2017. In general, sketch mapping also has an accuracy of ~68% (Johnson & Ross, 2008) at 50-m resolution, which is sufficient for comparing landscape scale patterns of die-off extent at 300-m.

We calculated ADS die-off for 2004 by taking the maximum of the annual mortality layers (combined mortality and flown area) for 1999-2004. We calculated ADS die-off for 2017 by taking the maximum of the annual mortality layers for 2012-2017. We used maximum TPA1 value to avoid double counting die-off and included all years of each time period plus two additional years to capture all observed die-off across different years, as each year of ADS observations is incomplete. To allow comparison between 1999-2004 and 2012-2017 ADS for die-off extent we converted TPA1 values into categorical presence or absence of mortality with TPA1 values of ≥ 5 trees $acre^{-1}$ assigned as tree mortality (1) and < 5 trees $acre^{-1}$ as no tree mortality (0).

1.2.3.3 Field Observations of Forest Basal Area (BA) and Die-off

We calculated basal area (BA) and mortality of needleleaf conifer trees using FIA observations (Bechtold & Patterson, 2005). The USFS FIA program measures inventory plots annually on a 10-year rotating schedule for California. Observations based on the current sampling protocol are available for 2001-2019. We retrieved FIA observations from https://apps.fs.usda.gov/fia/datamart/ using rFIA (Stanke et al., 2020). We calculated tree mortality as dead basal area for all trees and for the following tree genera: pine, fir, oak, juniper, and cedar. We selected plots that were sampled during only 2003-2006, only 2016-2019, or both time periods. We included only plots with the following plot disturbance conditions (DSTRBCD1): no disturbance (0), insect damage (10), insect

damage to understory (11), insect damage to trees (12), drought (54), unknown (70). We calculated the total live and dead basal area for each plot and for each tree genus in each plot using the plot adjustment factor (TPA_UNDADJ) for each tree counted in the plot with a diameter greater than 12.7 centimeters. For plots sampled in 2016-2019 we removed trees killed before 2013 using the morality year field (MORTYR). We removed any plots that had less than five percent total conifer basal area.

We calculated the mean SPI48 drought exposure for 1999-2002 and 2012-2015 in each Ecological Subsection. We used SPI48 values to assign the plots from each subsection to one of the two drought exposure sequences. We filtered drought exposure by Ecological Subsection because we did not have access to the precise geospatial locations of FIA plots due to United States federal regulations. The following subsections were exposed to Both Droughts: M262Bc, M262Bd, M262Be, M262Bf, M262Bg, M262Bh, M262Bi, M262Bl, M262Bm, M262Bo, M262Bp, and M261Es. The following subsections were exposed to the 2012-2015 Drought Only: M262Ba, M262Bb, M261Ep, M261Eq, M261Er, and M261Eu.

1.2.4 Geospatial Predictors of Forest Die-off

We compared three different geospatial predictors of die-off: cumulative moisture deficit from four-year Pr-ET which represents water availability, aboveground live biomass density (AGB), and annual mean maximum temperature (T_{max}).

1.2.4.1 Cumulative Moisture Deficit

We used four-year Pr-ET overdraft as a proxy for the spatial distribution of cumulative moisture deficit because it incorporates both water input and (Precipitation) water use (Evapotranspiration). We calculated Annual Precipitation minus Evapotranspiration (Pr-ET) in units of millimeters of water per year (mm yr^{-1}) by subtracting the annual ET from

down-sampled Pr for each water year (Fellows & Goulden, 2017; Goulden & Bales, 2019). We then calculated four-year Pr-ET for 1999-2002 by taking the sum of the water year Pr-ET layers for 1999 through 2002. We calculated four-year Pr-ET similarly for 2012-2015 by taking the sum of the Pr-ET layers for 2012 through 2015. Four-year Pr-ET is calculated in units of millimeters of water per four years (mm $4yr^{-1}$). A value of -1000 mm $4yr^{-1}$ for four-year Pr-ET overdraft means that over the previous four years of water use (ET) was greater than water input (Pr) by 1,000 mm.

We calculated ET for each water year by scaling between eddy covariance ET flux measurements and water year NDVI (Goulden et al., 2012; Goulden & Bales, 2019). We measured the net ET at four eddy covariance towers in the Sierra Nevada around the upper Kings River basin along a west to east transect at ~800 m elevation intervals beginning at 405 m, four in the San Jacinto Mountains at elevations ranging from 205 m to 1710 m and two in the Santa Ana Mountains at ~500 m (Goulden et al., 2012; Hinojo-Hinojo & Goulden, 2020). We retrieved ET field observations from https://www.ess.uci.edu/~california/. We calculated annual ET by integration after filling intervals with missing, calm, or otherwise unsuitable observations as a function of incoming solar radiation. We combined annual ET for the ten California flux towers to create a regression between annual ET and NDVI to extrapolate ET spatially and temporally (R^2 = 0.692; Fig. A.4). We created the same regression between annual ET and NDVI using only the six forested flux tower sites to confirm that our approach is robust in only our target ecosystem types (R^2 = 0.764; Fig. A.4). The NDVI values used for this regression were calculated using the approach described in the Landsat Observations section. We calculate the NDVI for each eddy covariance site as the mean of nine upwind Landsat pixels. As we have discussed in

previous papers, a strong correlation exists between annual NDVI and ET because of bidirectional linkages between Leaf Area Index (LAI) and canopy gas exchange (Goulden et al., 2012; Goulden & Bales, 2014, 2019). In semi-arid regions like California, site water balance, LAI, primary production, and ET are tightly correlated. LAI is also well correlated with NDVI, creating a tight relationship between annual NDVI and ET.

We used annual Pr to calculate annual Pr-ET. We calculated annual Pr for each water year (Oct 1 – Sep 30). We calculated annual Pr for each water year by taking the sum of monthly Pr. We retrieved monthly 4-kilometer (km) Pr for 1985 to 2019 from the Parameter-elevation Relationships on Independent Slopes Model (PRISM) retrieved from https://developers.google.com/earth-engine/datasets/catalog/OREGONSTATE_PRISM_AN81m. We down-sampled each year of Pr from 4-km to 30-m resolution with bilinear interpolation.

1.2.4.2 Annual Maximum Temperature (T_{max})

We used annual Maximum Temperature (T_{max}) as an alternative predictor of forest die-off. We calculated annual T_{max} for each water year (Oct 1 – Sep 30). We calculated annual T_{max} as the mean of monthly T_{max}. We retrieved monthly 4-kilometer (km) T_{max} for 1985 to 2019 from the Parameter-elevation Relationships on Independent Slopes Model (PRISM) retrieved from https://developers.google.com/earth-engine/datasets/catalog/OREGONSTATE_PRISM_AN81m. We down-sampled each year of T_{max} from 4-km to 30-m resolution with bilinear interpolation.

1.2.4.2 Aboveground Live Biomass (AGB)

We used the existing LandTrendr + Gradient Nearest Neighbor (LT-GNN) AGB data set for 1990-2017, which is publicly available and peer reviewed (Hooper & Kennedy, 2018;

Kennedy et al., 2018), as an alternative predictor of forest die-off severity. We used LT-GNN AGB for California retrieved from: http://emapr.ceoas.oregonstate.edu/pages/data/viz/index.html. LT-GNN AGB for 1999 represented forest density during the *1st Period*, and LT-GNN AGB for 2012 represented forest density during the *2nd Period*. We used the LT-GNN AGB data set created using LT-GNN imputation that combines Forest Inventory and Analysis (FIA) observations and annual time series of 30-m Landsat data (Kennedy et al., 2018). The LT-GNN AGB was validated with comparisons to AGB derived from > 6000 FIA plots (R^2 = 0.78) and airborne LiDAR (Kennedy et al., 2018). The data were most reliable when forest AGB was ≤ 450 Mg ha^{-1} and data was aggregated from 30-m to a larger spatial scale, both of which are true for our study (Kennedy et al., 2018).

1.2.5 Statistical Analysis.

We first compared observations of die-off (ADS, dNDMI, and FIA Mortality) and potential predictors of die-off (four-year Pr-ET, AGB, T_{max}, and FIA BA) between four experimental groups: *1st Period* of the *Both Droughts* sample, *2nd Period* of the *Both Droughts* sample, *1st Period* of the *2nd Drought Only* sample, and *2nd Period* of the *2nd Drought Only* sample. For the categorical ADS die-off data set, we compared the four experimental groups using a Chi-Squared Test. For all other variables, we compared observations between the *1st Period* and *2nd Period* within the *Both Droughts* and *2nd Drought Only* samples using paired t-tests. For these same data sets we compared the four experimental groups using Two-Way ANOVA and Tukey Honestly Significant Difference (HSD) tests. To conduct statistical tests we used base R (R Core Team, 2020).

We next compared four-year Pr-ET, AGB, T_{max}, drought sequence, time period and time period x drought sequence as predictors of dNDMI die-off severity using multiple linear regression and relative weight analysis (Groemping, 2006). We conducted the relative weight analysis using the relaimpo package (Groemping, 2006; Groemping & Matthias, 2018). To correct a sampling imbalance between drought exposure groups before applying the relative weight analysis we under-sampled the *2nd Drought Only* drought exposure group by 20% using the caret package (Kuhn et al., 2020) resulting in a sample size of 9,839 grid cells.

We next compared four-year Pr-ET as a predictor of dNDMI die-off severity within the four experimental groups using piecewise linear regression. We calculated the piecewise linear regression with an automated estimate of the breakpoint (Muggeo, 2003) using the segmented package (Muggeo, 2008). We tested for spatial autocorrelation in our data by creating semi-variograms with our geospatial data with a 5% random sample of each drought sequence using the gstat package (Pebesma, 2004).

For general data analysis and processing we used the tidyverse (Wickham, 2017), raster (Hijmans et al., 2015), sf (Pebesma, 2018), RSQLite (Wickham et al., 2015), and rFIA (Stanke et al., 2020) packages. To create figures and tables we used the tidyverse, RSToolbox (Leutner et al., 2017), patchwork (Pedersen, 2019), ggpubr (Kassambara, 2020) and kableExtra (H. Zhu, 2019) packages and base R (R Core Team, 2020).

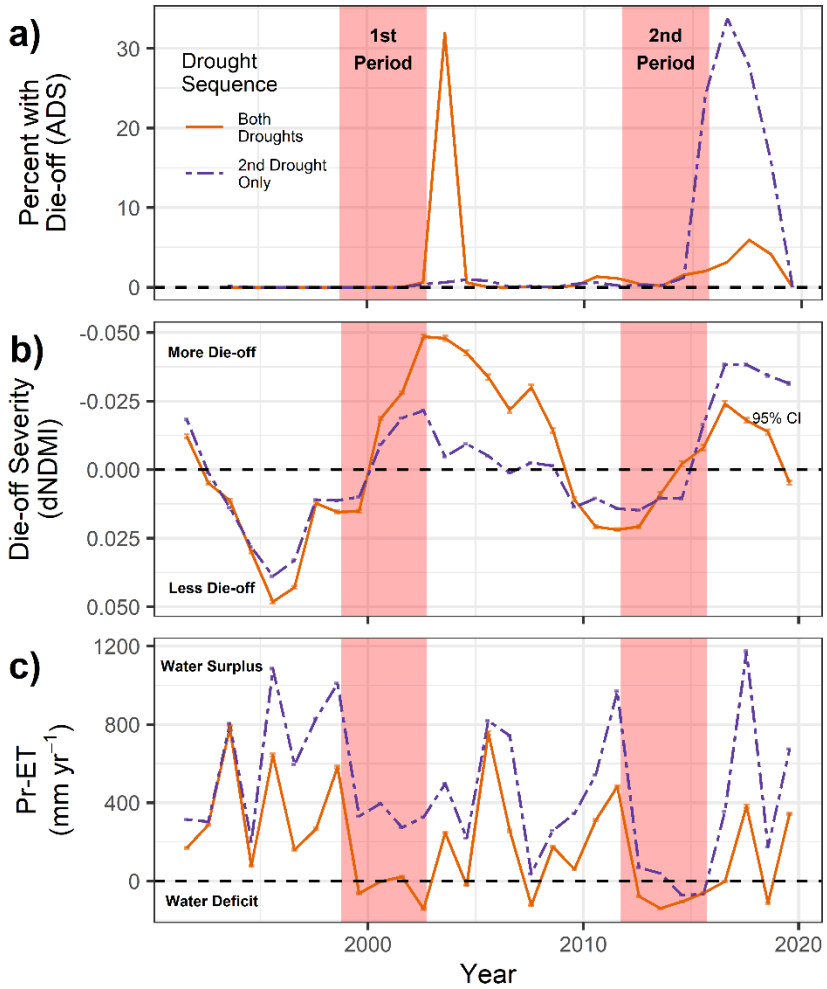

Figure 1.2. Time series of indicators of die-off extent, intensity, and drought stress for the two drought sequences. Panel (a) shows the proportion of grid cells with forest die-off, (b) shows dNDMI (c), and (c) shows annual Pr-ET for the region. The line in panel (a) is the proportion of grid cells with die-off according to Aerial Detection Surveys (ADS). The lines in panels (b) and (c) are the annual region means for dNDMI and Pr-ET. The uncertainty bars in (b) and (c) are 95% confidence intervals (CI). The red shading in each plot indicates the 1999-2002 and 2012-2015 water years. The sample size *Both Droughts* is N = 8,933. The sample size for the *2nd Drought Only* is N = 40,922.

1.3 Results

1.3.1 Spatial and Temporal Patterns of Die-off

Forest die-off was more widespread during the *1st Period* for the *Both Droughts* sample and during the *2nd Period* for the *2nd Drought Only* sample according to aerial detection surveys (ADS) of die-off extent. In the *Both Droughts* sample, die-off observed with ADS was significantly more widespread during the *1st Period* (30.7% of grid cells) than

in 2012-2015 (13.3% of grid cells), while in the *2nd Drought Only* sample, die-off was significantly more widespread during the *2nd Period* (50.7% of grid cells) than during the *1st Period* (2.6% of grid cells) according to a Chi-Square test ($p < 0.001$; Fig 1.2a; Fig. A.5; Fig. A.6).

Forest die-off was more severe during the *1st Period* for the *Both Droughts* sample and during the *2nd Period* for the *2nd Drought Only* sample. Negative dNDMI is a proxy for decreased live forest leaf area and die-off (Goodwin et al., 2008; Goulden & Bales, 2019; Hardisky et al., 1983), while forest inventory observations are a direct measure of dead trees. Positive values of dNDMI are a proxy for increased live leaf area (Goodwin et al., 2008; Goulden & Bales, 2019; Hardisky et al., 1983). In the *Both Droughts* sample, die-off severity quantified with dNDMI was significantly less negative during the *2nd Period* compared to the *1st Period* by 63 to 70% (95% CI; $p < 0.001$) using a paired t-test (Fig. 1.2b; Fig. 1.3; Fig. A.7; Table A.1). In the *2nd Drought Only* sample, dNDMI was significantly more negative during the *2nd Period* compared to the *1st Period* by 8.3 to 8.7-fold ($p < 0.001$) using a paired t-test (Fig. 1.2b; Fig 1.3; Fig. A.4; Table A.1). During the *2nd Period*, dNDMI was significantly less negative in the *Both Droughts* sample than the *2nd Drought Only* sample by 68 to 74% ($p < 0.001$) using a Tukey Honestly Significant Difference (HSD) test (Fig. 1.2b; Fig. 1.3; Fig. A.7; Table A.2). According to forest inventory observations, forests in the *Both Droughts* sample had significantly lower die-off by 17 to 154% during the *2nd Period* compared to the *1st Period* (95% CI; $p < 0.01$), while forests in the *2nd Drought Only* sample had significantly increased die-off by 13 to 30-fold during the *2nd Period* compared to the *1st Period* ($p < 0.001$) according to Tukey HSD tests (Fig. 1.4a, b; Table A.3).

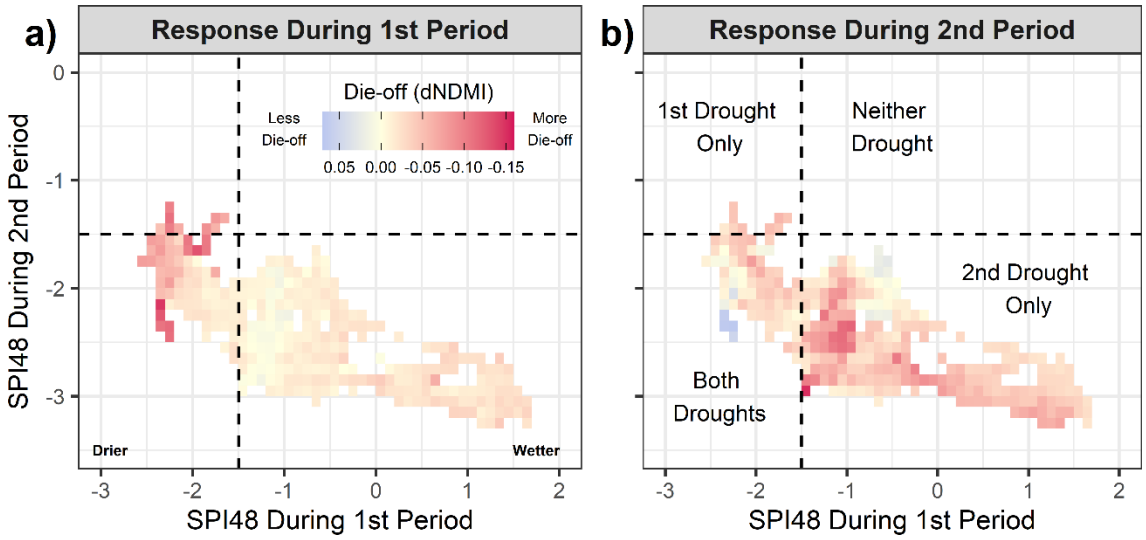

Figure 1.3. The distribution of forest die-off (dNDMI) arranged by SPI48 exposure. Panel (a) shows die-off and SPI48 exposure in the *1st Period* and panel (b) shows the *2nd Period*. In the color bar, red represents negative values of dNDMI or severe forest die-off, cream represents no change in dNDMI or forest condition, and blue represents positive dNDMI or possible forest regrowth. The sample size for both panels is N = 62,887.

Pine and fir mortality was greatest during the *1st Period* for the *Both Droughts* sample and during the *2nd Period* for the *2nd Drought Only* sample. Pine mortality was significantly greater ($p < 0.05$) than fir, oak, juniper, or cedar mortality during the *1st Period* for the *Both Droughts* sample, while fir mortality was not significantly greater than oak, juniper, or cedar mortality ($p > 0.9$). In the *Both Droughts* sample, pine mortality significantly decreased by 23 to 151% during the *2nd Period* compared to the *1st Period* ($p < 0.01$; Fig 1.4c, d; Table A.4) according to a Tukey HSD test. In the *2nd Drought Only* sample pine mortality significantly increased ($p < 0.001$) by 8 to 25-fold during the *2nd Period* compared to the *1st Period*, while fir morality significantly increased ($p < 0.001$) by 11 to 48-fold during the *2nd Period* compared to the *1st Period* according to Tukey HSD tests (Fig 1.4c, d; Table A.4, Table A.5).

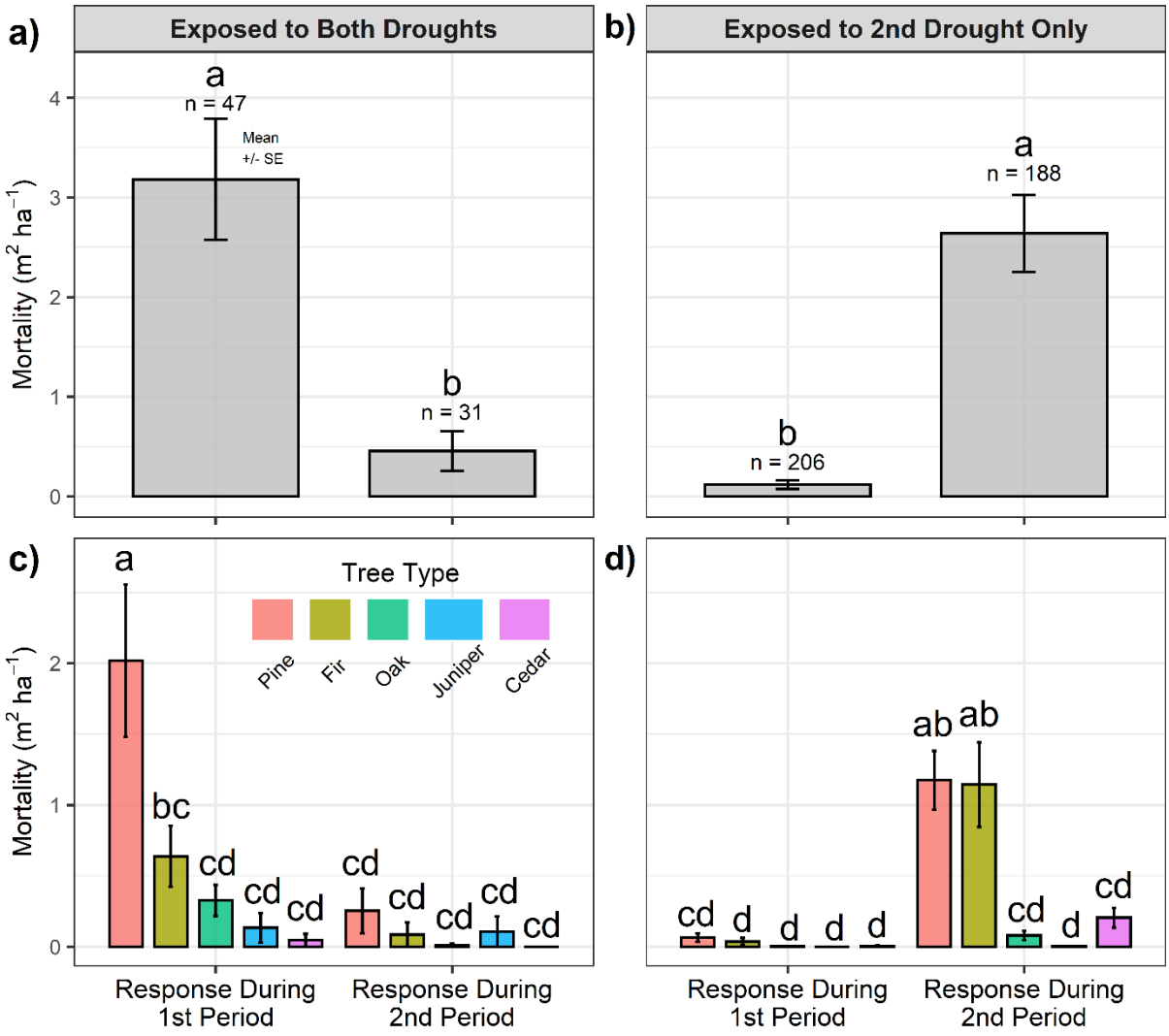

Figure 1.4. Comparison of needleleaf conifer mortality, from forest inventory observations, in *1st Period* and *2nd Period* and between locations exposed to *Both Droughts* and drought in *2nd Drought Only*. Panels (a) and (b) represent mortality for all tree species combined, while panels (b) and (c) represent mortality separated by tree genera. Tree mortality is reported in units of basal area (m^2 ha^{-1}). The letters represent comparison with a significant difference ($p<0.05$) using a Tukey Honestly Significant Difference Test. The n-values represent the number of forest inventory plots available to calculate the mortality for each time period and drought sequence combination.

3.2 Potential Biophysical Controls of Die-off Severity

Cumulative moisture deficit is a useful predictor of die-off because it allows for a test of whether changes in leaf area and therefore water use led to changes in water availability which altered die-off severity. Cumulative moisture deficit, quantified as negative four-year

water input (Pr) minus four-year water use (ET; four-year Pr-ET overdraft), was extreme during both the *1st Period* and *2nd Period* for the *Both Droughts* sample and during only the *2nd Period* for the *2nd Drought Only* sample (Figure 1.2c; Fig. A.8; Fig. A.9). In the *Both Droughts* sample, annual moisture deficit (Pr-ET) was also negative in 2004-2005 and 2007-2008 but was positive when combined into four-year cumulative moisture deficit (Figure 1.2c). Maximum temperatures (T_{max}) were higher during the *2nd Period* than the *1st Period* for the *Both Droughts* and *2nd Drought Only* samples (Fig. A.10; Fig. A.11). Four-year Pr-ET overdraft was significantly more negative during the *2nd Period* than the *1st Period* by 130 to 140 mm 4 yr^{-1} ($p < 0.001$) in the *Both Droughts* sample and by 1,020 to 1,030 mm 4 yr^{-1} ($p < 0.001$) in the *2nd Drought Only* sample using a paired t-test (Figure 1.2c; Fig A.8; Fig. A.9; Table A.1). T_{max} significantly increased during the 2*nd Period* compared to the *1st Period* by 0.46 to 0.48 ˚C (p-value < 0.001) in the *Both Droughts* sample and by 0.829 to 0.834 ˚C (p-value < 0.001) in the *2nd Drought Only* sample according to paired t-tests (Fig. A.9, Fig. A.10; Table A.1). T_{max} was significantly greater (p-value < 0.001) in the *Both Droughts* sample than the *2nd Drought Only* sample by 1.1 to 1.4 ˚C during the *1st Period* and by 0.8 to 1.1 ˚C during the *2nd Period* according to Tukey HSD tests (Table A.2).

There was little apparent change in forest density between the *1st Period* and *2nd Period* for the *2nd Drought Only* sample and mixed results for the *Both Droughts* sample (Fig. A.12; Fig. A.13; Fig. A.14). In the *Both Droughts* sample AGB significantly decreased during the *1st Period* compared to *2nd Period* by 4 to 5 Mg ha^{-1} or 3.3 to 4.0% ($p < 0.001$), while in the *2nd Drought Only* sample AGB significantly increased by 0.02 to 0.3 Mg ha^{-1} or 0.0 to 0.2% ($p < 0.05$) according to paired t-tests (Fig. A.12; Fig A.13; Table A.1). In the *Both Droughts* sample BA varied during the *2nd Period* compared to the *1st* Period from 6 m^2 ha^{-1}

greater to 19 $m^2 ha^{-1}$ less or 30% greater to 95% less ($p = 0.537$) sample, while in the *2nd Drought Only* BA varied from 5 $m^2 ha^{-1}$ greater to 6 $m^2 ha^{-1}$ less or 17% greater to 19% less ($p = 0.998$) sample according to Tukey HSD tests (Fig. A.14; Table A.3).

Both AGB and BA were greater in the *2nd Drought Only* sample compared to the *Both Droughts* sample. AGB was significantly greater by 54 to 60 Mg ha^{-1} during the *1st Period* and by 57 to 63 Mg ha^{-1} during the *2nd Period* ($p < 0.001$; Table A.2; Fig. A.11; Fig. A.12). BA was significantly greater by 2 to 19 $m^2 ha^{-1}$ during the *1st Period* ($p < 0.05$) and by 7 to 28 $m^2 ha^{-1}$ during *2nd Period* ($p < 0.001$; Fig A.14; Table A.3) according to Tukey HSD tests.

3.3 Comparing Predictors of Die-off Severity (dNDMI)

Cumulative moisture deficit (four-year Pr-ET overdraft) and severe die-off (dNDMI) were similarly correlated during the *1st Period* for the *Both Droughts* sample and the *2nd Period* for the *2nd Drought Only* sample, but for the *Both Droughts* sample four-year Pr-ET overdraft was not correlated with dNDMI during the *2nd Period*. We modeled die-off severity (dNDMI) using multiple linear regression ($R^2 = 0.234$, $p < 0.001$) with the following predictors: four-year Pr-ET, time period (*1st Period* or *2nd Period*), drought sequence (*Both Droughts* or *2nd Drought Only*), AGB, T_{max}, and the interaction between time period and drought sequence (time period x drought sequence; Fig. 1.5; Table A.6). Time period x drought sequence accounted for 45.8% of the explained variance in dNDMI, while four-year Pr-ET accounted for 36.6%, T_{max} accounted for 9.3%, time period accounted for 3.7%, AGB accounted for 2.7%, and drought sequence accounted for 2.0% in a relative weight analysis (Table A.6). There was a small amount of spatial autocorrelation in our data (Fig. A.15). We explored the effects of this spatial autocorrelation by taking a 5% random sub-sample from each drought sequence (Fig. A.14). The sub-sampled data

produced very similar results to the full data set (Fig. A.16); therefore, we used the full data set for further analysis. We explored differences in the drought sequence samples by comparing the responses of forests in the Sierra Nevada and Southern California regions. We found no evidence of differences in forest response by region (Fig. A.17).

Forests responded differently to predictors of die-off during the *1st Period* and *2nd Period* in the *Both Droughts* samples. In the *Both Droughts* sample, four-year Pr-ET overdraft was a strong predictor of die-off (negative dNDMI) during the *1st Period* (R^2 = 0.42, $p < 0.001$, piecewise linear regression; Figure 1.5a) while four-year Pr-ET was a weak predictor of lack of die-off or possible regrowth (positive dNDMI) during the *2nd Period* (R^2 = 0.095, $p < 0.001$, piecewise linear regression; Figure 1.5b). In the *2nd Drought Only* sample, four-year Pr-ET overdraft was a strong predictor of die-off (negative dNDMI) during the *2nd Period* (R^2 = 0.23; $p < 0.001$, piecewise linear regression; Figure 1.5d), but there was almost no relationship between four-year Pr-ET overdraft and dNDMI during the *2nd Period* (R^2 = 0.021, $p < 0.001$, piecewise linear regression; Figure 1.5c). As illustrated by four-year Pr-ET, in the *Both Droughts* samples the relationships between T_{max} and AGB with dNDMI were also different during the *1st Period* and *2nd Period* (Fig. A.18, Fig. A.19).

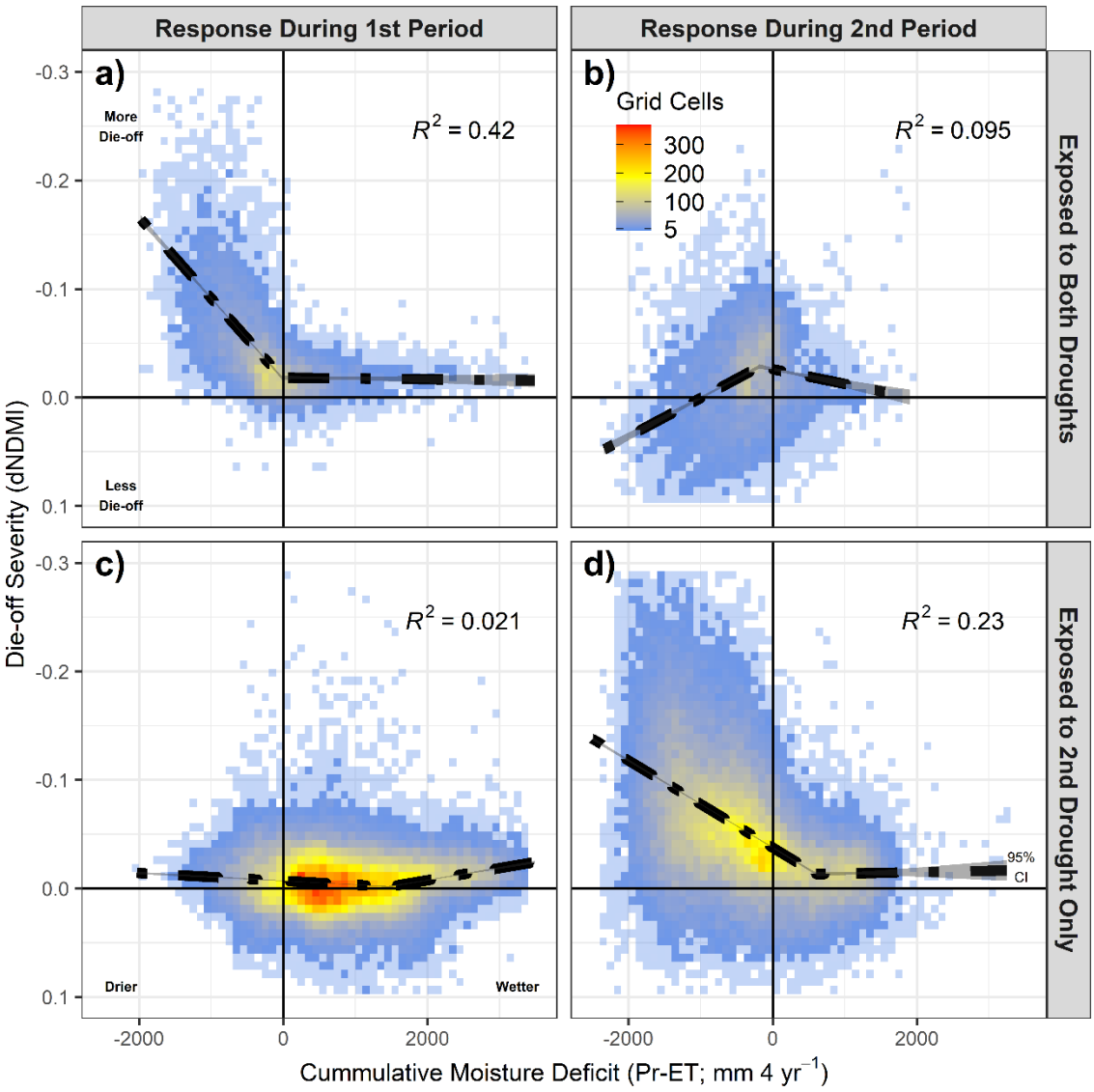

Figure 1.5. Comparison of four-year Pr-ET as a predictor of forest die-off severity (dNDMI) in four combinations of drought exposure and time period. The top two panels show the relationship between four-year Pr-ET and dNDMI for locations exposed to *Both Droughts* in the *1st Period* (a) and *2nd Period* (b). The bottom two panels show the relationship between four-year Pr-ET and dNDMI in locations exposed to drought in *2nd Drought Only* in the *1st Period*(c) and *2nd Period* (d). The solid black line in all panels shows the piecewise linear fit four-year Pr-ET as a predictor of dNDMI. The gray shaded ribbons are the 95% confidence intervals. The partially opaque blue squares represent combinations of dNDMI and four-year Pr-ET with less than 5 grid cell observations. The sample size for the top two panels is N = 8,933. The sample size the bottom two panels is N = 40,922.

1.4 Discussion

1.4.1 Observed Patterns of Die-off

We found that forests with previous drought exposure had dampened die-off severity during subsequent drought. Forest stands in the *2nd Drought Only* sample exhibited severe die-off during the *2nd Period*, as quantified with dNDMI, whereas stands in the *Both Droughts* sample experienced severe dNDMI during the *1st Period* but not the *2nd Period* (Fig. 1.2a, b; Fig. 1.3). Four-year Pr-ET overdraft was similarly correlated with dNDMI during the initial drought experienced by both samples (Figure 1.5a, d). This is consistent with previous studies showing that needleleaf conifers experience severe drought-induced die-off (Brodrick & Asner, 2017; Paz-Kagan et al., 2017; Stovall et al., 2019), especially in forests with high density (AGB or BA (Young et al., 2017); Fig. A.18), when exposed to high T_{max} (Goulden & Bales, 2019), and four-year Pr-ET overdraft (Goulden & Bales, 2019; Madakumbura et al., 2020). It is important to note that the *2nd Drought Only* sample occurs primarily in the Sierra Nevada and the *Both Droughts* sample occurs primarily in the Southern California Mountains (Fig. 1.1a, Fig. A.2). Forest density in the Sierra Nevada is on average greater than in the Southern California Mountains (Fig. A.12, Fig. A.13, Fig. A.14a, b), but the two regions do contain the same semi-arid conifer forest types and tree species (Fig. A.14c, d). Higher average forest density in *2nd Drought Only* sample could explain some of the greater die-off during the *2nd Period* in the *2nd Drought Only* sample compared to the *Both Droughts* samples. However, comparisons between the *1st Period* and *2nd Period* within each drought sequence are not impacted by these differences in forest density. Forest stands in the *Both Droughts* sample experienced similarly severe four-year Pr-ET overdraft during both the *1st Period* and *2nd Period* (Fig. 1.2c; Fig. A.2), but severe and widespread die-off only during the *1st Period* (Fig. 1.2a, b; Fig. 1.3; Fig. 1.4; Fig. 1.5a, b), implying that during

the *2nd Period* die-off had become decoupled from precipitation shortfall and cumulative moisture deficit.

Previous studies have proposed that reductions in forest leaf area from past die-off increase water availability (makes cumulative moisture deficit less negative) and therefore decrease subsequent die-off severity (Goulden & Bales, 2019; Young et al., 2017). Forest stands in the *Both Droughts* sample had an increase in cumulative moisture deficit in the *2nd Period* (~60 to 67% more negative four-year Pr-ET overdraft). If die-off severity is a function of changes in cumulative moisture deficit, we would have expected to see a ~60 to 67% increase in die-off severity (Fig. 1.5; Table A.4). This was in stark contrast to the large decreases we observed in die-off severity according to both geospatial (~63 to 70% decrease in dNDMI) and forest inventory data (~31 to 144% decrease). Pines shifted from severe mortality during the *1st Period* to negligible morality during the *2nd Period* (~31 to 150% decrease in pine mortality). Based on the severe mortality in the *Both Droughts* sample during the *1st Period* (~3 $m^2 ha^{-1}$) we expected to observe a decrease in forest density during the *2nd Period*. In the *Both Droughts* sample, we observed a small decrease in forest density from geospatial data (~3 to 4% in AGB) and no significant change in forest density from inventory data (30% increase to 95% decrease in BA). While forest density must have decreased due to die-off in the *1st Period*, tree growth following the *1st Period* and limited sampling in the *Both Droughts* region made decreases in forest density difficult to detect during the *2nd Period*. Despite this potential decrease in forest density, forest leaf area and water use remained high during the *2nd Period*. We interpret the decoupling of water availability from die-off severity as evidence for a dampening effect from recent tree mortality that reduced forest susceptibility to the subsequent drought.

1.4.2 Plausible Mechanisms

There are several potential mechanisms that could explain the dampening effect in the *Both Droughts* region. The simplest mechanism would result solely from a decrease in the number of trees to kill after initial die-off. It is true that forest stands in the *Both Droughts* region experienced tree mortality during the *1st Period* which must have decreased leaf area and the number of trees to kill. This relatively simple explanation likely accounts for at least some of the dampening effect we observed. However, three considerations illustrate that additional mechanisms likely also play a role: 1) mortality was species dependent; 2) there was negligible die-off regardless of remaining forest density; and 3) cumulative moisture deficit remained extreme. If a decrease in the number of trees to kill explained the protective effect we would have expected random die-off by tree species, continued mortality in high density forests, and decreased forest leaf area and therefore less negative cumulative water deficit. Instead, both initial mortality and decreases in mortality were greater in pines than among other tree species, in the *Both Droughts* sample there was negligible die-off during the *2nd Period* regardless of remaining living forest density, and cumulative moisture deficit remained extreme due to remaining forest leaf area.

Dampening effects may be caused by more nuanced mechanisms including decreased pathogen host density, physiological acclimation in surviving trees, decreased competition between surviving trees, or elimination of susceptible individuals (Anderegg et al., 2020b; McDowell et al., 2019; Seidl et al., 2017). We found that the greatest mortality occurred in pine and fir trees, which is consistent with past work showing the importance of tree species as a predictor of mortality (Fellows & Goulden, 2012; Fettig et al., 2019). One potential reason for this pattern is that some pine and fir species serve as hosts for

bark beetles that are implicated in drought-induced tree mortality, such as large Ponderosa pine for the western pine beetle (Das et al., 2016; Fettig et al., 2019). Past mortality may have decreased the density of bark beetle host trees so that there were fewer hosts to support a beetle outbreak and severe die-off during the *2nd Period* (McDowell et al., 2019). Alternatively, trees that survived the drought may have become less susceptible to die-off through physiological acclimations such as increased allocation to pathogen defense, root growth, or carbohydrate storage, and decreased allocation to stem and leaf growth (Allen et al., 2015). In addition, despite low overall water availability there may be reduced competition for water between trees in forest stands with reduced density and therefore more water available to individual trees (Young et al., 2017). Finally, pine mortality may have preferentially killed drought-susceptible trees so that the remaining living pines were intrinsically less susceptible to drought-induced die-off (Anderegg et al., 2020b; DeSoto et al., 2020). The limited number of forest inventory samples in the *Both Droughts* region and limited geographic scope of the region experiencing multiple droughts make it difficult to further differentiate between these possible mechanisms. Continued severe drought across the Southwestern United States will likely make it possible to further understand how widespread these types of dampening effects are across semi-arid conifer forests, and whether forest density will recover or persist at lower densities with repeated drought exposure. Regardless of which mechanism is correct, the existence of dampening effects will influence the long-term impact of drought stress in forests.

1.4.3 Implications

In forests where past tree morality reduces die-off severity in response to extreme drought, dampening effects will contribute to maintaining future forest density and ecosystem

services despite increased drought frequency and intensity. Forests that experience less severe die-off with drought as a result of previous exposure may better maintain long-term carbon stocks (Pan et al., 2011). However, in the short term the dampening effect was associated with carbon loss from recent tree mortality which is consistent with a recent projection of reduced carbon storage in California forests under climate change (Coffield et al., 2021). Die-off has been linked to increased fuels and wildfire risk, therefore changes to die-off severity may change wildfire risk, though the details of this effect are uncertain (Hicke et al., 2012; Stephens et al., 2018). Less severe needleleaf conifer die-off may maintain the current balance between pine and oak habitat in California forests (McIntyre et al., 2015). Similarly, forests with less severe die-off may maintain current water quality and quantity from mountain run-off (Goulden & Bales, 2014).

Past die-off that dampens forest disturbance during extreme drought has implications for projecting the impact of climate change. Ecological models that don't account for dampening effects project 50% or greater mortality in needleleaf evergreen forests by 2100 (Jiang et al., 2013; McDowell et al., 2016). However, if a dampening effect like the one we observed reduced die-off severity by ~63 to 70% during all future droughts we would expect ~15 to 19% mortality in needleleaf evergreen forests by 2100. Considering dampening effects that reduce die-off severity would improve prediction of drought-induced conifer forest die-off. Nonetheless, important uncertainties remain, such as how dampening effects dissipate with time and whether other disturbance types (e.g., wildfire) also dampen susceptibility to drought exposure. There is a near consensus that forests around the world will continue to experience increasing climate change-linked

drought stress; dampening effects of the type we identified will have a transient and perhaps long-term limit on the impacts of repeated drought exposure on forests.

1.5 Acknowledgments

This research was funded by the University of California Laboratory Fees Research Program grant number LFR-18-542511 and Strategic Growth Council grant number CCR20021 to The Center for Ecosystem Climate Solutions (CECS). CECS is supported by the California Strategic Growth Council's Climate Change Research Program with funds from California Climate Investments, a statewide initiative that puts billions of Cap-and-Trade dollars to work reducing greenhouse gas emissions, strengthening the economy, and improving public health and the environment – particularly in disadvantaged communities. CAN was supported in part by the Ridge to Reef Graduate Training Program funded in part by National Science Foundation Research Traineeship award DGE-1735040. This manuscript was greatly improved by comments from JA Wang, J Lin, CM Enweasor, KS Hemes, NM Fiore, SR Coffield, JT Randerson, and TE Huxman. We also acknowledge the indigenous peoples and land of California. UC Irvine, where most of this research took place, is located on the ancestral territories of the Acjachemen and Tongva peoples, many of whom maintain active physical, spiritual, and cultural ties to the region.

1.6 References

Abatzoglou, J. T., McEvoy, D. J., & Redmond, K. T. (2017). The West Wide Drought Tracker: Drought Monitoring at Fine Spatial Scales. Bulletin of the American Meteorological Society, 98(9), 1815–1820.

Adams, H. D., Williams, A. P., Xu, C., Rauscher, S. A., Jiang, X., & McDowell, N. G. (2013). Empirical and process-based approaches to climate-induced forest mortality models. Frontiers in Plant Science, 4, 438.

Allen, C. D., Breshears, D. D., & McDowell, N. G. (2015). On underestimation of global vulnerability to tree mortality and forest die-off from hotter drought in the Anthropocene. Ecosphere . https://esajournals.onlinelibrary.wiley.com/doi/abs/10.1890/ES15-00203.1

Anderegg, W. R. L., Trugman, A. T., Badgley, G., Anderson, C. M., Bartuska, A., Ciais, P., Cullenward, D., Field, C. B., Freeman, J., Goetz, S. J., Hicke, J. A., Huntzinger, D., Jackson, R. B., Nickerson, J., Pacala, S., & Randerson, J. T. (2020). Climate-driven risks to the climate mitigation potential of forests. Science, 368(6497), eaaz7005.

Anderegg, W. R. L., Trugman, A. T., Badgley, G., Konings, A. G., & Shaw, J. (2020). Divergent forest sensitivity to repeated extreme droughts. Nature Climate Change. https://doi.org/10.1038/s41558-020-00919-1

Asner, G. P., Brodrick, P. G., Anderson, C. B., Vaughn, N., Knapp, D. E., & Martin, R. E. (2016). Progressive forest canopy water loss during the 2012–2015 California drought. https://doi.org/10.1073/pnas.1523397113

Bechtold, W. A., & Patterson, P. L. (2005). The Enhanced Forest Inventory and Analysis Program--national Sampling Design and Estimation Procedures. USDA Forest Service, Southern Research Station.

Breshears, D. D., Cobb, N. S., Rich, P. M., Price, K. P., Allen, C. D., Balice, R. G., Romme, W. H., Kastens, J. H., Floyd, M. L., Belnap, J., Anderson, J. J., Myers, O. B., & Meyer, C. W. (2005). Regional vegetation die-off in response to global-change-type drought. Proceedings of the National Academy of Sciences of the United States of America, 102(42), 15144–15148.

Brodrick, P. G., & Asner, G. P. (2017). Remotely sensed predictors of conifer tree mortality during severe drought. Environmental Research Letters: ERL [Web Site], 12(11), 115013.

Byer, S., & Jin, Y. (2017). Detecting Drought-Induced Tree Mortality in Sierra Nevada Forests with Time Series of Satellite Data. Remote Sensing, 9(9), 929.

Coffield, S. R., Hemes, K. S., Koven, C. D., Goulden, M. L., & Randerson, J. T. (2021). Climate-Driven Limits to Future Carbon Storage in California's Wildland Ecosystems. AGU Advances, 2(3), e2021AV000384.

Crist, E. P., & Cicone, R. C. (1984). A Physically-Based Transformation of Thematic Mapper Data---The TM Tasseled Cap. IEEE Transactions on Geoscience and Remote Sensing: A Publication of the IEEE Geoscience and Remote Sensing Society, GE-22(3), 256–263.

Das, A. J., Stephenson, N. L., & Davis, K. P. (2016). Why do trees die? Characterizing the drivers of background tree mortality. Ecology, 97(10), 2616–2627.

DeSoto, L., Cailleret, M., Sterck, F., Jansen, S., Kramer, K., Robert, E. M. R., Aakala, T., Amoroso, M. M., Bigler, C., Camarero, J. J., Čufar, K., Gea-Izquierdo, G., Gillner, S., Haavik, L. J., Hereş, A.-M.,

Kane, J. M., Kharuk, V. I., Kitzberger, T., Klein, T., … Martínez-Vilalta, J. (2020). Low growth resilience to drought is related to future mortality risk in trees. Nature Communications, 11(1), 545.

Fellows, A. W., & Goulden, M. L. (2012). Rapid vegetation redistribution in Southern California during the early 2000s drought. Journal of Geophysical Research: Biogeosciences, 117(G3). https://doi.org/10.1029/2012JG002044

Fellows, A. W., & Goulden, M. L. (2017). Mapping and understanding dry season soil water drawdown by California montane vegetation. Ecohydrology, 10(1), e1772.

Fettig, C. J., Mortenson, L. A., Bulaon, B. M., & Foulk, P. B. (2019). Tree mortality following drought in the central and southern Sierra Nevada, California, U.S. Forest Ecology and Management, 432, 164–178.

Franklin, J. F., Shugart, H. H., & Harmon, M. E. (1987). Tree Death as an Ecological Process. Bioscience, 37(8), 550–556.

Goodwin, N. R., Coops, N. C., Wulder, M. A., Gillanders, S., Schroeder, T. A., & Nelson, T. (2008). Estimation of insect infestation dynamics using a temporal sequence of Landsat data. Remote Sensing of Environment, 112(9), 3680–3689.

Gorelick, N., Hancher, M., Dixon, M., Ilyushchenko, S., Thau, D., & Moore, R. (2017). Google Earth Engine: Planetary-scale geospatial analysis for everyone. Remote Sensing of Environment, 202, 18–27.

Goulden, M. L., Anderson, R. G., Bales, R. C., Kelly, A. E., Meadows, M., & Winston, G. C. (2012). Evapotranspiration along an elevation gradient in California's Sierra Nevada. Journal of Geophysical Research: Biogeosciences, 117(G3). https://doi.org/10.1029/2012JG002027

Goulden, M. L., & Bales, R. C. (2014). Mountain runoff vulnerability to increased evapotranspiration with vegetation expansion. Proceedings of the National Academy of Sciences, 111(39), 14071.

Goulden, M. L., & Bales, R. C. (2019). California forest die-off linked to multi-year deep soil drying in 2012–2015 drought. Nature Geoscience, 12(8), 632–637.

Groemping, U. (2006). Relative Importance for Linear Regression in R: The Package relaimpo. Journal of Statistical Software, 17(1), 1–27.

Groemping, U., & Matthias, L. (2018). Package 'relaimpo.' Relative Importance of Regressors in Linear Models (R Package Version). http://rsync.udc.es/CRAN/web/packages/relaimpo/relaimpo.pdf

Hardisky, M. A., Klemas, V., & Smart, R. M. (1983). The Influence of Soil-Salinity, Growth Form, and Leaf Moisture on the Spectral Radiance of Spartina-Alterniflora Canopies. Photogrammetric Engineering and Remote Sensing, 49(1), 77–83.

Hartmann, H., Moura, C. F., Anderegg, W. R. L., Ruehr, N. K., Salmon, Y., Allen, C. D., Arndt, S. K., Breshears, D. D., Davi, H., Galbraith, D., Ruthrof, K. X., Wunder, J., Adams, H. D., Bloemen, J., Cailleret, M., Cobb, R., Gessler, A., Grams, T. E. E., Jansen, S., … O'Brien, M. (2018). Research frontiers for improving our understanding of drought-induced tree and forest mortality. The New Phytologist, 218(1), 15–28.

Healey, S. P., Cohen, W. B., Zhiqiang, Y., & Krankina, O. N. (2005). Comparison of Tasseled Cap-based Landsat data structures for use in forest disturbance detection. Remote Sensing of Environment, 97(3), 301–310.

Hicke, J. A., Johnson, M. C., Hayes, J. L., & Preisler, H. K. (2012). Effects of bark beetle-caused tree mortality on wildfire. Forest Ecology and Management, 271, 81–90.

Hicke, J. A., Xu, B., Meddens, A. J. H., & Egan, J. M. (2020). Characterizing recent bark beetle-caused tree mortality in the western United States from aerial surveys. Forest Ecology and Management, 475, 118402.

Hijmans, R. J., Van Etten, J., Cheng, J., Mattiuzzi, M., Sumner, M., Greenberg, J. A., Lamigueiro, O. P., Bevan, A., Racine, E. B., Shortridge, A., & Others. (2015). Package 'raster.' R Package, 734. ftp://h64-50-233-100.mdsnwi.tisp.static.tds.net/pub/cran/web/packages/raster/raster.pdf

Hinojo-Hinojo, C., & Goulden, M. L. (2020). Plant Traits Help Explain the Tight Relationship between Vegetation Indices and Gross Primary Production. Remote Sensing, 12(9). https://doi.org/10.3390/rs12091405

Hooper, S., & Kennedy, R. E. (2018). A spatial ensemble approach for broad-area mapping of land surface properties. Remote Sensing of Environment, 210, 473–489.

Jiang, X., Rauscher, S. A., Ringler, T. D., Lawrence, D. M., Park Williams, A., Allen, C. D., Steiner, A. L., Michael Cai, D., & McDowell, N. G. (2013). Projected Future Changes in Vegetation in Western North America in the Twenty-First Century. Journal of Climate, 26(11), 3671–3687.

Johnson, E. W., & Ross, J. (2008). Quantifying error in aerial survey data. Australian Forestry, 71(3), 216–222.

Jump, A. S., Ruiz-Benito, P., Greenwood, S., Allen, C. D., Kitzberger, T., Fensham, R., Martínez-Vilalta, J., & Lloret, F. (2017). Structural overshoot of tree growth with climate variability and the global spectrum of drought-induced forest dieback. Global Change Biology, 23(9), 3742–3757.

Kassambara, A. (2020). ggpubr: 'ggplot2' Based Publication Ready Plots. R Package Version, 1.

Kelly, A. E., & Goulden, M. L. (2008). Rapid shifts in plant distribution with recent climate change. Proceedings of the National Academy of Sciences of the United States of America, 105(33), 11823–11826.

Kennedy, R. E., Ohmann, J., Gregory, M., Roberts, H., Yang, Z., Bell, D. M., Kane, V., Hughes, M. J., Cohen, W. B., Powell, S., Neeti, N., Larrue, T., Hooper, S., Kane, J., Miller, D. L., Perkins, J., Braaten, J., & Seidl, R. (2018). An empirical, integrated forest biomass monitoring system. Environmental Research Letters: ERL [Web Site], 13(2), 025004.

Kleinman, J. S., Goode, J. D., Fries, A. C., & Hart, J. L. (2019). Ecological consequences of compound disturbances in forest ecosystems: a systematic review. Ecosphere , 10(11), e02962.

Kuhn, M., Wing, J., Weston, S., Williams, A., Keefer, C., Engelhardt, A., Cooper, T., Mayer, Z., Kenkel, B., Team, R. C., & Others. (2020). Package 'caret.' The R Journal, 223(7). http://cran.radicaldevelop.com/web/packages/caret/caret.pdf

Leutner, B., Horning, N., & Leutner, M. B. (2017). Package 'RStoolbox.' R Foundation for Statistical Computing, Version 0. 1. http://cran.hafro.is/web/packages/RStoolbox/RStoolbox.pdf

Madakumbura, G. D., Goulden, M. L., Hall, A., Fu, R., Moritz, M. A., Koven, C. D., Kueppers, L. M., Norlen, C. A., & Randerson, J. T. (2020). Recent California tree mortality portends future increase in drought-driven forest die-off. Environmental Research Letters: ERL [Web Site]. http://iopscience.iop.org/article/10.1088/1748-9326/abc719

McDowell, N. G., Barnard, H., Bond, B., Hinckley, T., Hubbard, R., Ishii, H., Köstner, B., Magnani, F., Marshall, J., Meinzer, F., Phillips, N., Ryan, M., & Whitehead, D. (2002). The relationship between tree height and leaf area: sapwood area ratio. Oecologia, 132(1), 12–20.

McDowell, N. G., Beerling, D. J., Breshears, D. D., Fisher, R. A., Raffa, K. F., & Stitt, M. (2011). The interdependence of mechanisms underlying climate-driven vegetation mortality. Trends in Ecology & Evolution, 26(10), 523–532.

McDowell, N. G., Grossiord, C., Adams, H. D., Pinzón-Navarro, S., Mackay, D. S., Breshears, D. D., Allen, C. D., Borrego, I., Dickman, L. T., Collins, A., Gaylord, M., McBranch, N., Pockman, W. T., Vilagrosa, A., Aukema, B., Goodsman, D., & Xu, C. (2019). Mechanisms of a coniferous woodland persistence under drought and heat. Environmental Research Letters: ERL [Web Site], 14(4), 045014.

McDowell, N. G., Pockman, W. T., Allen, C. D., Breshears, D. D., Cobb, N., Kolb, T., Plaut, J., Sperry, J., West, A., Williams, D. G., & Yepez, E. A. (2008). Mechanisms of plant survival and mortality during drought: why do some plants survive while others succumb to drought? The New Phytologist, 178(4), 719–739.

McDowell, N. G., Williams, A. P., Xu, C., Pockman, W. T., Dickman, L. T., Sevanto, S., Pangle, R., Limousin, J., Plaut, J., Mackay, D. S., Ogee, J., Domec, J. C., Allen, C. D., Fisher, R. A., Jiang, X., Muss, J. D., Breshears, D. D., Rauscher, S. A., & Koven, C. (2016). Multi-scale predictions of massive conifer mortality due to chronic temperature rise. Nature Climate Change, 6(3), 295–300.

McIntyre, P. J., Thorne, J. H., Dolanc, C. R., Flint, A. L., Flint, L. E., Kelly, M., & Ackerly, D. D. (2015). Twentieth-century shifts in forest structure in California: Denser forests, smaller trees, and increased dominance of oaks. Proceedings of the National Academy of Sciences of the United States of America, 112(5), 1458–1463.

Minnich, R. A. (2007). Southern California conifer forests. In M. G. Barbour, T. Keeler-Wolf, & A. A. Schoenherr (Eds.), Terrestrial Vegetation of California, 3rd Edition (pp. 502–538). University of California Press.

Miura, S., Amacher, M., Hofer, T., San-Miguel-Ayanz, J., Ernawati, & Thackway, R. (2015). Protective functions and ecosystem services of global forests in the past quarter-century. Forest Ecology and Management, 352, 35–46.

Mueller-Dombois, D. (1987). Natural Dieback in Forests. Bioscience, 37(8), 575–583.

Muggeo, V. M. R. (2003). Estimating regression models with unknown break-points. Statistics in Medicine, 22(19), 3055–3071.

Muggeo, V. M. R. (2008). Segmented: an R package to fit regression models with broken-line relationships. R News, 8(1), 20–25.

Pachauri, R. K., Allen, M. R., Barros, V. R., Broome, J., Cramer, W., Christ, R., Church, J. A., Clarke, L., Dahe, Q., Dasgupta, P., Dubash, N. K., Edenhofer, O., Elgizouli, I., Field, C. B., Forster, P., Friedlingstein, P., Fuglestvedt, J., Gomez-Echeverri, L., Hallegatte, S., … Meyer, L. (2014). Climate Change 2014: Synthesis Report. Contribution of Working Groups I, II and III to the Fifth Assessment Report of the Intergovernmental Panel on Climate Change. IPCC.

Pan, Y., Birdsey, R. A., Fang, J., Houghton, R., Kauppi, P. E., Kurz, W. A., Phillips, O. L., Shvidenko, A., Lewis, S. L., Canadell, J. G., Ciais, P., Jackson, R. B., Pacala, S. W., McGuire, A. D., Piao, S., Rautiainen, A., Sitch, S., & Hayes, D. (2011). A Large and Persistent Carbon Sink in the World's Forests. Science, 333(6045), 988.

Paz-Kagan, T., Brodrick, P. G., Vaughn, N. R., Das, A. J., Stephenson, N. L., Nydick, K. R., & Asner, G. P. (2017). What mediates tree mortality during drought in the southern Sierra Nevada? Ecological Applications: A Publication of the Ecological Society of America, 27(8), 2443–2457.

Pebesma, E. J. (2004). Multivariable geostatistics in S: the gstat package. Computers & Geosciences, 30(7), 683–691.

Pebesma, E. J. (2018). Simple features for R: standardized support for spatial vector data. R J., 10(1), 439.

Pedersen, T. L. (2019). Patchwork: The composer of plots. R Package Version, 1(0).

R Core Team. (2020). R: A language and environment for statistical computing. R Foundation for Statistical Computing. https://www.R-project.org/

Roy, D. P., Kovalskyy, V., Zhang, H. K., Vermote, E. F., Yan, L., Kumar, S. S., & Egorov, A. (2016). Characterization of Landsat-7 to Landsat-8 reflective wavelength and normalized difference vegetation index continuity. Remote Sensing of Environment, 185, 57–70.

Ryan, M. G., Phillips, N., & Bond, B. J. (2006). The hydraulic limitation hypothesis revisited. Plant, Cell & Environment, 29(3), 367–381.

Ryan, M. G., & Yoder, B. J. (1997). Hydraulic Limits to Tree Height and Tree Growth. Bioscience, 47(4), 235–242.

Savage, M. (1994). Anthropogenic and natural disturbance and patterns of mortality in a mixed conifer forest in California. Canadian Journal of Forest Research. Journal Canadien de La Recherche Forestiere, 24(6), 1149–1159.

Savage, M. (1997). The role of anthropogenic influences in a mixed-conifer forest mortality episode. Journal of Vegetation Science: Official Organ of the International Association for Vegetation Science, 8(1), 95–104.

Seidl, R., Thom, D., Kautz, M., Martin-Benito, D., Peltoniemi, M., Vacchiano, G., Wild, J., Ascoli, D., Petr, M., Honkaniemi, J., Lexer, M. J., Trotsiuk, V., Mairota, P., Svoboda, M., Fabrika, M., Nagel, T. A., & Reyer, C. P. O. (2017). Forest disturbances under climate change. Nature Climate Change, 7(6), 395–402.

Stanke, H., Finley, A. O., Weed, A. S., Walters, B. F., & Domke, G. M. (2020). rFIA: An R package for estimation of forest attributes with the US Forest Inventory and Analysis database. Environmental Modelling & Software, 127, 104664.

Stephens, S. L., Collins, B. M., Fettig, C. J., Finney, M. A., Hoffman, C. M., Knapp, E. E., North, M. P., Safford, H., & Wayman, R. B. (2018). Drought, Tree Mortality, and Wildfire in Forests Adapted to Frequent Fire. BioScience, 68(2), 77–88.

Stovall, A. E. L., Shugart, H., & Yang, X. (2019). Tree height explains mortality risk during an intense drought. Nature Communications, 10(1), 1–6.

Thom, D., & Seidl, R. (2016). Natural disturbance impacts on ecosystem services and biodiversity in temperate and boreal forests. Biological Reviews of the Cambridge Philosophical Society, 91(3), 760–781.

Waring, R. H. (1987). Characteristics of Trees Predisposed to Die. Bioscience, 37(8), 569–574.

Wickham, H. (2017). The tidyverse. R Package Ver, 1(1), 836.

Wickham, H., James, D. A., Falcon, S., Healy, L., & Wickham, M. H. (2015). Package 'RSQLite.' mran.microsoft.com. https://mran.microsoft.com/snapshot/2016-10-12/web/packages/RSQLite/RSQLite.pdf

Young, D. J. N., Stevens, J. T., Earles, J. M., Moore, J., Ellis, A., Jirka, A. L., & Latimer, A. M. (2017). Long-term climate and competition explain forest mortality patterns under extreme drought. Ecology Letters, 20(1), 78–86.

Zhu, H. (2019). KableExtra: Construct complex table with'kable'and pipe syntax. R Package Version, 1(0).

Zhu, Z., Wang, S., & Woodcock, C. E. (2015). Improvement and expansion of the Fmask algorithm: cloud, cloud shadow, and snow detection for Landsats 4–7, 8, and Sentinel 2 images. Remote Sensing of Environment, 159, 269–277.

CHAPTER 2

Recent fire history enhances semi-arid conifer forest drought resistance

Adapted From:

Norlen, C.A., Hemes, K.S., Wang, J.A., Randerson, J.A., Goulden, M.L. Recent fire history enhances semi-arid conifer forest drought resistance (in preparation)

2.1 Introduction

Changes to fire regimes are impacting forests around the world in conjunction with other climate change amplified threats such as drought induced tree mortality or die-off (Anderegg, Trugman, Badgley, Anderson, et al., 2020; McLauchlan et al., 2020). Forests are essential for humans as they regulate climate, provide water, and store carbon among many other ecosystem services (Bonan, 2008; Fargione et al., 2018; Griscom et al., 2017; McDowell et al., 2020; Pan et al., 2011). Fire is a fundamental ecological process in forests that has large impacts on each of these ecosystem properties (Bowman et al., 2009; McLauchlan et al., 2020). Climate change is driving increases in fire weather around the world and burned area in mesic forests where fire has been excluded for decades due to human fire suppression (Abatzoglou et al., 2019; Iglesias et al., 2022; M. W. Jones et al., 2022; MacDonald et al., 2023). This changing fire regime has large immediate initial impacts on forest structure and recovery (Hemes et al., 2023; Wang et al., 2022). While it is possible that initial climate change impacts from fire could lead to feedbacks (Lloret et al., 2012; Seidl et al., 2017) on subsequent drought induced forest die-off (Allen et al., 2015; McDowell et al., 2011), there is limited understanding of the feedbacks due to interactions between initial and subsequent disturbances.

2.1.1 Disturbance Interactions

Initial climate change amplified impacts on forests due to disturbances such as wildfires and drought induced forest die-off are well documented (Anderegg, Trugman, Badgley, Anderson, et al., 2020; McDowell et al., 2020). The changes to forest structure caused by initial climate change impacts can translate into ecological feedbacks which can either amplify or dampen subsequent disturbances (Lloret et al., 2012; Seidl et al., 2017). Emerging research shows that past drought induced forest die-off dampens the severity of subsequent drought induced die-off in semi-arid conifer forest*s* (Anderegg, Trugman, Badgley, Konings, et al., 2020; Norlen & Goulden, 2023). Increases to California fire size over the last few decades and especially the last few years (Williams

et al., 2019) increase the possibility of interactions between past fires and subsequent disturbances like drought induced die-off (Anderegg, Trugman, Badgley, Anderson, et al., 2020). Drought followed by fire resulted in destructive impacts in mature conifer forests in the Sierra Nevada (Steel et al., 2022).

2.1.2 Fire Impacts on Forests in California

California conifer forests represent diverse forest types that are currently experiencing the effects of initial climate change impacts. Recent changes to the California fire regime are driven by both climate change (Williams et al., 2019) and other factors such as fuels and human settlement (Keeley & Syphard, 2016). Before European colonization frequent fire due to both wildfire and Native American practices was an important driver of vegetation heterogeneity across the landscape, with a fire interval of less than 50 years in ecosystems below 2500 meters (Fites-Kaufman et al., 2007). However, since the early 1900s western forest practices focused on fire suppression have increased fire return intervals at lower elevations and have contributed to changes in forest composition including a greater dominance of intermediate age forest patches across the landscape (Fites-Kaufman et al., 2007). In recent years climate change is reversing some of the trends produced by fire suppression by driving increases to fire size (Gutierrez et al., 2021; Turco et al., 2023) and rate of spread (Hantson et al., 2022). In addition to reducing the fire return interval in some forests, this changing fire regime has large impacts on forests such as reducing evapotranspiration (ET) following fire, with fires that produced that greatest reductions in forest basal area also producing the greatest reductions in ET (Ma et al., 2020). Fires are also driving a decrease in tree cover across California (Wang et al., 2022) and decreases in the ability of forests to take up carbon following fire (Hemes et al., 2023). At the same time, following decades of fire suppression people are attempting to reintroduce historical levels of high frequency and low severity fire (Fites-Kaufman et al., 2007; Knight, Anderson, et al., 2022) through increased application of prescribed fire (Hankins, 2015; Knight, Tompkins, et al., 2022). Prescribed fire and

other forest management treatments also change forest structure by reducing ET and tree cover (Roche et al., 2018) and reducing wildfire risk (Stephens, Moghaddas, Hartsough, et al., 2009; van Mantgem et al., 2011; Walker et al., 2006).

2.1.3 Influence of Fire History on Forest Drought Vulnerability

Fire history has been hypothesized to either act as a dampening feedback that reduces the impact of drought or an amplifying feedback that increases the impact of drought. The dampening hypothesis could operate through a mechanism where more frequent fire history changes forest composition and structure (Bernal et al., 2023) to be more heterogenous and less susceptible to drought (Minnich, 2000; Minnich et al., 1995; Savage, 1994, 1997). Alternatively the dampening hypothesis could operate through a mechanism where exposure to low severity fire produces physiological induced defense responses that increase drought tolerance and resistance to herbivory in surviving trees (Hood et al., 2015). The amplifying hypothesis could operate through a mechanism where injury from fire increases susceptibility to mortality from bark beetle attack for a few years after burn (Fettig et al., 2010; Nelson et al., 2016). Alternatively, the amplifying hypothesis could operate through a mechanism where fire history favors the growth of fire resistant trees such as ponderosa pine which are particularly susceptible to drought induced die-off (Fettig et al., 2019; Fites-Kaufman et al., 2007). Increasing severe wildfires have well documented impacts on forests through reductions in tree cover, water use, and carbon uptake compared to similar unburned forests. Changes in forest properties such as the number of susceptible trees, number of bark beetle host trees, and forest water could explain potential post-fire feedbacks. Whatever effect fires have on subsequent disturbances, these impacts could vary depending on the type (e.g., wildfires or prescribed fires) and severity of fires.

2.1.4 Research Questions and Hypotheses

Semi-arid conifer forests in the Sierra Nevada of California provide a useful study system to investigate how forest water use and structure change following fires and the implications of those

changes for forest drought sensitivity as they have experienced both extensive fires and widespread drought induced die-off during a severe 2012-2015 drought. We used the well-documented forest die-off episode in the Southern Sierra Mixed conifer forests during the 2012-2015 drought as our study system (Asner et al., 2016; Byer & Jin, 2017; Goulden & Bales, 2019; Paz-Kagan et al., 2017; Young et al., 2017). We constructed a forest chrono-sequence by combining geospatial information on historical fire with satellite data on die-off, vegetation cover, and water use (evapotranspiration, ET). We measured vegetation cover with a peer-reviewed data set created by scaling Landsat observations with field observations. We measured forest water use as annual ET calculated by scaling satellite-based Normalized Difference Vegetation Index observations with flux tower ET. We measured forest die-off with aerial detection surveys (ADS) of forest die-off performed by the United States Forest Service (USFS) and tree cover time series derived from satellite remote sensing. We used these data sets to answer three **research questions**: **1.) How does water use and forest structure change following exposure to prescribed fire compared to wildfire? 2.) How do changes in water use and forest structure following fire vary according to fire severity? 3.) How do changes to forest structure and water use following fire alter forest sensitivity to drought?**

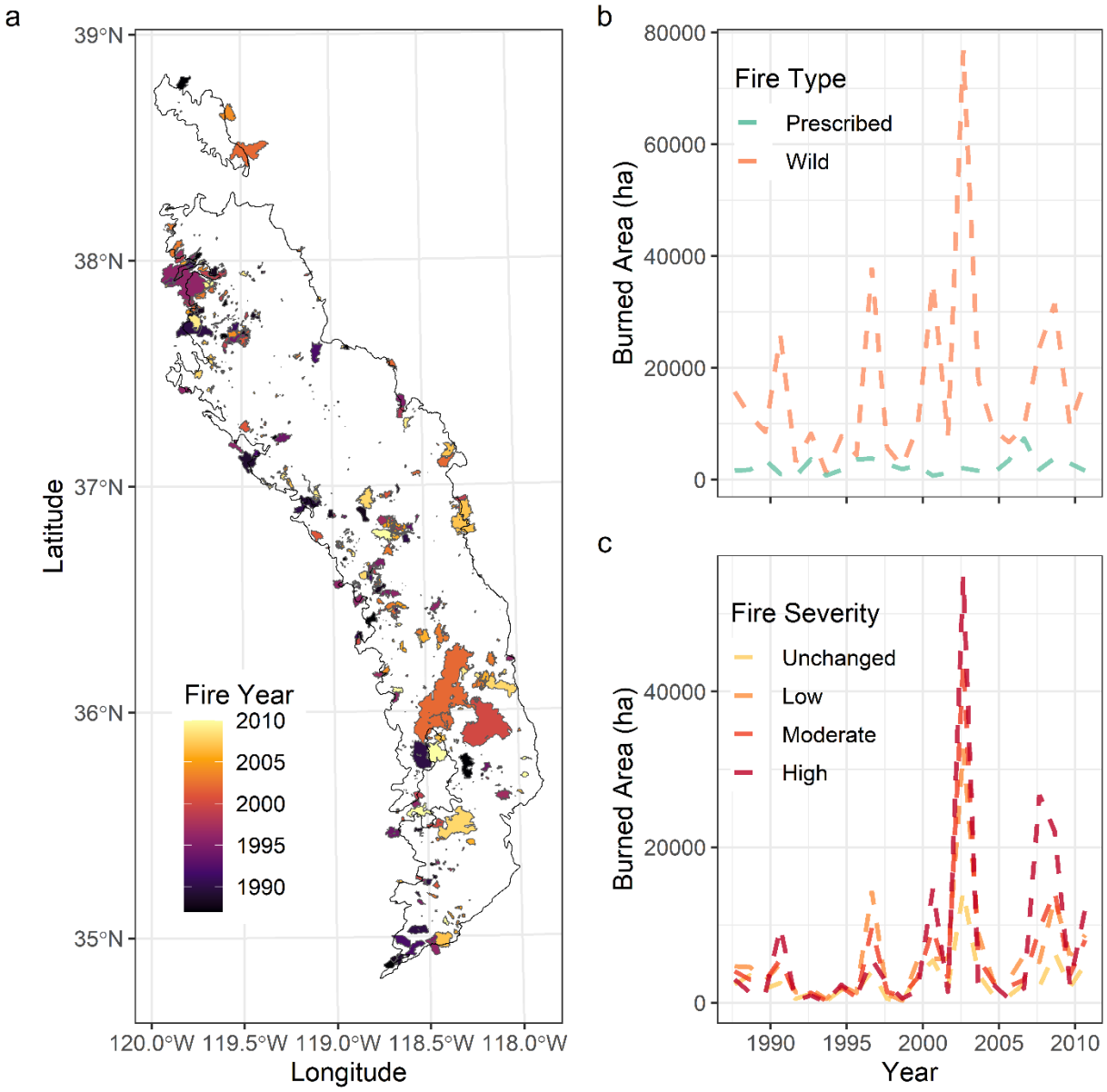

Figure 2.1. Fire area in the South Sierra from 1987-2010. The locations of fire perimeters are shown in panel a, annual area burned is shown in panel b, and annual burned area for different classes of wildfire severity are shown in panel c.

2.2 Materials & Methods

2.2.1 Study Design

We used a combined chrono-sequence and time series analysis approach to isolate the effects of fire history on vegetation cover, water use, and forest die-off. We used spatial controls to account for the changes to the characteristics of forests across time and between fire types and severity levels. We used temporal controls to account for variations in the growth of forest vegetation due to climatic conditions.

Semi-arid conifer forests in the south Sierra Nevada region provide a useful study system because they have a history of wildfires of varying severity, prescribed fires, and drought induced forest die-off (Figure 2.1; Figure B.1). The entire south Sierra region contains 2,530,236 hectares and intersects with 547 wildfire perimeters, 463 prescribed fire perimeters, and 206 wildfire perimeters with additional fire severity information during our study period of 1987 to 2010. We re-gridded all data to 300-meters by calculating the mean of all intersecting 30-meter pixels using Google Earth Engine (Gorelick et al., 2017). After random sampling from these fire perimeters and their 2-km buffers and matching between treatments and controls, we used 10,763 grid cells from the wildfire treatments and 13,332 from controls, 1,515 grid cells from the prescribed fire treatments and 1,913 from controls, and 12,257 grid cells from the fire severity treatments and 15,054 grid cells from controls.

2.2.2 Data Set Creation and Processing

2.2.2.1 Generating Water Flux Datasets

To create annual gridded data sets of ET and Precipitation minus ET (Pr-ET), we combined the record of Landsat from 1984-2021 with observations of ET from a network

of ten eddy covariance flux towers across California (Goulden et al., 2012; Goulden & Bales, 2014). We used the U.S. Geological Survey Collection 2 surface reflectance product screened for clouds, sensor saturation and other quality issues for the Landsat 5 Thematic Mapper, Landsat 7 Enhance Thematic Mapper+, and Landsat 8 Operational Land Imager (Wulder et al., 2012). We retrieved all 1984-2020 USGS Collection 2 Landsat 5, 7, and 8 scenes intersecting a state of California perimeter. We masked for clouds, cloud shadows, and snow using the FMask layer provided by USGS (Zhu & Woodcock, 2012). As a proxy for vegetation leaf area we calculated the Normalized Difference Vegetation Index (NDVI) surface reflectance index (Tucker, 1979) for each Landsat scene. We harmonized the surface reflectance bands and NDVI across the Landsat 7 and 8 by applying linear models calculated for all the Landsat 7 and 8 surface reflectance pixels across the continental united states (Goulden & Bales, 2019; Roy et al., 2016). We calculated the Tasseled Cap Brightness index for each Landsat pixel as a measure of total surface reflectance (Crist & Cicone, 1984; Crist et al., 1984). We removed pixels that were three standard deviations darker (shadows) or brighter (clouds or snow) than the time series mean Tasseled Cap Brightness (Goulden & Bales, 2019; Norlen & Goulden, 2023; Zhu & Woodcock, 2014). We calculated monthly NDVI for each Landsat pixel across California as the mean of the NDVI values for each calendar month using the masked and harmonized Landsat 5, 7, and 8 stack.

To calculate maximum monthly ET, we created a linear model of monthly NDVI from Landsat and monthly ET from eddy covariance data for each of the nine upwind Landsat pixels at each eddy covariance flux tower site. We applied the linear model of ET based on gridded NDVI to create monthly ET for all of California. We first analyzed the relationship

between monthly NDVI and monthly ET at the ten eddy covariance locations (Goulden et al., 2012; Goulden & Bales, 2014) for the 130 site years of data (eddy covariance towers were in operation from 2006-2018). We then applied the relationship between ET and NDVI to convert monthly NDVI across California to ET from 1984 to 2021. We then calculated the annual water year summed ET by taking the sum of the twelve months (Oct 1 – September 30) for each water year at each pixel for both the predicted and observed ET data sets (Fig B.2, R^2 = 0.8). We assigned the end year of each water year as the year. We used annual water year precipitation from PRISM from 1984-2021 (Daly et al., 2015). We converted the PRISM data from 4-km to 30-m resolution using linear interpolation. We retrieved PRISM precipitation from: https://developers.google.com/earth-engine/datasets/catalog/OREGONSTATE_PRISM_AN81m.

We define annual water stress (WS, Eq. 3) as current year precipitation (Pr) minus current water year evapotranspiration (ET). We summed annual water stress over the 2012-2015 water years (October 1, 2012 to September 30, 2015) to align with a four-year time scale that is related for forest drought stress (Goulden & Bales, 2019; Madakumbura et al., 2020).

$$(Eq.\,1)\; WS = \sum_{t+3}^{t} Pr_t - ET_t$$

2.2.2.2 Generating Forest Die-off Datasets

We measure forest die-off in two different ways: 1) as the sum of aerial detection surveys of die-off (ADS Die-off) conducted from 2015-2018, and 2) the change in tree cover between 2010-2011 and 2017-2018 (ΔTree Die-off). The two metrics of forest die-off had a moderate correlation with each other (Fig B.3, R^2 = 0.22).

Vegetation Cover

We used a gridded vegetation cover (tree, shrub, annual grass, perennial grass, litter, and bare ground) both to assess the presence and relative presence of trees and shrubs in forest stands and to detect decreases in tree cover following the 2012-2015 drought as a measure of forest die-off. The 30-meter annual (1984-2021) data set was generated by training Landsat data with vegetation percent cover from the Bureau of Land Management rangeland monitoring field data (Allred et al., 2021; M. O. Jones et al., 2018). The full data set can be retrieved as GeoTiffs from http://rangeland.ntsg.umt.edu/data/rap/rap-vegetation-cover/ or with Google Earth Engine (Gorelick et al., 2017) as an Image Collection at 'projects/rap-data-365417/assets/vegetation-cover-v3'.

Die-off (ΔTree)

We calculated forest die-off from tree cover as the difference between pre-drought and post-drought tree cover. We calculated pre-drought tree cover as the mean of 2010 and 2011 tree cover. We calculated post-drought tree cover as the mean of 2017 and 2018 tree cover. We calculated die-off (ΔTree) as post-drought tree cover minus pre-drought tree cover (Eq. 2).

$$(Eq.2)\ \Delta Tree = mean(Tree_{2017}, Tree_{2018}) - mean(Tree_{2010}, Tree_{2011})$$

Die-off (ADS)

We USFS used aerials detection surveys (ADS) of forest die-off intensity as a measure of forest die-off. The observations include both polygons that enclose areas with detected die-off and larger polygons that represent the entire area surveyed which included areas without detected die-off. We rasterized the ADS polygons for each year

2010-2019. We rasterized both the layers with the total area surveyed and the polygons enclosing areas where die-off was detected. We assigned a value of zero dead trees ha^{-1} to the survey area polygons. For each grid cell, we took the sum of the die-off detection and survey areas pixels for the rasterized layers from 2015-2018. That means that areas that were surveyed but did not overlap with mortality areas were assigned a die-off severity of 0 trees ha^{-1}. We assigned grid cells that were not surveyed a value of -9999 to represent no data. We retrieved ADS data from https://www.fs.usda.gov/detail/r5/forest-grasslandhealth/?cid=fsbdev3_046696.

2.2.2.3 Processing Fire Perimeter Datasets

We used fire perimeters from the California Department of Forestry and Fire Protection (CAL FIRE) and the United States Forest Service (USFS) to identify fire history, years since the last wildfire, and the severity of the previous wildfire (Figure 2.1). We used the fire perimeters provided by CAL FIRE to identify where and when wildfires and prescribed fires had occurred in our study region. We rasterized each year of the wildfire and prescribed fire data using GEE. We retrieved the wild and prescribed fire perimeters from https://frap.fire.ca.gov/media/ly2jyr4j/fire21_2.zip. We used the fire perimeters generated by USFS to identify the severity of a subset of fires from 1984-2017. The USFS fire severity perimeters contain calibrated burn severity with the following categories: 1 = lowest, 2 = low, 3 = moderate, and 4 = high (Miller et al., 2009; Miller & Quayle, 2015). We retrieved the USFS fire perimeters from https://www.fs.usda.gov/detail/r5/landmanagement/gis/?cid=STELPRDB5327833. The calibrated burn severity is based on the Relative change in Normalized Burn Ratio calculated with Landsat combined and field measurements of the actual proportion of

vegetation killed by fire (Miller & Thode, 2007). We rasterized each year and severity category of the data using GEE.

2.2.3 Experimental Design and Statistical Analyses

2.2.3.1 Experimental Design

We used the combination of a traditional chrono-sequence or space for time approach with time series analysis to isolate the effect of fire history on vegetation cover, water use, and forest die-off. We used controls of spatial variability to address non-random patterns of wildfire and prescribed fire occurrence and controls of temporal variability to address changes in forest growth in our study period from 1987-2010. Annual wildfire burned area varied year-to-year according to weather and other factors and has been increasing. Prescribed fire varies widely year-to-year depending on federal and state funding availability and has tended to be applied in forests that are denser than average. The biases and trends in wildfire and prescribed fire occurrence from 1987-2010 across our study area create issues for identifying statistically comparable burned and unburned control forests stands due to large fire years dominating our sample and decreases in sample size for older fires due to lower burned areas in previous decades (Figure B.3, Figure B.5). We used temporal controls to address variations in forest growth due to interannual temperature and precipitation variability that can be mistaken for changes due to disturbance recovery. This hybrid approach allows us to control for both changes in the composition of forests in our sample over time due to changes in the fire regime as well as variations in forest growth due to interannual climatic variability so that we can isolate the effect of forest recovery following fire.

Controls of Temporal Variability

Where wildfires occur, and the severity of fire at specific locations, is related to forest density. For example, historically fires in higher density conifer forests are typically less severe as many trees in these forests are resistant to fire which leads to less severe ground fires. However, under climate change this dynamic appears to be changing with severe crown fires occurring in dense conifer forests (Steel et al., 2022). We used a spatial matching approach between samples in burned and unburned control forest stands to control for temporal variability. To sample potential unburned spatial matches for burned forest stands we added a 2-km exterior buffer to each fire perimeter for the FRAP wildfire, FRAP prescribed fire, and USFS wildfire severity. We sampled from these unburned buffers by using two stratification layers: 1) the pre-fire tree cover and, 2) fire year. Our tree stratification layer had 20 five-percent tree cover bins (e.g., 0-5%, 6-10%, 11-15%, etc.) calculated as the tree cover two-years before the fire year (see Equation 3) for each of the three fire data sets with the reported fire year (*fyr*), and the two years before the fire (*fyr – 1, fyr – 2*). We based our spatial controls approach on previous studies in California ecosystems (Coffield et al., 2022; Hemes et al., 2023).

$$(Eq.3)\ Pre-Fire\ Tree = mean(Tree_{fyr-1} + Tree_{fyr-2})$$

The fire year stratification layer used the 1987-2010 fire years for the FRAP wildfire, FRAP prescribed fire, and USFS wildfire severity data sets. We excluded locations with a fire recorded from 2011-2019 to avoid considering the impacts of drought induced die-off in our analysis of fire history impacts on vegetation cover and water use. For the combined tree cover and fire year stratification, we drew a random sample of 500 grid cells from each bin for fire locations as burned grid cells, and 2-km fire buffers as unburned grid cells. For unburned stratification bins with fewer pixels than the corresponding burned

stratification bin, we used all available unburned grid cells and a random sample of the same number of burned grid cells. We then randomly drew the same number of unburned pixels from each stratification bin of the unburned 2-km buffer for each of the three fire datasets.

Controls of Spatial Variability

As described previously, the fire regime in California is changing, which leads to systematic positive trends in burned area and changes the geographic footprint of fires over our study period. For that reason, we subtracted the pre-fire vegetation cover (see Eq. 3, 4, and 5) for each burned and unburned control stand time series to calculate the post-fire deficits of tree cover, shrub cover, and ET in burned forests and growth in unburned control forests. We calculate these deficits by calculating the average pre-fire tree cover, shrub cover, and ET as the mean of the last two observed years before a fire (See Eq. 3, 4, and 5). For example, for a fire that occurred in 1987 (*fyr*) we used the mean of the observations for 1985 (*fyr – 1*) and 1986 (*fyr – 2*) as the pre-fire conditions. We then subtract the pre-fire conditions for each pixel from all the other observations for tree cover, shrub cover, and ET for that location.

$$(Eq.4)\ Pre-Fire\ Shrub = mean(Shrub_{fyr-1} + Shrub_{fyr-2})$$

$$(Eq.5)\ Pre-Fire\ ET = mean(ET_{fyr-1} + ET_{fyr-2})$$

Recovery after fire includes both variability in growth due to annual variations in the conditions controlling growth, such as precipitation and temperature, as well as changes in the composition of years since fire samples due to changes in the fire regime. For that reason, we calculated the mean and standard deviation across burned and unburned forest stands for each fire year (Figure B.4, Figure B.6). We then subtracted the

unburned control values from the burned values for each fire year and calculated the combined standard error as the sum of squared errors (Eq. 6). To assess pre-drought fire recovery, we plotted the fire recovery through 20-years post fire using the 1987 – 2012 observation years before the drought.

$$(Eq. 6)\ Combined\ Standard\ Error = \sqrt{\frac{sd_{burned}^2 + sd_{unburned}^2}{n}}$$

Statistical Analysis

To understand the impact of fire type (wild or prescribed) and fire severity, we compared the tree mortality, pre-drought evapotranspiration (ET), pre-drought tree cover, and water stress between fire type and fire severity levels using one-way analysis of variance (ANOVA) and Tukey Honestly Significant Difference (HSD) test.

We quantified the recovery of tree cover, shrub cover, and ET following wildfire, prescribed fire, and within fire severity categories by calculating the deficits of tree cover, shrub cover, and water use at the following post-fire intervals: *fyr + 1*, the year of greatest change after fire, and *fry + 20*.

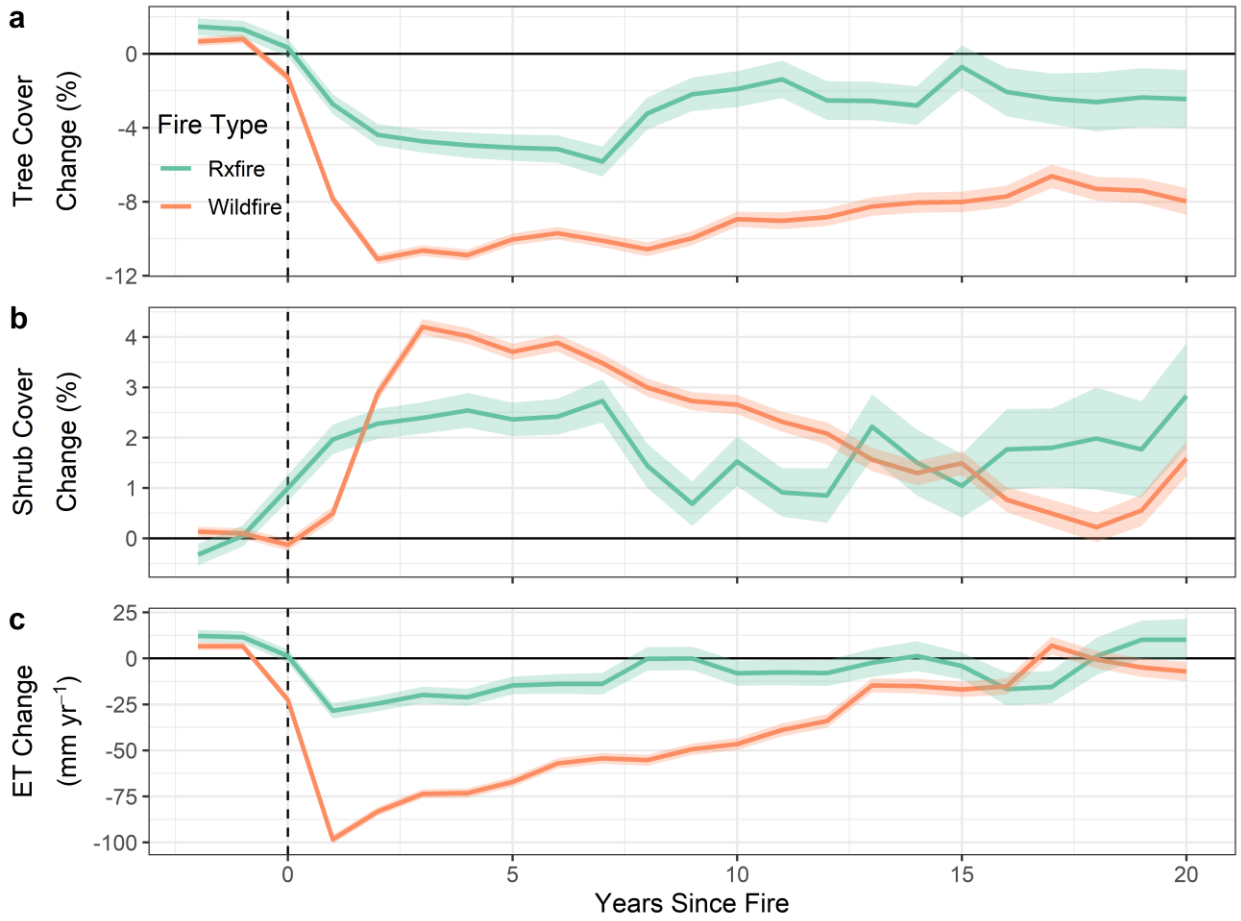

Figure 2.2. The impact of wildfire and prescribed (Rx) fire on tree cover (a), shrub cover (b), and ET (c) following exposure to wildfire or prescribed fire. The lines show means across fire pixels across the Sierra Nevada. The error bars show the 95% confidence intervals.

2.3 Results

2.3.2 Recovery of Vegetation Cover and Water Use Following Fire

Tree cover decreased and shrub cover increased due to wildfire and prescribed fire compared to unburned controls, with wildfire producing more considerable reductions in vegetation cover (Figure 2.2a, b). Tree cover in forest stands exposed to wildfire compared to unburned controls was 7.6 to 8.1% (95% Confidence Interval) lower after one year, 10.8 to 11.4% lower after two years, and 7.3 to 8.7% lower after 20 years. Tree cover in forest stands exposed to prescribed fire compared to unburned controls was 2.2 to 3.3% lower

after one year, 5.0 to 6.6% lower after seven years, and 0.9 to 4.0% lower after 20 years. Visible shrub cover in forest stands exposed to wildfire compared to unburned controls was 0.4 to 0.6% greater after one year, 2.7 to 3.0% greater after two years, and 1.2 to 1.9% greater after 20 years. Visible shrub cover in forest stands exposed to prescribed fire compared to unburned controls was 1.7 to 2.3% greater after one year, 2.3 to 3.2% greater after seven years and 1.0 to 2.6% greater after two years.

ET decreased following both wildfires and prescribed fires compared to unburned controls, with wildfires producing larger decreases in ET (Figure 2.2c). ET in forest stands impacted by wildfire returned to pre-fire levels after 17 years whereas ET in stands impacted by prescribed fire returned to pre-fire levels after 7 years. ET in forest stands exposed to wildfire compared to unburned controls was 96 to 101 mm yr^{-1} lower after 1 year and 2 to 12 mm yr^{-1} lower after 20 years. ET in forest stands exposed to prescribed fire compared to unburned controls was 24 to 33 mm yr^{-1} lower after 1 year and from 1 mm yr^{-1} lower to 2 mm yr^{-1} greater after 20 years.

Tree cover decreased due to all fire severity categories compared to unburned controls, with the highest severity fires producing the strongest decreases in tree cover (Figure 2.3a). Tree cover in forest stands exposed to high severity fire compared to unburned controls was 20.0 to 20.6% lower after one year, 24.9 to 25.6% lower after two years, and 10.9 to 13.6% lower after 20 years. Tree cover in forest stands exposed to moderate severity fire compared to unburned controls was 12.2 to 12.8% lower after one year, 16.8 to 17.5% lower after two years, and 5.9 to 8.0% lower after 20 years. Tree cover in forest stands exposed to low severity fire compared to unburned controls was 6.0 to 6.5% lower after one year, 9.9 to 10.5% lower after four years, and 4.4 to 6.4% lower after

20 years. Tree cover in forest stands exposed to the lowest severity fire compared to unburned controls was 0.9 to 1.6% lower after one year, 2.3 to 3.2% lower after four years, and 1.1 to 3.4% lower after 20 years.

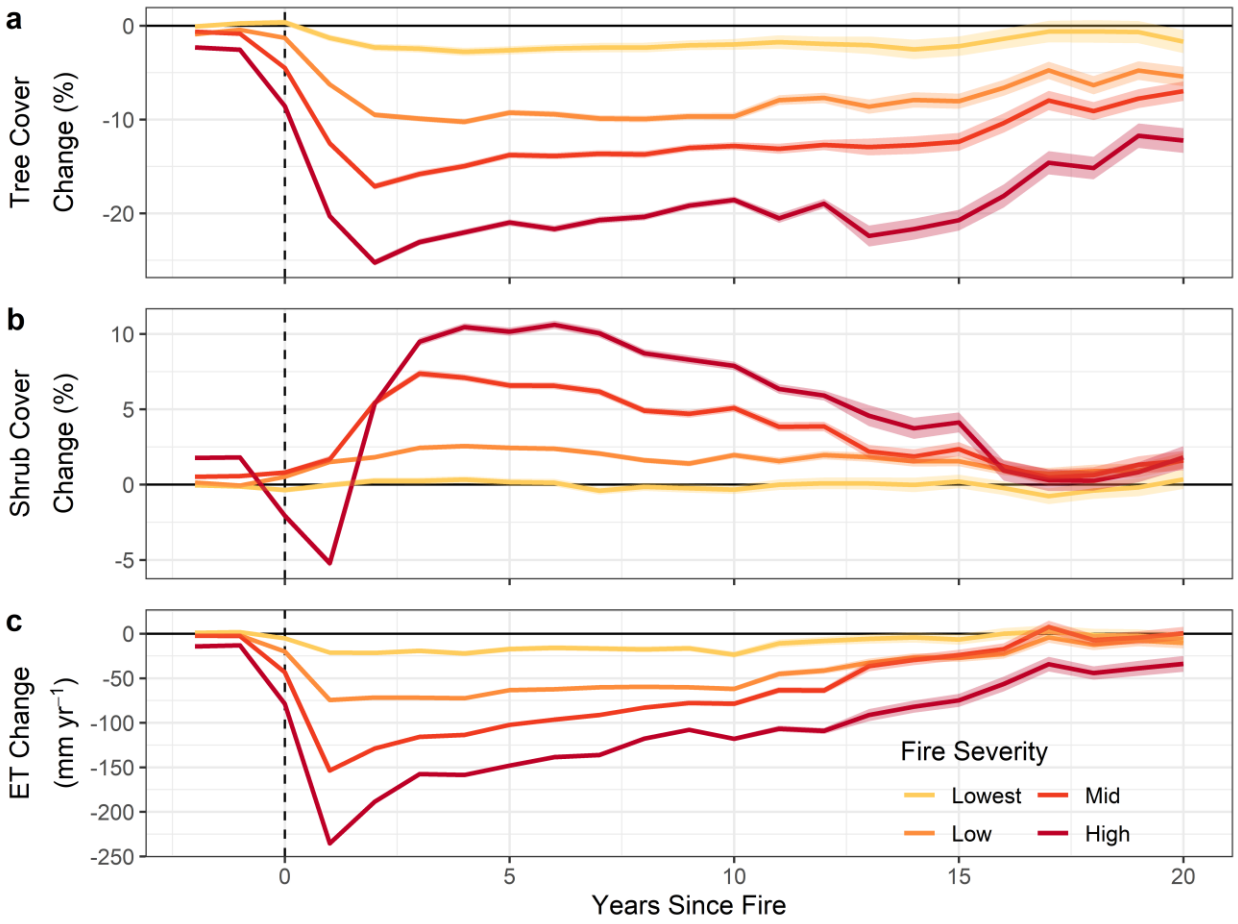

Figure 2.3. The impact of low, moderate, and high severity fires on tree cover (a), shrub cover (b), and ET over time. The lines show means across fire pixels across the Sierra Nevada. The error bars show the 95% confidence intervals.

Shrub cover increased due to all fire severity categories compared to unburned controls, with the highest severity fires producing the largest increases (Figure 2.3a). Visible shrub cover in forest stands exposed to high severity fire compared to unburned controls was 5.0 to 5.5 lower after one year, 10.3 to 10.9% greater after six years, and 1.1 to

2.6% greater after 20 years. Visible shrub cover in forest stands exposed to moderate severity fire compared to unburned controls was 1.5 to 1.9 greater after one year, 7.1 to 7.6% greater after three years, and 0.9 to 2.2% greater after 20 years. Visible shrub cover in forest stands exposed to low severity fire compared to unburned controls was 1.4 to 1.6 greater after one year, 2.4 to 2.7% greater after four years, and 1.1 to 2.1% greater after 20 years. Visible shrub cover in forest stands exposed to the lowest severity fire compared to unburned controls was 0.2% lower to 0.2% greater after one year, 0.1 to 0.6% greater after three years, and 0.3% lower to 1.0% greater after 20 years.

ET decreases in all fire severity categories, with the most severe fires producing the largest decreases (Figure 2.3c). ET in forest stands impacted by higher severity fires had not returned to pre-fire ET levels by 20 years, in forest stands affected by moderate and low severity fires had first returned to pre-fire ET levels after 17 years and in forest stands affected by the lowest severity fires returned to pre-fire ET after 14 years. In forest stands exposed to high severity fire ET compared to unburned controls was 233 to 238 mm yr^{-1} lower after one year, and 25 to 43 mm yr^{-1} lower after 20 years. In forest stands exposed to moderate severity fire ET compared to unburned controls was 151 to 156 mm yr^{-1} lower after one year, and 7 lower to 8 mm yr^{-1} greater after 20 years. In forest stands exposed to low severity fire ET compared to unburned controls was 72 to 77 mm yr^{-1} lower after one year and 4 to 17 mm yr^{-1} lower after 20 years. In forest stands exposed to the lowest severity fire ET compared to unburned controls was 19 to 24 mm yr^{-1} lower after one year, 19 to 25 mm yr^{-1} lower after four years, and 13 lower to 1 mm yr^{-1} greater after 20 years.

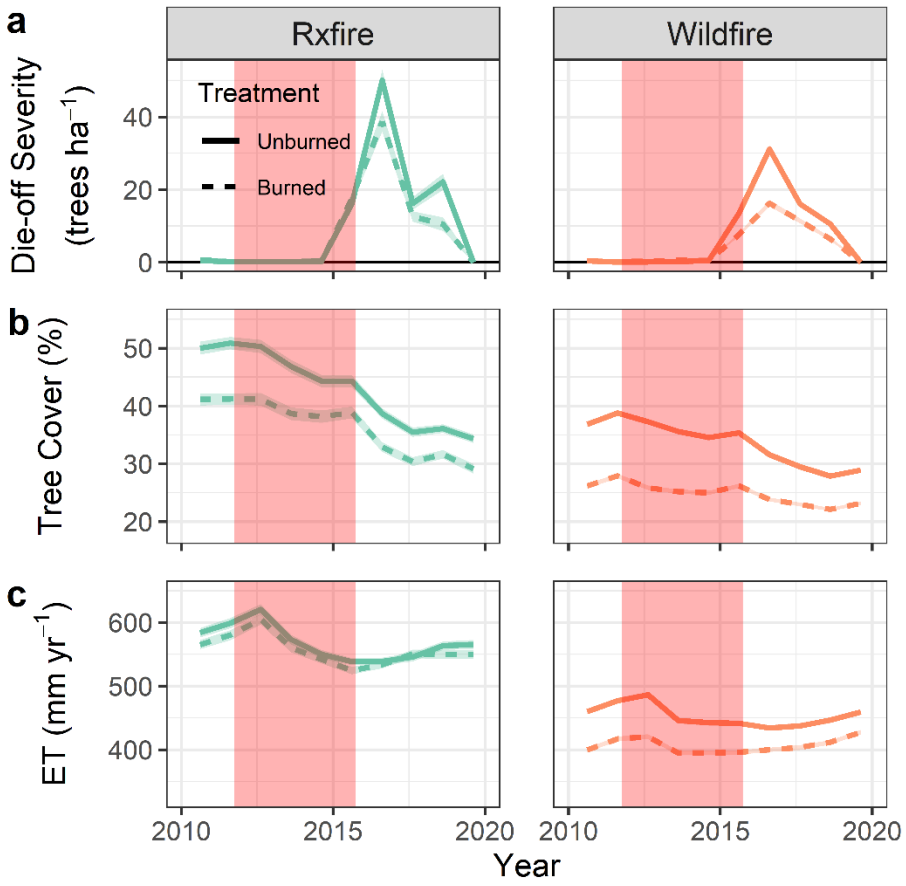

Figure 2.4. Tree mortality (a), tree cover (b), and ET (c) over time burned and unburned control locations from prescribed fires (Rxfires) and wildfires. The red bands across the 2012-2015 water years represent exposure to severe drought. The unburned controls are spatial controls matched to have similar to pre-fire burned pixels.

2.3.3 Wildfire versus Prescribed Fire Impacts on Forest Die-off

According to both ADS and ΔTree metrics for drought induced die-off, stands previously exposed to fire had lower levels of tree mortality following the 2012-2015 drought than unburned controls. Wildfire also conferred greater resistance to drought induce tree mortality than prescribed fire. (Figure 2.4a, b Table 2.5, Table B.1). According to the ADS die-off metric, die-off was lower in forest stands exposed to wildfire compared to unburned controls by 35.2% to 45.9 (29.9 to 39.0 trees ha^{-1}) according to a Tukey HSD test ($p < 0.001$). Die-off was lower in forest stands exposed to prescribed compared to

unburned controls by 12.1 to 28.7% (14.4 to 34.0 trees ha^{-1}) according to a Tukey HSD test ($p < 0.001$). According to the change in tree cover die-off metric, die-off was lower in forest stands exposed to wildfire than unburned controls by 45.7 to 55.5% (3.9 to 4.8% in absolute tree cover) according to a Tukey HSD test ($p < 0.001$). Die-off was lower in forest stands exposed to prescribed fire compared unburned controls by 24.9 to 38.3% (3.6 to 5.6% in absolute tree cover) according to a Tukey HSD test ($p < 0.001$).

Tree cover and ET also decreased in forest stands exposed to fire compared to unburned controls, which was greater in stands exposed to wildfire than in stands exposed to prescribed fire (Figure 2.4b, c, Figure 2.5, Table B.1). Tree cover was lower in forest stands exposed to wildfire compared to unburned controls by 25.6 to 30.1% (9.2 to 10.8% in absolute tree cover) according to a Tukey HSD test ($p < 0.001$). Tree cover was lower in forests stands exposed to prescribed fire compared to unburned controls by 14.8 to 22.3% (7.2 to 10.8% in absolute tree cover) according to a Tukey HSD test ($p < 0.001$). ET was lower in forest stands exposed to wildfire compared to unburned controls by 10.7 to 13.7% (49 to 62 mm yr^{-1}) or according to a Tukey HSD test ($p < 0.001$). ET was lower in forest stands exposed to prescribed compared to unburned controls by 0.0 to 5.2 % (0 to 30 mm yr^{-1}) or according to a Tukey HSD test ($p < 0.05$).

Four-year Pr-ET was less negative in forest stands exposed to wildfire compared to unburned controls, but not in forest stand exposed to prescribed fire (Fig B.8b; Figure 2.5; Table B.1). Four-year Pr-ET was less negative in forest stands exposed to wildfire compared to unburned controls increased by 3.6-to-5.1-fold (136 to 190 mm $4yr^{-1}$) according to a Tukey HSD test ($p < 0.001$). Four-year Pr-ET varied from more negative to more positive in forest stands exposed to prescribed fire compared to unburned controls

from 3.4% lower to 31.5% greater (12 mm 4yr^{-1} more negative to 110 less negative mm 4yr^{-1}) according to a Tukey HSD test (p = 0.165).

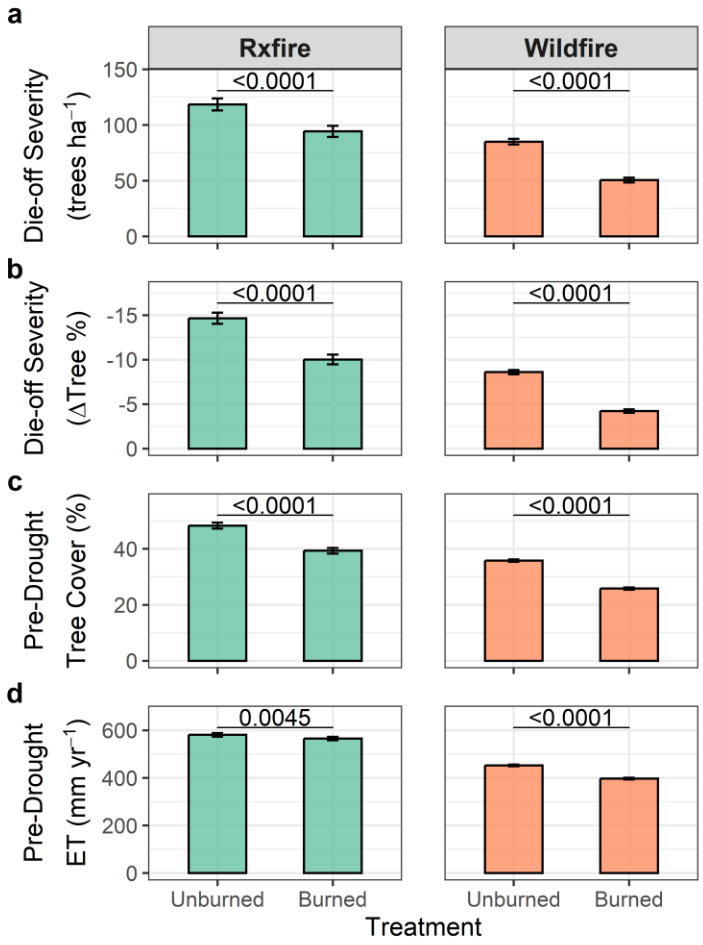

Figure 2.5. Comparisons of post-drought die-off (ADS), die-off (% tree cover), pre-drought tree cover, pre-drought ET, and four-year Pr-ET between forest stands exposed to wildfire and prescribed fire and matched to unburned control pixels using a Tukey Honestly Significant Difference test. The error bars represent 95% confidence intervals. The values shown between the two bars in a panel report the p-value from a Tukey Honestly Significant Difference test.

2.3.4 Fire Severity Impacts on Forest Stands

According to the ADS die-off metric, die-off decreased in stands exposed to fire compared to unburned controls, with greater decreases in locations exposed to higher severity fires (Figure 2.6 a, Figure 2.7a, Table B.2). Die-off was 60.3 to 86.1% lower (decrease of 36.4 to 52.0 trees ha^{-1}) in forest stands exposed to high severity wildfire

compared to unburned controls by according to a Tukey HSD test ($p < 0.001$). Die-off was lower in forest stands exposed to moderate severity wildfire compared to unburned controls by 39.1 to 62.4% (25.1 to 40.1 trees ha^{-1}) according to a Tukey HSD test ($p < 0.001$). Die-off was lower in forest stands exposed to low severity wildfire compared to unburned controls by or 31.8 to 47.4% (24.8 to 37.0 trees ha^{-1}) according to a Tukey HSD test ($p < 0.001$). Die-off was lower in forest stands exposed to the lowest severity wildfire compared to unburned controls by 10.5 to 36.6% (8.2 to 28.7 trees ha^{-1}) according to a Tukey HSD test ($p < 0.001$).

According to the tree cover change die-off metric, die-off decreased in stands exposed to fire compared to unburned controls, with greater decreases in locations exposed to higher severity fires (Figure 2.6a, Figure 2.7a, Table B.2). Die-off was lower in forest stands exposed to high severity wildfire compared to unburned controls by 94.2 to 117.8% (5.1 to 6.4% in absolute tree cover) according to a Tukey HSD test ($p < 0.001$). Die-off was lower in forest stands exposed to moderate severity wildfire compared to unburned controls by 67.6 to 88.1% (4.3 to 5.6% in absolute tree cover) according to a Tukey HSD test ($p < 0.001$). Die-off was lower in forest stands exposed to low severity wildfire compared to unburned controls by 37.4 to 51.4% (3.0 to 4.1% in absolute tree cover) according to a Tukey HSD test ($p < 0.001$). Die-off varied from lower to higher in forest stands exposed to the lowest severity wildfire compared to unburned controls from 20.6 lower to 2.7% greater (1.6 lower to 0.2% greater in absolute tree cover) according to a Tukey HSD test ($p = 0.256$).

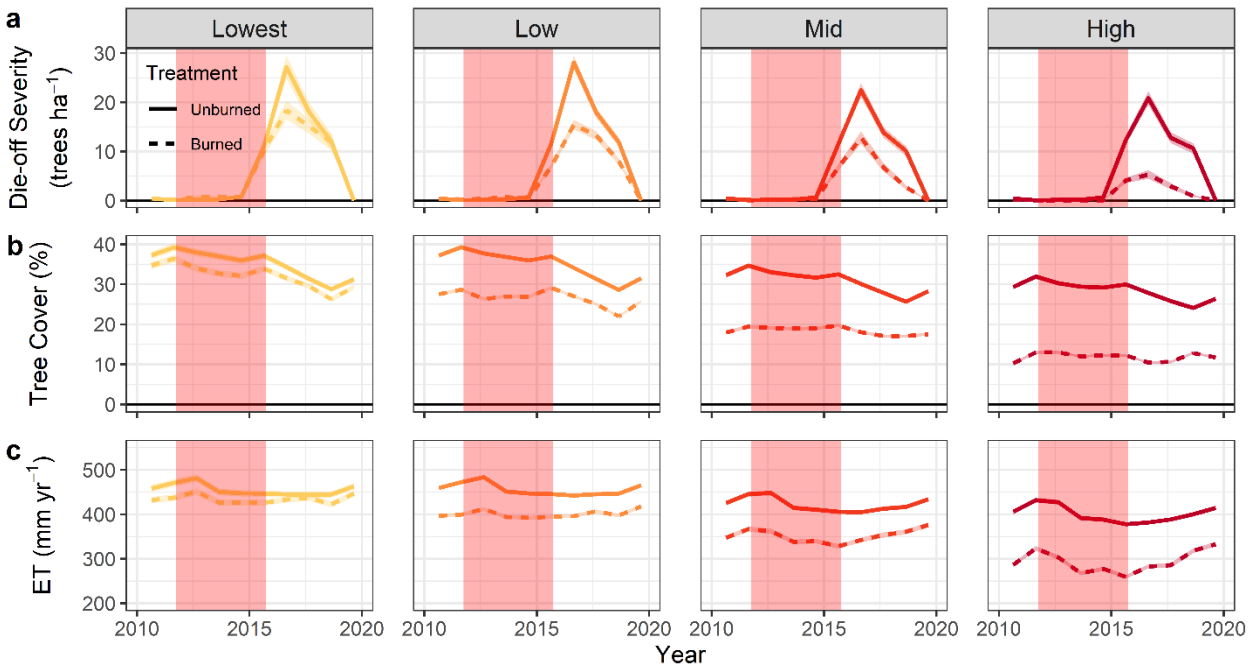

Figure 2.6. Tree mortality (a), tree cover (b), and ET (c) over time in burned and unburned control locations for different levels of fire severity. The red band across the 2012-2015 water years represents exposure to severe drought. The unburned controls are spatial controls matched to have tree cover similar to pre-fire burned pixels.

Tree cover decreased the most in the highest severity fires compared to unburned controls according to a USFS fire severity data sets (Figure 2.6b, Figure 2.7c, Table B.2). Tree cover decreased in forest stands exposed to high severity fire compared to unburned controls by 59.3 to 67.4% (17.7 to 20.1% in absolute tree cover) according to a Tukey HSD test ($p < 0.001$). Tree cover decreased in forest stands exposed to moderate severity fire compared to unburned controls by 40.5 to 48.0% (13.2 to 15.7% in absolute cover) according to a Tukey HSD test ($p < 0.001$). Tree cover decreased in forest stands exposed to low severity fire compared to unburned controls by 23.0 to 28.6% (8.7 to 10.8% in absolute cover) according to a Tukey HSD test ($p < 0.001$). Tree cover decreased in forest stands exposed to the lowest severity fire compared to unburned controls by 1.2 to 8.3% (0.8 to 4.3% in absolute tree cover) according to a Tukey HSD test ($p < 0.001$).

ET decreased the most in the highest severity fires compared to unburned controls according to a USFS fire severity data set (Figure 2.5c, Table 2.2, Table B.2). ET was lower in forest stands exposed to high severity fire compared to unburned controls by 25.4 to 30.9% (102 to 125 mm yr^{-1}) according to a Tukey HSD test ($p < 0.001$). ET was lower in forest stands exposed to moderate severity fire compared to unburned controls by 15.5 to 20.8% (66 to 88 mm yr^{-1}) according to a Tukey HSD test ($p < 0.001$). ET was lower in forest stands exposed to low severity fire compared to unburned controls by 12.0 to 16.3% (51 to 71 mm yr^{-1}) according to a Tukey HSD test ($p < 0.001$). ET was lower in forest stands exposed to the lowest severity fire compared to unburned controls by 2.1 to 11.4% (6 to 38 mm yr^{-1}) according to a Tukey HSD test ($p < 0.01$).

Four-year Pr-ET became less negative most drastically in forest stands exposed to the highest severity fires compared to unburned controls according to the USFS fire severity data sets (Fig. B.9b, Table B.2). Four-year Pr-ET was less negative in forest stands exposed to high severity fire compared to unburned controls by 1.8 to 3.0-fold (134 to 226 mm $4yr^{-1}$) according to a Tukey HSD test ($p < 0.001$). Four-year Pr-ET was less negative in forest stands exposed to moderate severity fire compared to unburned controls increased by 2.7 to 5.0-fold (107 to 200 mm $4yr^{-1}$) according to a Tukey HSD test ($p < 0.001$). Four-year Pr-ET was less negative in forest stands exposed to low severity fire compared to unburned controls by 9.0 to 14.5-fold (132 to 212 mm $4yr^{-1}$) or according to a Tukey HSD test ($p < 0.001$). Four-year Pr-ET was less negative in forest stands exposed to the lowest severity fire compared to unburned controls increased by 7.1% to 2.2-fold (5 to 138 mm $4yr^{-1}$) compared to unburned controls according to a Tukey HSD test ($p < 0.05$).

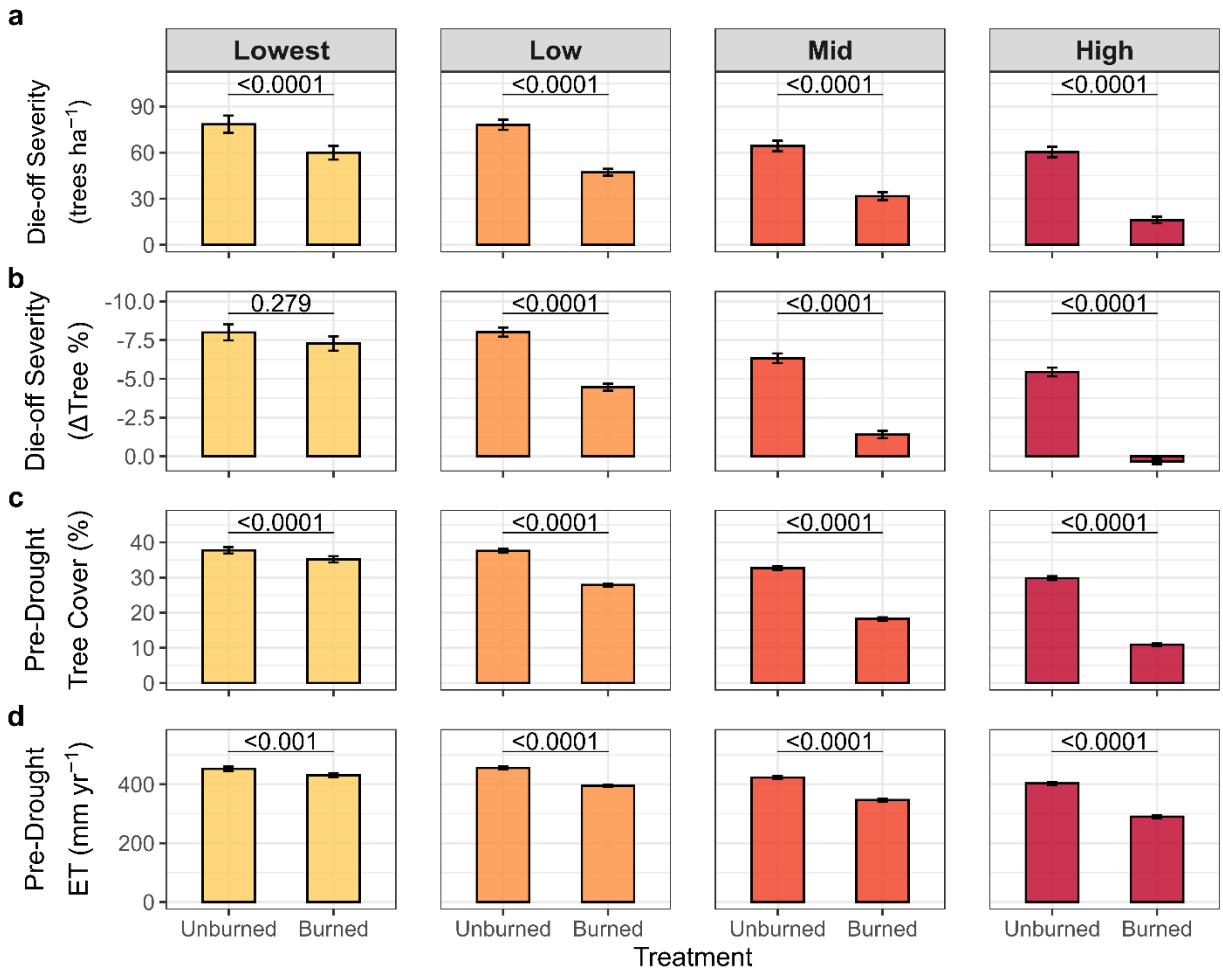

Figure 2.7. Comparisons die-off (trees ha^{-1}), die-off (Δ Tree %), pre-drought tree cover, pre-drought ET, and four-year Pr-ET between forest stands into four fire severity groups and matched to unburned control pixels using a Tukey Honestly Significant Difference test. The error bars represent 95% confidence intervals. The values shown between the two bars in a panel report the p-value from a Tukey Honestly Significant Difference test.

2.4 Discussion

2.4.1 Fire Recovery Trends

Recent fire history reduced tree cover, increased shrub cover, and decreased water use (ET) across all fire types and fire severities, with the largest post-fire changes observed for high severity wildfire fires. The reductions in ET were shorter-lived than reductions in tree cover because of rapid expansion of shrub cover and, therefore rapid recovery of ET

following fire. The reduction in ET led to greater water availability indicated by less negative four-year Pr-ET in all fire severities and in wildfires, but not in prescribed fires. The decreases in ET and tree cover led to dampened forest die-off severity according to both ADS and tree cover measures of die-off except for the lowest severity fires according to the tree cover change die-off metric. Die-off decreased the most in forests with a history of wildfire and high severity fire. These results support the dampening feedback hypothesis that decreases in tree cover and ET from fire history decrease the severity of forest die-off and increase the ability of semi-arid conifer forests to resist drought.

2.4.2 Mechanistic Explanations

The pattern of vegetation and ET recovery we observed follow theoretical patterns of forest succession following fire in conifer-dominated forests (Bonan, 2008). The post-fire decreases in ET, tree cover and shrub cover in high severity fires follows the general pattern of recruitment and recovery following fire in temperate forests. According to classical theories of succession post-fire decrease in tree cover allows additional light to reach the understory along with reduced competition for water from trees which in turn allows for increases in shrub cover (Finegan, 1984; Odum, 1969). The rapid increase and later decline in shrub cover, which is replaced by tree cover, aligns with the rapid initial decline of ET following fire and later gradual recovery. Across much of the Western United States, a century of fire suppression has decreased the occurrence of this fire recovery pattern (Fites-Kaufman et al., 2007). As burned area increases due to climate change and human settlement, post-fire recovery may begin to shift from these observed patterns due to changing climate conditions, as has been observed with forest photosynthesis during post-fire recovery (Coop et al., 2020; Hemes et al., 2023; Rodman et al., 2020).

There are at least three plausible mechanisms that could explain how post-fire recovery dampens die-off in semi-arid conifer forests. First, forests recovering from fire may simply have fewer susceptible trees remaining to kill (Norlen & Goulden, 2023; Young et al., 2017). Second, forests recovering from fire may have fewer host trees available for bark beetles to inhabit, which then limits their ability to produce widespread forest die-off during drought (Allen et al., 2015; Anderegg, Trugman, Badgley, Konings, et al., 2020; Fettig et al., 2019; McDowell et al., 2019; Seidl et al., 2017). Third, forests recovering from fire may have reduced leaf area and therefore reduced water use and competition for water so that individual surviving trees have increased water availability when precipitation decreases during drought (Goulden & Bales, 2019; Greenwood et al., 2017).

Our results support the idea that reductions in susceptible trees and forest water use (mechanisms one and three) dampen forest die-off following wildfire. The reductions in forest die-off severity were in general greater than proportional reductions in overall tree cover and water use due to fire. This suggests that the combination of reduced tree cover (Fig 2.2a, Fig 2.3a) and reduced water use (Fig 2.2b, Fig 2.3b) due to fire enhances forest drought resistance more than either reduction would individually. Changes in host trees (mechanism two) do not seem to have played a role in the dampened die-off we observed. This is consistent with understanding of post-fire forest succession tree mortality due to fire does not kill drought vulnerable pines and firs at a disproportionate rate. As a result, it is not surprising that mechanism two is not a key driver of the dampening feedback due to fire. It is important to note that due to the lack of a gridded time series that measures forest species composition and tree size we were not able to quantify the potential contribution of hypothesis two to the dampening feedback.

2.4.3 Benefits and Limitations of Fire

Both prescribed and wildfire history's ability to dampen forest die-off highlights the importance of returning fire to western US semi-arid forests. Increased application of prescribed fire and low severity fire provides many well-known benefits, such as reducing wildfire risk (Stephens, Moghaddas, Edminster, et al., 2009) and increasing water yield (Roche et al., 2018), and appear to provide the added benefit of dampening forest die-off. Other studies have highlighted that pre-drought management strategies such as thinning and prescribed fire lead to other benefits such as improved habitat due to increased hardwood dominance (Young et al., 2020) and increased growth and resistance in forests exposed to severe drought (Bernal et al., 2023; Young et al., 2023). The ability of fire history to dampen the impact of forest die-off raises important unanswered questions, such as how fire history impacts forest die-off risk at time intervals greater than about 20 years and whether management techniques such as prescribed fire combined with thinning, repeated prescribed fire, or selective thinning also reduce tree mortality during drought. The fact that prescribed fires can act as a proxy for wildfire to dampen the effects of drought induced die-off highlight one of the many additional co-benefits that will arise from ambitious plans to reintroduce frequent prescribed fire to Western U.S. forests.

Some trade-offs are inherent in selecting management strategies to improve overall forest health while also working to mitigate climate change. Even if ambitious plans to increase prescribed low severity fire to reduce fuel loads in western US semi-arid forests – such as the million-acre fuel treatment strategy in California – are successful, they will lead to reductions in overall tree cover and therefore greenhouse gas uptake (Crowfoot et al., 2021). These benefits come at the cost of reduced forest density and thus, at least in the

short term, decreased greenhouse gas removals from forests. This cost should not diminish the importance of reintroducing frequent low severity fire through prescribed fire. In the absence of prescribed fire, drought induced mortality can be followed be high severity fire leading to massive overall mortality as was the case when drought-induced forest die-off was followed by high severity fire in parts of the Sierra Nevada (Steel et al., 2022). This highlights that managing ecosystems for climate mitigation and adaptation requires consideration of trade-offs across temporal scales such as short-term reductions in carbon uptake linked to increased drought resistance.

2.4.4 Limitations

There are several limitations to this study including the two-decade timeline of our chrono-sequence analysis and comparison of ΔTree and ADS die-off metrics. Our study only considers the effects of fire followed by drought and spans includes a fire history record of about 20 years. How long it takes the dampening feedback from fire history to dissipate is an open question that could be answered by considering a longer fire history chrono sequence. This study only considers the effect of fire followed by severe drought. Other studies have shown that when the sequence is reversed and severe drought induced die-off is followed by fire massive overall tree mortality results (Steel et al., 2022). The two forest die-off metrics that we presented forest die-off in different ways and are presented as independent measure of die-off to increase confidence in our results. The ΔTree die-off metric indirectly measures forest die-off as a change in tree cover and therefore detects both increases in tree cover due to growth as well as some decreases that could be due to other land cover changes such as harvest. The ADS die-off metric is targeted to observe only tree mortality and forest die-off but has limited accuracy because it is collected

through digital sketch mapping in airplanes by human observers. It is encouraging and unsurprising that the two metrics are correlated, but at a modest level. The process for converting NDVI to ET is a useful approach, but likely saturates at LAI levels above 3.0 and especially above LAI of 5.0 (Granier et al., 2000).

2.4.4 Implications

Both prescribed and climate change induced wildfires produce a subsequent dampening feedback that enhances subsequent drought resistance in semi-arid California forests. This is in contrast to potentially catastrophic positive climate ecological-feedbacks that are hypothesized may lead to forest conversions into shrublands (Rising et al., 2022). The potential for initial climate change impacts to produce amplifying and dampening feedbacks raises important questions for research, modeling, and management. As climate change progress the ability of prescribed fire to increase forest drought resistance in semi-arid forests highlights the need to better understand and quantify how prescribed fire and other land management can mitigate the effects of climate change. In semi-arid conifer forests and ecosystems that behave similarly, increases to burned area through climate change induced wildfire and prescribed fire will decrease produce decreases tree cover and water use during post-fire forests that in turn increases forest resistance to drought.

2.5 Acknowledgements

This research was funded by the Ridge to Reef Graduate Training Program funded in part by the National Science Foundation Research Traineeship award DGE-1735040 and Strategic Growth Council grant number CCR20021 to The Center for Ecosystem Climate Solutions (CECS). CECS is supported by the California Strategic Growth Council's Climate Change Research Program with funds from California Climate Investments, a statewide

initiative that puts billions of Cap-and-Trade dollars to work reducing greenhouse gas emissions, strengthening the economy, and improving public health and the environment – particularly in disadvantaged communities. This manuscript was greatly improved by comments from VN Boot. We also acknowledge the indigenous peoples and land of California. UC Irvine, where most of this research took place, is located on the ancestral territories of the Acjachemen and Tongva peoples, many of whom maintain active physical, spiritual, and cultural ties to the region.

2.6 References

Abatzoglou, J. T., Williams, A. P., & Barbero, R. (2019). Global emergence of anthropogenic climate change in fire weather indices. *Geophysical Research Letters*, *46*(1), 326–336.

Allen, C. D., Breshears, D. D., & McDowell, N. G. (2015). On underestimation of global vulnerability to tree mortality and forest die-off from hotter drought in the Anthropocene. *Ecosphere* , *6*(8), art129.

Allred, B. W., Bestelmeyer, B. T., Boyd, C. S., Brown, C., Davies, K. W., Duniway, M. C., Ellsworth, L. M., Erickson, T. A., Fuhlendorf, S. D., Griffiths, T. V., Jansen, V., Jones, M. O., Karl, J., Knight, A., Maestas, J. D., Maynard, J. J., McCord, S. E., Naugle, D. E., Starns, H. D., … Uden, D. R. (2021). Improving Landsat predictions of rangeland fractional cover with multitask learning and uncertainty. *Methods in Ecology and Evolution / British Ecological Society*, *2041-210X.13564*. https://doi.org/10.1111/2041-210x.13564

Anderegg, W. R. L., Trugman, A. T., Badgley, G., Anderson, C. M., Bartuska, A., Ciais, P., Cullenward, D., Field, C. B., Freeman, J., Goetz, S. J., Hicke, J. A., Huntzinger, D., Jackson, R. B., Nickerson, J., Pacala, S., & Randerson, J. T. (2020). Climate-driven risks to the climate mitigation potential of forests. *Science*, *368*(6497). https://doi.org/10.1126/science.aaz7005

Anderegg, W. R. L., Trugman, A. T., Badgley, G., Konings, A. G., & Shaw, J. (2020). Divergent forest sensitivity to repeated extreme droughts. *Nature Climate Change*. https://doi.org/10.1038/s41558-020-00919-1

Asner, G. P., Brodrick, P. G., Anderson, C. B., Vaughn, N., Knapp, D. E., & Martin, R. E. (2016). Progressive forest canopy water loss during the 2012-2015 California drought. *Proceedings of the National Academy of Sciences of the United States of America*, *113*(2), E249-55.

Bernal, A. A., Kane, J. M., Knapp, E. E., & Zald, H. S. J. (2023). Tree resistance to drought and bark beetle-associated mortality following thinning and prescribed fire treatments. *Forest Ecology and Management*, *530*, 120758.

Bonan, G. B. (2008). Forests and climate change: forcings, feedbacks, and the climate benefits of forests. *Science*, *320*(5882), 1444–1449.

Bowman, D. M. J. S., Balch, J. K., Artaxo, P., Bond, W. J., Carlson, J. M., Cochrane, M. A., D'Antonio, C. M., Defries, R. S., Doyle, J. C., Harrison, S. P., Johnston, F. H., Keeley, J. E., Krawchuk, M. A., Kull, C. A., Marston, J. B., Moritz, M. A., Prentice, I. C., Roos, C. I., Scott, A. C., … Pyne, S. J. (2009). Fire in the Earth system. *Science*, *324*(5926), 481–484.

Byer, S., & Jin, Y. (2017). Detecting Drought-Induced Tree Mortality in Sierra Nevada Forests with Time Series of Satellite Data. *Remote Sensing*, *9*(9), 929.

Coffield, S. R., Vo, C. D., Wang, J. A., Badgley, G., Goulden, M. L., Cullenward, D., Anderegg, W. R. L., & Randerson, J. T. (2022). Using remote sensing to quantify the additional climate benefits of California forest carbon offset projects. *Global Change Biology*, *28*(22), 6789–6806.

Coop, J. D., Parks, S. A., Stevens-Rumann, C. S., Crausbay, S. D., Higuera, P. E., Hurteau, M. D., Tepley, A., Whitman, E., Assal, T., Collins, B. M., Davis, K. T., Dobrowski, S., Falk, D. A., Fornwalt, P. J., Fulé, P. Z., Harvey, B. J., Kane, V. R., Littlefield, C. E., Margolis, E. Q., … Rodman, K. C. (2020). Wildfire-Driven Forest Conversion in Western North American Landscapes. *Bioscience*, *70*(8), 659–673.

Crist, E. P., & Cicone, R. C. (1984). A Physically-Based Transformation of Thematic Mapper Data---The TM Tasseled Cap. *IEEE Transactions on Geoscience and Remote Sensing: A Publication of the IEEE Geoscience and Remote Sensing Society*, *GE-22*(3), 256–263.

Crist, E. P., Cicone, R. C., & Others. (1984). Application of the tasseled cap concept to simulated thematic mapper data. *Photogrammetric Engineering and Remote Sensing*, *50*(3), 343–352.

Crowfoot, W., Blumenfeld, J., & Porter, T. (Eds.). (2021). *California's Wildfire and Forest Resilience Action Plan*. California Department of Water Resources.

Daly, C., Smith, J. I., & Olson, K. V. (2015). Mapping Atmospheric Moisture Climatologies across the Conterminous United States. *PloS One*, *10*(10), e0141140.

Fargione, J. E., Bassett, S., Boucher, T., Bridgham, S. D., Conant, R. T., Cook-Patton, S. C., Ellis, P. W., Falcucci, A., Fourqurean, J. W., Gopalakrishna, T., Gu, H., Henderson, B., Hurteau, M. D., Kroeger, K. D., Kroeger, T., Lark, T. J., Leavitt, S. M., Lomax, G., McDonald, R. I., … Griscom, B. W. (2018). Natural climate solutions for the United States. *Science Advances*, *4*(11), eaat1869.

Fettig, C. J., McKelvey, S. R., Cluck, D. R., Smith, S. L., & Otrosina, W. J. (2010). Effects of prescribed fire and season of burn on direct and indirect levels of tree mortality in Ponderosa and Jeffrey Pine Forests in California, USA. *Forest Ecology and Management*, *260*(2), 207–218.

Fettig, C. J., Mortenson, L. A., Bulaon, B. M., & Foulk, P. B. (2019). Tree mortality following drought in the central and southern Sierra Nevada, California, U.S. *Forest Ecology and Management*, *432*, 164–178.

Finegan, B. (1984). Forest succession. *Nature*, *312*(5990), 109–114.

Fites-Kaufman, J. A., Rundel, P., Stephenson, N., & Weixelman, D. A. (2007). Montane and subalpine vegetation of the Sierra Nevada and Cascade ranges. *Terrestrial Vegetation of California*, 456–501.

Gorelick, N., Hancher, M., Dixon, M., Ilyushchenko, S., Thau, D., & Moore, R. (2017). Google Earth Engine: Planetary-scale geospatial analysis for everyone. *Remote Sensing of Environment*, *202*, 18–27.

Goulden, M. L., Anderson, R. G., Bales, R. C., Kelly, A. E., Meadows, M., & Winston, G. C. (2012). Evapotranspiration along an elevation gradient in California's Sierra Nevada. *Journal of Geophysical Research: Biogeosciences*, *117*(G3). https://doi.org/10.1029/2012JG002027

Goulden, M. L., & Bales, R. C. (2014). Mountain runoff vulnerability to increased evapotranspiration with vegetation expansion. *Proceedings of the National Academy of Sciences*, *111*(39), 14071.

Goulden, M. L., & Bales, R. C. (2019). California forest die-off linked to multi-year deep soil drying in 2012–2015 drought. *Nature Geoscience*, *12*(8), 632–637.

Granier, A., Loustau, D., & Bréda, N. (2000). A generic model of forest canopy conductance dependent on climate, soil water availability and leaf area index. *Annals of Forest Science*, *57*(8), 755–765.

Greenwood, S., Ruiz-Benito, P., Martínez-Vilalta, J., Lloret, F., Kitzberger, T., Allen, C. D., Fensham, R., Laughlin, D. C., Kattge, J., Bönisch, G., Kraft, N. J. B., & Jump, A. S. (2017). Tree mortality across biomes is promoted by drought intensity, lower wood density and higher specific leaf area. *Ecology Letters*, *20*(4), 539–553.

Griscom, B. W., Adams, J., Ellis, P. W., Houghton, R. A., Lomax, G., Miteva, D. A., Schlesinger, W. H., Shoch, D., Siikamäki, J. V., Smith, P., Woodbury, P., Zganjar, C., Blackman, A., Campari, J., Conant, R. T., Delgado, C., Elias, P., Gopalakrishna, T., Hamsik, M. R., … Fargione, J. (2017). Natural climate solutions. *Proceedings of the National Academy of Sciences of the United States of America*, *114*(44), 11645–11650.

Gutierrez, A. A., Hantson, S., Langenbrunner, B., Chen, B., Jin, Y., Goulden, M. L., & Randerson, J. T. (2021). Wildfire response to changing daily temperature extremes in California's Sierra Nevada. *Science Advances*, *7*(47), eabe6417.

Hankins, D. L. (2015). Restoring indigenous prescribed fires to California oak woodlands. *Gen. Tech. Rep. PSW-GTR-251. Berkeley, CA: US*. https://www.fs.usda.gov/treesearch/pubs/49977

Hantson, S., Andela, N., Goulden, M. L., & Randerson, J. T. (2022). Human-ignited fires result in more extreme fire behavior and ecosystem impacts. *Nature Communications*, *13*(1), 2717.

Hemes, K. S., Norlen, C. A., Wang, J. A., Goulden, M. L., & Field, C. B. (2023). The magnitude and pace of photosynthetic recovery after wildfire in California ecosystems. *Proceedings of the National Academy of Sciences*, *120*(15), e2201954120.

Hood, S., Sala, A., Heyerdahl, E. K., & Boutin, M. (2015). Low-severity fire increases tree defense against bark beetle attacks. *Ecology*, *96*(7), 1846–1855.

Iglesias, V., Balch, J. K., & Travis, W. R. (2022). U.S. fires became larger, more frequent, and more widespread in the 2000s. *Science Advances*, *8*(11), eabc0020.

Jones, M. O., Allred, B. W., Naugle, D. E., Maestas, J. D., Donnelly, P., Metz, L. J., Karl, J., Smith, R., Bestelmeyer, B., Boyd, C., Kerby, J. D., & McIver, J. D. (2018). Innovation in rangeland monitoring: annual, 30 m, plant functional type percent cover maps for U.S. rangelands, 1984–2017. *Ecosphere* , *9*(9), e02430.

Jones, M. W., Abatzoglou, J. T., Veraverbeke, S., Andela, N., Lasslop, G., Forkel, M., Smith, A. J. P., Burton, C., Betts, R. A., van der Werf, G. R., Sitch, S., Canadell, J. G., Santín, C., Kolden, C., Doerr, S. H., & Le Quéré, C. (2022). Global and regional trends and drivers of fire under climate change. *Reviews of Geophysics* , *60*(3). https://doi.org/10.1029/2020rg000726

Keeley, J. E., & Syphard, A. D. (2016). Climate Change and Future Fire Regimes: Examples from California. *Geosciences Journal*, *6*(3), 37.

Knight, C. A., Anderson, L., Bunting, M. J., Champagne, M., Clayburn, R. M., Crawford, J. N., Klimaszewski-Patterson, A., Knapp, E. E., Lake, F. K., Mensing, S. A., Wahl, D., Wanket, J., Watts-Tobin, A., Potts, M. D., & Battles, J. J. (2022). Land management explains major trends in forest structure and composition over the last millennium in California's Klamath Mountains. *Proceedings of the National Academy of Sciences of the United States of America*, *119*(12), e2116264119.

Knight, C. A., Tompkins, R. E., Wang, J. A., York, R., Goulden, M. L., & Battles, J. J. (2022). Accurate tracking of forest activity key to multi-jurisdictional management goals: A case study in California. *Journal of Environmental Management*, *302*(Pt B), 114083.

Lloret, F., Escudero, A., Iriondo, J. M., Martínez-Vilalta, J., & Valladares, F. (2012). Extreme climatic events and vegetation: the role of stabilizing processes. *Global Change Biology*, *18*(3), 797–805.

Ma, Q., Bales, R. C., Rungee, J., Conklin, M. H., & Collins, B. M. (2020). Wildfire controls on evapotranspiration in California's Sierra Nevada. *Journal Of*. https://www.sciencedirect.com/science/article/pii/S0022169420308246

MacDonald, G., Wall, T., Enquist, C. A. F., LeRoy, S. R., Bradford, J. B., Breshears, D. D., Brown, T., Cayan, D., Dong, C., Falk, D. A., Fleishman, E., Gershunov, A., Hunter, M., Loehman, R. A., van Mantgem, P. J., Middleton, B. R., Safford, H. D., Schwartz, M. W., & Trouet, V. (2023). Drivers of California's changing wildfires: a state-of-the-knowledge synthesis. *International Journal of Wildland Fire*, *32*(7), 1039–1058.

Madakumbura, G. D., Goulden, M. L., Hall, A., Fu, R., Moritz, M. A., Koven, C. D., Kueppers, L. M., Norlen, C. A., & Randerson, J. T. (2020). Recent California tree mortality portends future increase in drought-driven forest die-off. *Environmental Research Letters: ERL [Web Site]*. http://iopscience.iop.org/article/10.1088/1748-9326/abc719

McDowell, N. G., Allen, C. D., & Anderson-Teixeira, K. (2020). Pervasive shifts in forest dynamics in a changing world. *Science*. https://www.science.org/doi/abs/10.1126/science.aaz9463?casa_token=BN2Jpf5tT9sAAAAA:q9l0O7UJXg4Xk8YB4YlURsrt11d8nAznGOprLfang9uH-vLkqg7II94W7bd2pEUDl59lmsaVhB2wKIQ

McDowell, N. G., Beerling, D. J., Breshears, D. D., Fisher, R. A., Raffa, K. F., & Stitt, M. (2011). The interdependence of mechanisms underlying climate-driven vegetation mortality. *Trends in Ecology & Evolution*, *26*(10), 523–532.

McDowell, N. G., Grossiord, C., Adams, H. D., Pinzón-Navarro, S., Mackay, D. S., Breshears, D. D., Allen, C. D., Borrego, I., Dickman, L. T., Collins, A., Gaylord, M., McBranch, N., Pockman, W. T., Vilagrosa, A., Aukema, B., Goodsman, D., & Xu, C. (2019). Mechanisms of a coniferous woodland persistence under drought and heat. *Environmental Research Letters: ERL [Web Site]*, *14*(4), 045014.

McLauchlan, K. K., Higuera, P. E., Miesel, J., Rogers, B. M., Schweitzer, J., Shuman, J. K., Tepley, A. J., Varner, J. M., Veblen, T. T., Adalsteinsson, S. A., Balch, J. K., Baker, P., Batllori, E., Bigio, E., Brando, P., Cattau, M., Chipman, M. L., Coen, J., Crandall, R., … Watts, A. C. (2020). Fire as a fundamental ecological process: Research advances and frontiers. *The Journal of Ecology*, *108*(5), 2047–2069.

Miller, J. D., Knapp, E. E., Key, C. H., Skinner, C. N., Isbell, C. J., Creasy, R. M., & Sherlock, J. W. (2009). Calibration and validation of the relative differenced Normalized Burn Ratio (RdNBR) to three measures of fire severity in the Sierra Nevada and Klamath Mountains, California, USA. *Remote Sensing of Environment*, *113*(3), 645–656.

Miller, J. D., & Quayle, B. (2015). Calibration and Validation of Immediate Post-Fire Satellite-Derived Data to Three Severity Metrics. *Fire Ecology*, *11*(2), 12–30.

Miller, J. D., & Thode, A. E. (2007). Quantifying burn severity in a heterogeneous landscape with a relative version of the delta Normalized Burn Ratio (dNBR). *Remote Sensing of Environment*, *109*(1), 66–80.

Minnich, R. A. (2000). Californian mixed-conifer forests under unmanaged fire regimes in the Sierra San Pedro Mártir, Baja California, Mexico. *Journal of Biogeography*.

Minnich, R. A., Barbour, M. G., Burk, J. H., & Fernau, R. F. (1995). Sixty Years of Change in Californian Conifer Forests of the San Bernardino Mountains. *Conservation Biology: The Journal of the Society for Conservation Biology*, *9*(4), 902–914.

Nelson, M. F., Ciochina, M., & Bone, C. (2016). Assessing spatiotemporal relationships between wildfire and mountain pine beetle disturbances across multiple time lags. *Ecosphere* , *7*(10), e01482.

Norlen, C. A., & Goulden, M. L. (2023). Recent tree mortality dampens semi-arid forest die-off during subsequent drought. *AGU Advances*, *4*(3). https://doi.org/10.1029/2022av000810

Odum, E. P. (1969). The strategy of ecosystem development. *Science*, *164*(3877), 262–270.

Pan, Y., Birdsey, R. A., Fang, J., Houghton, R., Kauppi, P. E., Kurz, W. A., Phillips, O. L., Shvidenko, A., Lewis, S. L., Canadell, J. G., Ciais, P., Jackson, R. B., Pacala, S. W., McGuire, A. D., Piao, S., Rautiainen, A., Sitch, S., & Hayes, D. (2011). A large and persistent carbon sink in the world's forests. *Science*, *333*(6045), 988–993.

Paz-Kagan, T., Brodrick, P. G., Vaughn, N. R., Das, A. J., Stephenson, N. L., Nydick, K. R., & Asner, G. P. (2017). What mediates tree mortality during drought in the southern Sierra Nevada? *Ecological Applications: A Publication of the Ecological Society of America* , *27*(8), 2443–2457.

Rising, J., Tedesco, M., Piontek, F., & Stainforth, D. A. (2022). The missing risks of climate change. *Nature*, *610*(7933), 643–651.

Roche, J. W., Goulden, M. L., & Bales, R. C. (2018). Estimating evapotranspiration change due to forest treatment and fire at the basin scale in the Sierra Nevada, California. *Ecohydrology*, *11*(7), e1978.

Rodman, K. C., Veblen, T. T., Battaglia, M. A., Chambers, M. E., Fornwalt, P. J., Holden, Z. A., Kolb, T. E., Ouzts, J. R., & Rother, M. T. (2020). A changing climate is snuffing out post-fire recovery in montane forests. *Global Ecology and Biogeography: A Journal of Macroecology*, *29*(11), 2039–2051.

Roy, D. P., Kovalskyy, V., Zhang, H. K., Vermote, E. F., Yan, L., Kumar, S. S., & Egorov, A. (2016). Characterization of Landsat-7 to Landsat-8 reflective wavelength and normalized difference vegetation index continuity. *Remote Sensing of Environment*, *185*, 57–70.

Savage, M. (1994). Anthropogenic and natural disturbance and patterns of mortality in a mixed conifer forest in California. *Canadian Journal of Forest Research. Journal Canadien de La Recherche Forestiere*, *24*(6), 1149–1159.

Savage, M. (1997). The role of anthropogenic influences in a mixed-conifer forest mortality episode. *Journal of Vegetation Science: Official Organ of the International Association for Vegetation Science*, *8*(1), 95–104.

Seidl, R., Thom, D., Kautz, M., Martin-Benito, D., Peltoniemi, M., Vacchiano, G., Wild, J., Ascoli, D., Petr, M., Honkaniemi, J., Lexer, M. J., Trotsiuk, V., Mairota, P., Svoboda, M., Fabrika, M., Nagel, T. A., & Reyer, C. P. O. (2017). Forest disturbances under climate change. *Nature Climate Change*, *7*(6), 395–402.

Steel, Z. L., Jones, G. M., Collins, B. M., & Green, R. (2022). Mega-disturbances cause rapid decline of mature conifer forest habitat in California. *Ecological*. https://esajournals.onlinelibrary.wiley.com/doi/abs/10.1002/eap.2763

Stephens, S. L., Moghaddas, J. J., Edminster, C., Fiedler, C. E., Haase, S., Harrington, M., Keeley, J. E., Knapp, E. E., McIver, J. D., Metlen, K., Skinner, C. N., & Youngblood, A. (2009). Fire treatment effects on vegetation structure, fuels, and potential fire severity in western U.S. forests. *Ecological Applications: A Publication of the Ecological Society of America*, *19*(2), 305–320.

Stephens, S. L., Moghaddas, J. J., Hartsough, B. R., Moghaddas, E. E. Y., & Clinton, N. E. (2009). Fuel treatment effects on stand-level carbon pools, treatment-related emissions, and fire risk in a Sierra Nevada mixed-conifer forestPublication No. 143 of the National Fire and Fire Surrogate Project. *Canadian Journal of Forest Research. Journal Canadien de La Recherche Forestiere*, *39*(8), 1538–1547.

Tucker, C. J. (1979). Red and photographic infrared linear combinations for monitoring vegetation. *Remote Sensing of Environment*, *8*(2), 127–150.

Turco, M., Abatzoglou, J. T., Herrera, S., Zhuang, Y., Jerez, S., Lucas, D. D., AghaKouchak, A., & Cvijanovic, I. (2023). Anthropogenic climate change impacts exacerbate summer forest fires in California. *Proceedings of the National Academy of Sciences*, *120*(25), e2213815120.

van Mantgem, P. J., Stephenson, N. L., Knapp, E., Battles, J., & Keeley, J. E. (2011). Long-term effects of prescribed fire on mixed conifer forest structure in the Sierra Nevada, California. *Forest Ecology and Management*, *261*(6), 989–994.

Walker, R. F., Fecko, R. M., Frederick, W. B., Murphy, J. D., Johnson, D. W., & Miller, W. W. (2006). Thinning and Prescribed Fire Effects on Forest Floor Fuels in the East Side Sierra Nevada Pine Type. *Journal of Sustainable Forestry*, *23*(2), 99–115.

Wang, J. A., Randerson, J. T., Goulden, M. L., Knight, C. A., & Battles, J. J. (2022). Losses of tree cover in California driven by increasing fire disturbance and climate stress. *AGU Advances*, *3*(4). https://doi.org/10.1029/2021av000654

Williams, A. P., Abatzoglou, J. T., Gershunov, A., Guzman-Morales, J., Bishop, D. A., Balch, J. K., & Lettenmaier, D. P. (2019). Observed impacts of anthropogenic climate change on wildfire in California. *Earth's Future*, *7*(8), 892–910.

Wulder, M. A., Masek, J. G., Cohen, W. B., Loveland, T. R., & Woodcock, C. E. (2012). Opening the archive: How free data has enabled the science and monitoring promise of Landsat. *Remote Sensing of Environment*, *122*, 2–10.

Young, D. J. N., Estes, B. L., Gross, S., Wuenschel, A., Restaino, C., & Meyer, M. D. (2023). Effectiveness of forest density reduction treatments for increasing drought resistance of ponderosa pine growth. *Ecological Applications: A Publication of the Ecological Society of America*, *33*(4), e2854.

Young, D. J. N., Meyer, M., Estes, B., & Gross, S. (2020). Forest recovery following extreme drought in California, USA: natural patterns and effects of pre-drought management. *Ecological*. https://esajournals.onlinelibrary.wiley.com/doi/abs/10.1002/eap.2002

Young, D. J. N., Stevens, J. T., Earles, J. M., Moore, J., Ellis, A., Jirka, A. L., & Latimer, A. M. (2017). Long-term climate and competition explain forest mortality patterns under extreme drought. *Ecology Letters*, *20*(1), 78–86.

Zhu, Z., & Woodcock, C. E. (2012). Object-based cloud and cloud shadow detection in Landsat imagery. *Remote Sensing of Environment*, *118*, 83–94.

Zhu, Z., & Woodcock, C. E. (2014). Automated cloud, cloud shadow, and snow detection in multitemporal Landsat data: An algorithm designed specifically for monitoring land cover change. *Remote Sensing of Environment*, *152*, 217–234.

CHAPTER 3

Where are forests most vulnerable to drought?

Adapted from:

Norlen, C.A., Randerson, J.T., Bhoot, V.N., Goulden, M.L. Where are forests most vulnerable to drought? (in preparation).

3.1 Introduction

3.1.1 Global Implications of Forest Disturbance

Global forests face significant threats from climate change amplified natural disasters like droughts (Allen et al., 2015; Anderegg, Trugman, Badgley, Anderson, et al., 2020), but forest restoration and improved forest management are often viewed as potential natural climate solutions (Fargione et al., 2018; Griscom et al., 2017). Forests are rightly given high global importance for their global role in the carbon cycle (Pan et al., 2011) and high regional importance for ecosystem services such as climate control, water production, and reduced fire risk (Ninan & Inoue, 2013). Forest disturbances due to fire, climate stress, and insect infestation are typically expected to increase as climate change progresses (Anderegg et al., 2022). Research has uncovered many potential die-off risk factors and frameworks for understanding forest die-off (Allen et al., 2015; Breshears et al., 2005). The global importance of forests in our climate system and high potential of restoration and forest management to act as natural climate solutions make understanding longer term climate change impacts of critical importance to policy makers and land managers (Field et al., 2020).

3.1.2 Die-off Risk Framework

The impact of natural disasters like droughts on human communities or ecosystems depends on a combination of exposure and the vulnerability or resiliency of the impacted community or ecosystem (Kim & Marcouiller, 2015). In assessing drought risk in a human community, social vulnerability factors such as the number of older adults and young children, the number of people with disabilities, and the number of people without access to transportation are taken into consideration (Essen et al., 2023; Zarghami & Dumrak,

2021). In forests, there are a variety of proposed vulnerabilities or risk factors that make the impact of drought induced die-off more severe such as: water balance, drought exposure, forest leaf area, climate conditions, and bark beetle host characteristics (Table 1). In both forests and human communities, drought exposure is a necessary initiating factor for drought risk (Brodrick et al., 2019; Madakumbura et al., 2020; Young, Stevens, Earles, & Moore, 2017). The density of trees (basal area) has been proposed as an indicator of competition for resources and a predictor of die-off (Young, Stevens, Earles, & Moore, 2017). Tree height has been identified as a risk factor and predictor of die-off (Hemming-Schroeder et al., 2023; Stovall et al., 2019). Negative water balance during drought or water input that is less than water use can explain spatial patterns of forest die-off (Goulden & Bales, 2019). However, negative water balance alone is not enough to explain how repeated droughts impact forests (Norlen & Goulden, 2023). High forest leaf area called canopy overshoot area due to favorable growth conditions has also been proposed as a potential predictor of die-off (Jump et al., 2017). Forests loss has also been observed and predicted in locations that are near either their precipitation or temperature climate limits (Coffield et al., 2021; Hill et al., 2023). Tree characteristics that promote act by bark beetles and other forest pathogens are another key risk factor proposed risk factor (Fettig et al., 2019; Robbins et al., 2022). Each of these risk factors likely contributes to forest die-off, but many are related to each other and there is limited understanding of which risk factors are most important and how they interact with each other which limits understanding of which forests have the highest vulnerability to drought.

Table 3.1. Die-off risk factors (predictors) with mechanistic explanations

Die-off Risk Factor	Potential Predictors	Proposed Mechanism	Supporting Literature
Water Balance	Pr – ET (mm yr^{-1})	Locations with greater water use (ET) than water input (Pr) experience high levels of die-off	(Goulden & Bales, 2019; Madakumbura et al., 2020; Norlen & Goulden, 2023)
	ET Fraction (%)	Forests close to their climatic water limit are more vulnerable to die-off	(Madakumbura et al., 2020; Wang et al., 2022)
Forest Leaf Area	Pre-Drought ET (mm yr^{-1})	High water use due to canopy overshoot could increase vulnerability to drought	(Goulden & Bales, 2019; Jump et al., 2017; Madakumbura et al., 2020; Norlen et al., 2023)
	Pre-Drought Tree Cover (%)	Canopy overshoot during favorable conditions could increase vulnerability to drought	(Norlen et al., 2023; Wang et al., 2022)
Drought Exposure	Forty-Eight Month Standardized Precipitation Index (SPI48)	The four-year precipitation anomaly is a biologically relevant indicator of drought severity due to water availability	(Goulden & Bales, 2019; Madakumbura et al., 2020)
	Twelve Month Temperature Anomaly (Temp Anomaly)	High temperature anomalies combined with drought can amplify die-off	(Brodrick et al., 2019; Young, Stevens, Earles, Moore, et al., 2017)
Forest Structure and Density	Basal Area (m^2 ha^{-1})	Forest density can be an indicator of competition for resources and vulnerability to insects	(Young, Stevens, Earles, Moore, et al., 2017)
	Conifer Basal Area (m^2 ha^{-1})	Conifer trees die at higher rates due to drought induced die-off than other trees in semi-arid conifer forests	(Anderegg, Trugman, Badgley, Konings, et al., 2020; Goulden & Bales, 2019; Norlen & Goulden, 2023)
	Stand Height (m)	Tall trees are more vulnerable to forest die-off either due to increased hydraulic stress, species, or exposure to the atmosphere	(Hemming-Schroeder et al., 2023; Stovall et al., 2019)
Climate Conditions	Climate Precipitation (mm yr^{-1})	Trees that are near their climatic limit in water availability or temperature have had high observed mortality	(Coffield et al., 2021; Hill et al., 2023)
	Climate Temperature (C°)		
Bark Beetle Host Tree Characteristics	Tree species and size distribution	Pine trees, especially above a particular size threshold, tend to be bark beetle hosts and have high mortality	(Fettig et al., 2019; Robbins et al., 2022)

3.1.3 Die-off Mortality Observation

Many die-off risk factors have been proposed based on theory, but which of these is most important remains uncertain. This uncertainty is important because land managers do not have guidance on what practices could be beneficial for reducing forest drought vulnerability and promoting forest health. There has been a lot of great research describing how various combinations of risk factors can predict forest die-off (Brodrick & Asner, 2017; Goulden & Bales, 2019; Madakumbura et al., 2020; Young, Stevens, Earles, Moore, et al., 2017). There have also been efforts to detect early warning signs of tree mortality due to drought stress using satellite data that appear promising (Anderegg et al., 2019; Liu et al., 2019; Rogers et al., 2018). Ultimately, process-based models will likely provide the best predictions of drought impacts on forest density in the long term and at a larger spatial scale. There has been progress in developing these models and making them relevant to California (Robbins et al., 2022). However, process-based models do not currently address the need for fast and high-resolution measurements of forest health that can be implemented for land managers to strategically plan efforts to mitigate the impacts of climate change.

3.1.4 Research Approach

California provides a useful system to study forest die-off risk due to the large suite of geospatial and forest inventory data sets available, the presence of a diverse area of high-density forested ecosystems, and exposure to recent high-severity drought. Here we created a framework to diagnose patterns of die-off and used that framework to predict forest die-off risk using a statistical modeling approach. To build our statistical models we used the forest plot information available through the USFS FIA program, geospatial data

on forest die-off, and Landsat-derived data on water use and forest density. Through our analysis, we answered three research questions: 1.) What environmental variables are the most important predictors of historical patterns of forest drought vulnerability 2.) Which forests currently have the highest vulnerability to die-off? 3.) How has forest drought vulnerability changed?

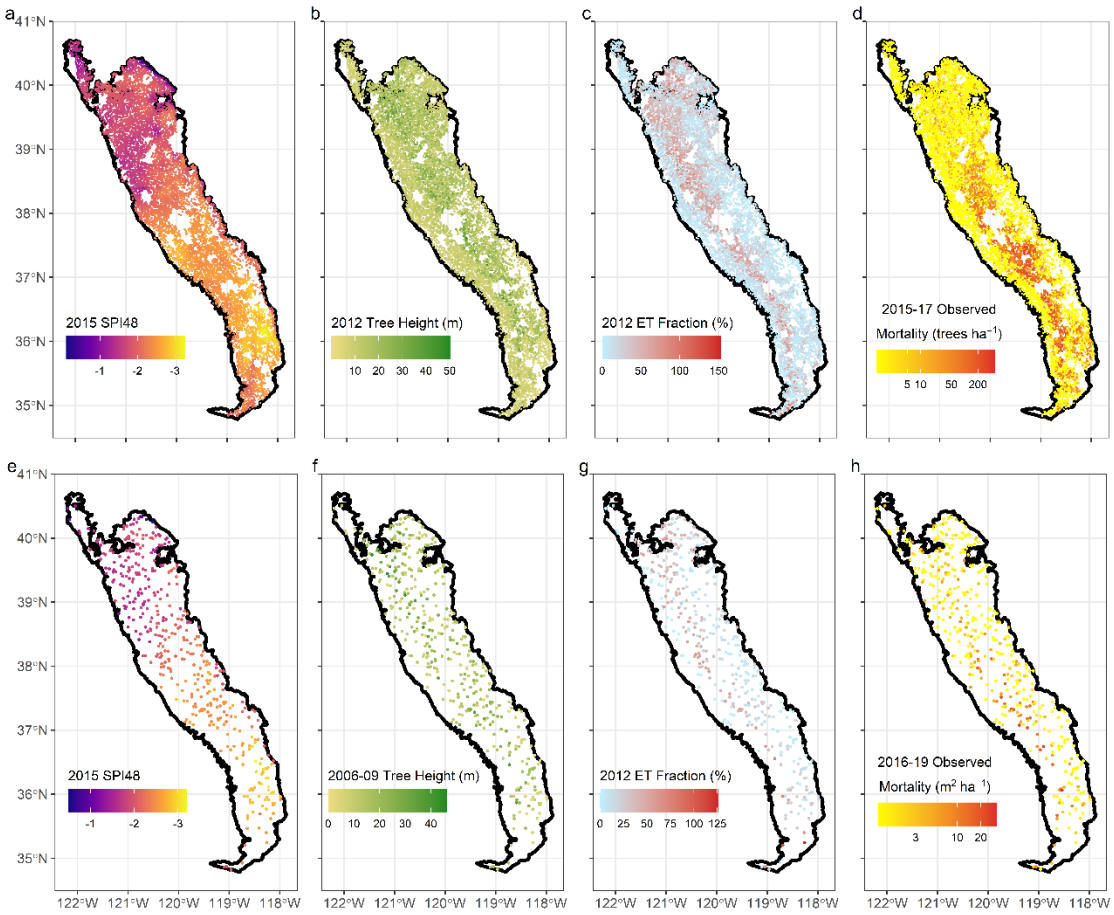

Figure 3.1. Spatial patterns of drought induced die-off intensity and risk factors for the Sierra Nevada and foothills for remote sensing and FIA data sets the Sierra Nevada and foothills. Panels a, b, c, and d show remote sensing data with N = 12,319 randomly selected pixels. Panel f shows FIA data with 4 = 409 plots from inventory years 2016-2019. Panels e and g show data from the nearest 4-km grid cell to the publicly available FIA plot locations. The panels show drought severity (a, e) according to the forty-eight-month standardized precipitation index (SPI48), pre-drought stand

tree height (b, f), and pre-drought corrected evapotranspiration (ET) fraction (c, g), and die-off intensity (d, h).

3.2 Methods

3.2.1 Experimental Design

Study Region

We focused on the Sierra Nevada and foothills region that experienced severe drought in 2012-2015 in its southern extent. This region covers a wide range of forest habitats in California and potential responses to severe drought and covers 6,967,752 hectares (Figure 3.1). We used FIA plots and a random sample 0.2% of 30-meter Landsat pixels in the Sierra Nevada and Sierra Nevada Foothill ecoregions as our study region (Figure 3.1). We excluded remote sensing grid cells with a record of harvest, wildfire, or prescribed fire from 2011-2019 from the remote sensing pixels. We excluded FIA plots with a history of wildfire from our samples. Our final analysis used 12,319 Landsat pixels and 409 FIA plots.

FIA Analysis

We selected FIA plots within the Sierra Nevada and Sierra Nevada foothills USFS Ecological Subsections (ECOSUBCD: M261Ea, M261Eb, M261Ec, M261Ed, M261Ef, M261Eg, M261Eh, M261Ej, M261Fa, M261Fb, M261Fc, M261Fd, and M261Fe) that were sampled during both the 2001-2009 inventory periods and 2011-2019 inventory periods. We included plots with a disturbance code relevant to drought-induced mortality (DSTRBCD1 = 0, 10, 11, 12, 54, 70) with a mortality year (MORTYR) of 2013-2019. We removed plots with a fire disturbance code (DSTRBCD1 = 30, 31, or 32).

Remote Sensing Analysis

We selected a 0.2% random sample of 30-meter Landsat pixels from within the Sierra Nevada and Sierra Nevada foothills ecoregions. We masked pixels that burned or had a record of management from 2011-2019 using wildfire and prescribed fire perimeters from the California Department of Forestry and Fire Protection (CALFIRE) and forest harvest and management perimeters from the United States Forest Service's (USFS) Forest Activity Tracking System (FACTS) and CALFIRE forest harvest and management perimeters (FACTS) from 2011-2019.

3.2.2 Data Processing

We modeled and predicted drought induced forest die-off using a combination of geospatial and forest inventory and analysis (FIA) datasets. For datasets available in the FIA database or that can be derived from it (basal area, conifer basal area, tree cover, and dominant stand height) we used Landsat data translated into the same units for the remote sensing analysis. For geospatial datasets not available in the FIA data (*SPI48*, *ET*, $Pr_{climate}$), we calculated 4-km grid cell versions of the 30-meter resolution data sets as the mean of all intersecting 30-meter pixels. Then we extracted the nearest 4-km grid cell for the "fuzzed" location of a FIA plot. The fuzzed locations of the FIA plots should be sufficient to find an appropriate 4-km value as fuzzing as reported fuzzing values are ± 0.8 to 1.6 km. The additional 20% plot swapping that the FIA program applies to the publicly available FIA data to protect private landowner information likely introduces extra noise into this data, which should be considered when interpreting our analysis. The relationships we report

with the FIA analysis would likely be stronger if we used the using 30-meter Landsat data and the absolute FIA plot locations.

USFS Aerial Detection Surveys (ADS) Mortality

We used the USFS ADS data set as a measure of drought induced forest die-off. The major advantage of the ADS data set is that human observers screen for the likely cause of mortality and actively avoid measuring live tree removal due to fires or harvest. It is important to note that ADS data set has limited accuracy and has experienced a series of protocol changes over time (Hicke et al., 2020; Johnson & Ross, 2008). However, despite their higher accuracy in tracking changes in tree cover the lack of accurate drought induced die-off attribution in available remote sensing data sets is an even greater problem for predicting die-off (Koltunov et al., 2020; Slaton et al., 2021). We used rasterized ADS data sets from 1978 – 2022 at 30-meter resolution using the TPA_MORT field of ADS. We used only disturbance polygons with the "Mortality" disturbance class. We also rasterized the flown area polygons and assigned a tree mortality column (TPA_MORT) with a value of 0 trees ha^{-1}. We used the sum of three years of ADS data to calculate the mortality for each drought event. We used the sum of ADS 2015-2017 to track mortality for the 2012-2015 drought (SPI48 2015). We retrieved ADS data from https://www.fs.usda.gov/detail/r5/forest-grasslandhealth/?cid=fsbdev3_046696.

FIA Mortality

We used the basal area of dead trees to calculate mortality in the FIA data (Bechtold & Patterson, 2005; Burrill et al., 2018; Smith, 2002). We filtered the FIA mortality data to include only mortality that was labeled with mortality years (MORTYR) of 2013-2019 and

for inventory years (INVYR) 2016-2019. We used FIA plot data to measure mortality in units of basal area (m^2 ha^{-1}).

Forest Structure and Density (LEMMA-GNN)

We used basal area (m^2 ha^{-1}), conifer basal area (m^2 ha^{-1}), and dominant stand height (m) from LEMMA-GNN as predictors of die-off (Ohmann & Gregory, 2002; Ohmann et al., 2014). We used the conifer basal area divided by live basal area to calculate conifer fraction. We used the mean of 2010, 2011, and 2012 basal area (m^2 ha^{-1}), conifer basal area (m^2 ha^{-1}), and stand height (m) as pre-drought predictors for die-off induced by the 2012-2015 drought. We used the 2017 versions of the same data sets as predictors for current (2019) levels of die-off likelihood and magnitude because they are the most recent data layers available. We retrieved LEMMA-GNN data from: https://lemmadownload.forestry.oregonstate.edu/index.

Tree Cover (Remote Sensing)

We used the Landsat base tree cover data set to track pre-drought forest density and changes in forest density. This data set was created by training Landsat data with vegetation data from the Bureau of Land Management rangeland surveys (Allred et al., 2021; Jones et al., 2018). We retrieved the data with Google Earth Engine (Gorelick et al., 2017) as an Image Collection at 'projects/rap-data-365417/assets/vegetation-cover-v3'. The data can also be data set can also be retrieved as GeoTiffs from http://rangeland.ntsg.umt.edu/data/rap/rap-vegetation-cover/.

Tree Cover (FVS and FIA)

We used the Forest Vegetation Simulator (FVS) model to calculate tree cover for each FIA plot in our sample (Crookston & Dixon, 2005). The FVS model uses live trees to calculate tree cover. To avoid using tree cover reduced by die-off to predict die-off we used the tree cover values from the 2001-2009 inventory plots. We used tree cover calculated from the 2011-2019 inventory plots to calculate post-drought levels of die-off likelihood and magnitude.

Fire Perimeters (FRAP)

We used fire perimeters from CALFIRE to identify where and when wildfires and prescribed fires occurred in our study region. We rasterized the fire perimeter to 30-meter resolution using GEE. We calculate the most recent year of fire occurrence from 2011-2019 using the rasterized layers for each year. We used the locations identified with fire occurrence to exclude these pixels from our analysis to avoid confusion between drought induced die-off and fires. We retrieved the fire perimeters from https://frap.fire.ca.gov/media/ly2jyr4j/fire21_2.zip

Forest Management Perimeters (FACTS and CAL FIRE)

We used combined perimeters of forest management and harvest projects from CALFIRE and USFS to identify where harvest and forest management occurred in our study region (Knight et al., 2022). We rasterized the fire perimeters to 30-meter resolution using GEE. We calculated the most recent year of management from 2011-2018 using the rasterized layers for each year. We excluded the pixels where management occurred to avoid confusion between drought induced die-off and forest management.

Standardized Precipitation Index over 48-months (SPI48)

We used 4-km SPI48 as a measure of the four-year precipitation anomaly (Abatzoglou et al., 2017), which is an important indicator of drought stress for forests (Goulden & Bales, 2019; Madakumbura et al., 2020). We used the 4-km version of this dataset for our FIA analysis and for the remote sensing analysis, we converted this data set to 30-m resolution using bilinear interpolation. We used September SPI48 for 2015 to represent the precipitation anomaly for the 2012-2015 drought water years. We retrieved this data set from https://wrcc.dri.edu/wwdt/archive.php.

Temperature Anomaly over 12-months ($Temp_{anom}$)

We used 4-km $Temp_{anom}$ as a measure of the 12-month temperature anomaly (Abatzoglou et al., 2017), which has been highlighted as potential risk factor for die-off (Brodrick et al., 2019; Young, Stevens, Earles, Moore, et al., 2017). We used the 4-km version of this dataset for our FIA analysis and for the remote sensing analysis, we converted this data set to 30-m resolution using bilinear interpolation. We used September SPI48 for 2015 to represent the temperature anomaly for the 2015 water year. We retrieved this data set from https://wrcc.dri.edu/wwdt/archive.php.

Evapotranspiration ($ET_{Pre\text{-}Drought}$)

We used annual evapotranspiration data created by combining flux tower data and Monthly NDVI, which is described in detail in the following manuscripts (Goulden et al., 2012; Goulden & Bales, 2019; Norlen & Goulden, 2023; Norlen et al., 2023). For our FIA analysis we calculated the mean ET in each 4-km grid cell, while in the remote sensing analysis we used the 30-meter Landsat scale data set. We calculate Pre-Drought ET as the

mean of 2010, 2011, and 2012 ET for the 2012-2015 drought and the mean of 2017, 2018, and 2019 ET for current conditions.

Climatological Mean Precipitation ($Pr_{climate}$)Temperature ($Temp_{climate}$)

We used 4-km climate (1981-2010) precipitation ($Pr_{climate}$) and temperature ($Temp_{climate}$) from the PRISM data set (Daly et al., 2008). We calculated $Pr_{climate}$ as the sum of the twelve climate precipitation months. We calculated $Temp_{climate}$ as the mean of the twelve climate maximum temperature months. For our FIA analysis we used the 4-km resolution data. For our remote sensing analysis, we converted the 4-km dataset to 30-m resolution using bilinear interpolation. We retrieved the PRISM data set from https://developers.google.com/earth-engine/datasets/catalog/OREGONSTATE_PRISM_Norm91m.

ET Fraction

We calculated how close forest stands were to their climate water limit by dividing $Pr_{climate}$ by $ET_{Pre\text{-}Drought}$. We used 4-km data for the FIA analysis and 30-meter data for the remote sensing data set.

$$(Eq.1) ET\ Fraction = \frac{ET_{Pre-Drought}}{Pr_{climate}} * 100$$

Correct ET Fraction

We calculated a tree cover corrected version of the *ET Fraction* to account for the tree cover in each grid cell. For the remote sensing data, we multiplied the 30-meter ET fraction by the fraction pre-drought tree cover. For the FIA analysis we used tree cover

derived from the FIA data using FVS, while for the remote sensing analysis we used 30-meter tree cover data derived from Landsat data.

$$(Eq. 2)\ Corrected\ ET_{Fraction} = ET_{Fraction} * \frac{Tree\ Cover}{100}$$

Water Balance (Pr – ET)

We calculated Pre-Drought Climate Water Balance as an alternative method to calculate how close forest stand were to their climate limit. We calculated pre-drought water balance as $Pr - ET$ (see Eq. 3). We used 4-km data for the FIA analysis and 30-meter data for the remote sensing analysis.

$$(Eq. 3)\ Pr - ET = Pr_{climate} - ET_{Pre-Drought}$$

3.2.3 Modeling and Statistical Analysis

Comparison of Predictors

To determine which variables to include in our models we calculated the correlations between potential die-off predictors and die-off magnitude. We also calculated the correlation between die-off predictors and each other to select predictor variables that were relatively independent from each other. We calculated correlations using the *cor* function from the *stats* package in R (R Core Team, 2020).

Model Training

Modeling forest die-off is difficult for a variety of reasons, including the high frequency of die-off absence or zero inflation in observations of die-off (Trugman et al., 2021; Young, Stevens, Earles, & Moore, 2017). To address the zero inflation problem we

used a two-step or hurdle model approach where we first modeled the presence or absence of mortality, and then in locations where mortality was present, we modeled the magnitude of mortality (Young, Stevens, Earles, Moore, et al., 2017). The first step of the model is a logistic regression model created with the *glm* function from the stats package in R with the binomial family and a logit link (R Core Team, 2020). The second part of the model is a multiple linear regression model created with the *lm* function from the stats package in R (R Core Team, 2020).

We trained both the remote sensing and FIA models using 60% of the data with the remaining 40% held out for testing. We used the *tidymodels* set of packages to create the training and testing datasets and train the models (Max Kuhn & Silge, 2022). For both the logistic regression model we also stratified the selection of testing and training data by the presence of die-off above background levels. We defined die-off above background using the definition used by the USFS ADS program or as > 2.5 trees ha^{-1} (> 1 tree $acre^{-1}$). For both the logistic regression and multiple linear regression models we used the following predictors pre-drought stand height (m), ET Fraction (%), forty-eight-month standardized precipitation index (SPI48), the interaction between stand height and SPI48 (Stand Height x SPI48), and the interaction between ET Fraction and SPI48 (ET Fraction x SPI48).

Model Testing

We assessed the overall performance of our models as well as the relative importance of the predictors in each model. We calculated the root mean square error (RMSE) and coefficient of determination (R^2) to assess the linear regression models. We calculated the *accuracy* and for R^2 to assess the logistic regression models. We tested the

models using 40% of the data held out for testing held out data and compared the predictions to observed values of die-off magnitude and occurrence. To calculate *RMSE*, R^2, and *accuracy* we used the *rmse*, *rsq_trad*, and *accuracy* functions from the *yardstick* package (M. Kuhn et al., 2021). We calculated the importance of each predictor variable for the logistic regression and linear regression models using *vip* function from the *vip* package in R (Greenwell et al., 2020).

Predicting Die-off Risk & Change

We used SPI48 set to -2.5 and forest conditions in 2012 and 2019 to predict die-off likelihood and die-off magnitude as well as change in die-off likelihood, Δ Die-off (%), and change in die-off magnitude, Δ Die-off (trees ha^{-1}). We replaced the observed SPI48 with a value of -2.5 to consider the risk of severe drought. To calculate 2012 die-off likelihood and die-off magnitude, we used 2012 Stand Height and Corrected ET Fraction along with fixed SPI48 (Figure C.6). To calculate 2019 die-off likelihood, we used 2017 *Stand Height* and 2019 *Corrected ET Fraction* (Figure C.6, Figure C.7). We calculated Δ *Die-off* (%) and Δ *Die-off* (trees ha^{-1}) as the 2019 predicted value minus the 2012 predicted value (Figure C.8). We also calculated changes in *Stand Height*, *Corrected ET Fraction*, *Tree Cover*, and *ET* using this same approach (Figure C.9).

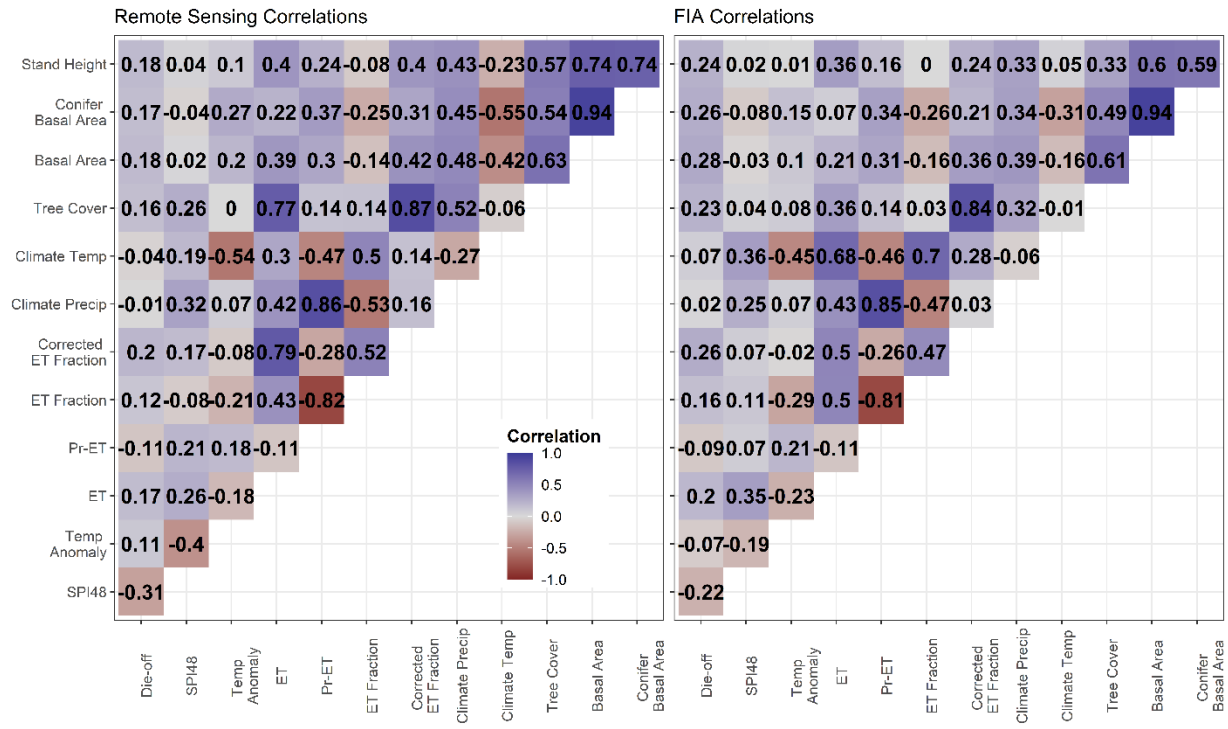

Figure 3.2. Comparison of correlations between die-off magnitude and predictors of die-off magnitude. The left-hand panel (a) shows the correlations for remote sensing data sets. The right-hand panel (b) shows the correlations for the FIA data sets.

3.3 Results

3.3.1 Relationships Between Potential Model Predictors

The relationships between each predictor with die-off magnitude were similar for the remote sensing and FIA analyses, with some variations in the relative strength of the correlations. For the remote sensing analysis, the strongest correlations with die-off magnitude were SPI48 (r = -0.31), corrected ET Fraction (r = 0.2), stand height (r = 0.18), basal area (r = 0.18), conifer basal area (r = 0.17), and ET (r = 0.17; Figure 2a). For the FIA analysis, the strongest correlations with die-off magnitude were basal area (r = 0.28), conifer basal area (r = 0.26), corrected ET fraction (r = 0.26), stand height (r = 0.24), and SPI48 (r = -0.22; Figure 3.2b).

All the predictors were correlated with at least one other predictor in both the remote sensing and FIA data sets (Figure 3.2). The forest structure density data sets (basal area, conifer basal, and stand height) were highly correlated with each other in both the remote sensing and FIA analyses. Tree cover was strongly associated with ET and corrected ET Fraction in the remote sensing analysis and moderately correlated with ET and corrected ET in the FIA analysis. *Pr-ET* was highly correlated with *ET Fraction* and $Pr_{climate}$ and moderately correlated with $Temp_{climate}$. $Temp_{climate}$ was also moderately correlated with *ET Fraction*, *ET*, and *Corrected ET Fraction*. Tree cover was moderately correlated with all three forest density metrics in both analyses. *ET* was moderately correlated with *ET Fraction* and $Pr_{climate}$ in both analyses. $Temp_{anom}$ was moderately correlated with *SPI48*.

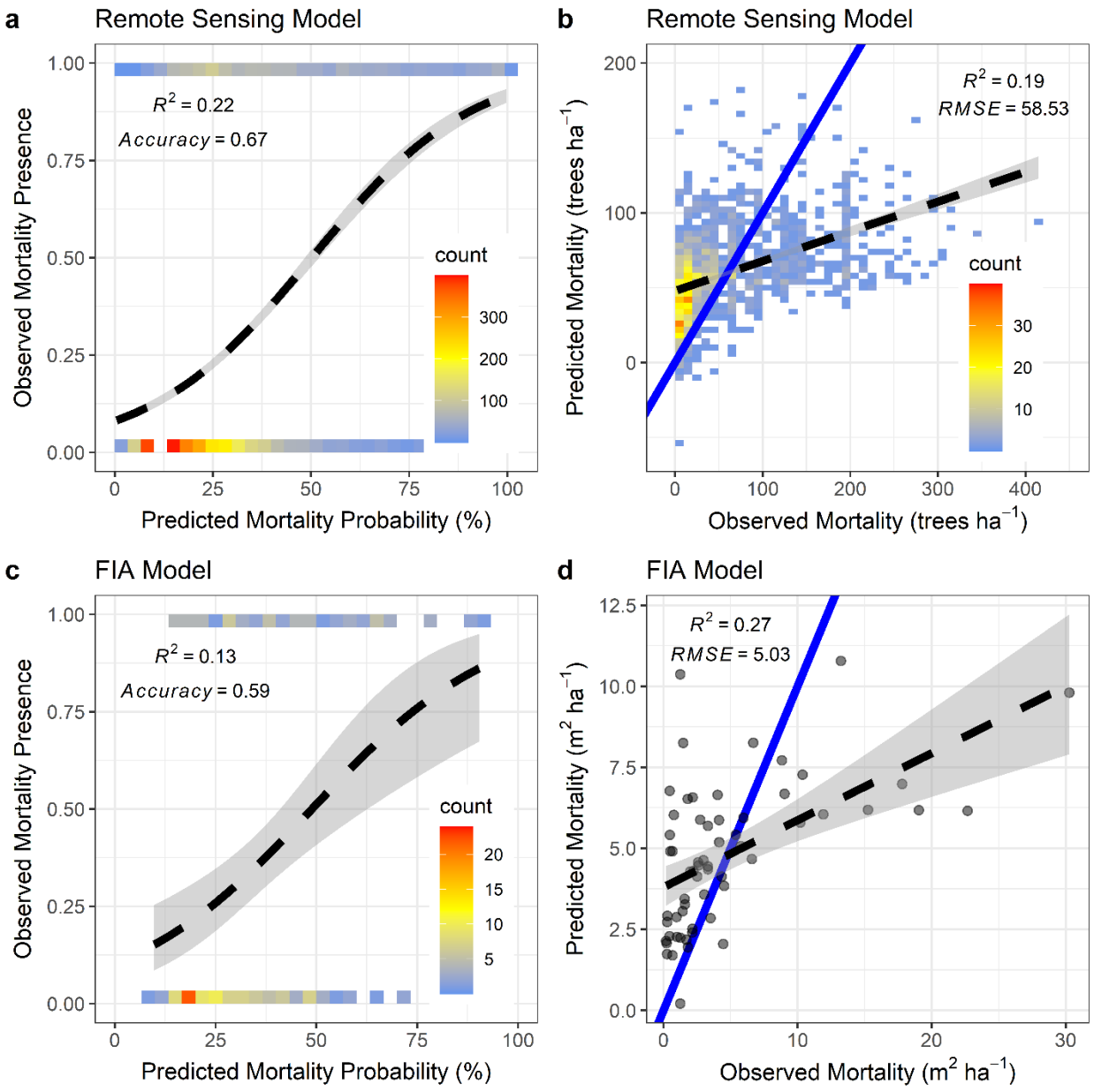

Figure 3.3. Predictions of die-off probability and magnitude based on logistic and linear regression models trained with remote sensing and FIA data. Each panel displays 40% of the original sample held out for model testing. The shading represents 95% confidence intervals. The first panel (a) shows the fit of a logistic model to predict the probability of die-off occurrence with a sample size of N = 4,822. The second panel (b) shows the fit of a linear regression model to predict the magnitude of die-off trained with locations with mortality present with a sample size of N = 1,498. The third panel (c) shows the fit of a logistic model to predict the probability of die-off occurrence with a sample size of N = 164. The fourth panel (d) shows the fit of a linear regression model to predict the magnitude of die-off from locations where die-off occurred with a sample size of N = 61. The blue line in the second and fourth panels (b, d) represents the one-to-one line.

3.3.2 Model Performance and Testing

The two analyses produced similar models of die-off likelihood and die-off magnitude. The remote sensing model of die-off likelihood performed better (R^2 = 0.23, *accuracy* = 0.67; Figure 3.3a) than the FIA model of die-off likelihood (R^2 = 0.13, *accuracy* = 0.59; Figure 3.3c). According to R^2, the FIA model of die-off magnitude (R^2 = 0.27; Figure 3.3d) performed better than the remote sensing model (R^2 = 0.19; Figure 3.3b), while according to *RMSE* the remote sensing model (*RMSE* = 58.53; Figure 3.3a) performed better than the FIA model (*RMSE* = 5.03; Figure 3.3d). The die-off magnitude values from the remote sensing and FIA analyses have different units, so they should be compared to the overall range of values in the observed data set before comparing them to each other. The models of die-off likelihood and magnitude created with the two analyses are similar. The models of die-off magnitude both tend to underpredict high levels of observed mortality and overpredict mortality that is close to zero. The models for magnitude of mortality also generally agree with each other, with the remote sensing model producing slightly stronger correlations.

After comparing the relationship between the predictors and die-off magnitude as well as with each other we selected relatively independent from each other and represented important potential risk factors for die-off (Table 3.1). We selected predictors for our final model that were correlated with die-off magnitude in both the remote sensing and FIA data sets, were relatively independent from each other, and that measured three of the important potential predictors of die-off documented in the literature: forest structure (*Stand Height*), water balance (*Corrected ET Fraction*), and drought exposure (*SPI48*). We did not include a term for forest leaf area or water use because those predictors were

highly correlated with either *Stand Height* or *Corrected ET Fraction*. We did not include a term to measure potential for bark beetle infestation because there were no appropriate metrics available at the forest stand level. It is possible that forest density metrics such as *Stand Height* provide some information about potential bark beetle hosts, but critical information about species and stand structure is missing. We also included the interactions of drought exposure with water balance and forest density in the final models (*SPI48* x *Corrected ET Fraction*, *SPI48* x *Stand Height*).

SPI48 x *Corrected ET Fraction* was the most important predictor in all the models with the other predictors ranked in the same order in both the remote sensing and FIA analyses (Figure C.3). The other predictors in the logistic regression models were ranked in importance with *SPI48* x *Stand Height* second most important followed by *Corrected ET Fraction*, *SPI48*, and *Stand Height* (Figure C.3a, c). The other predictors in the multiple linear regression models were ranked in importance with *Corrected ET Fraction* second most important followed by *SPI48* x *Stand Height*, *Stand Height*, and *SPI48* (Figure C.3b, d).

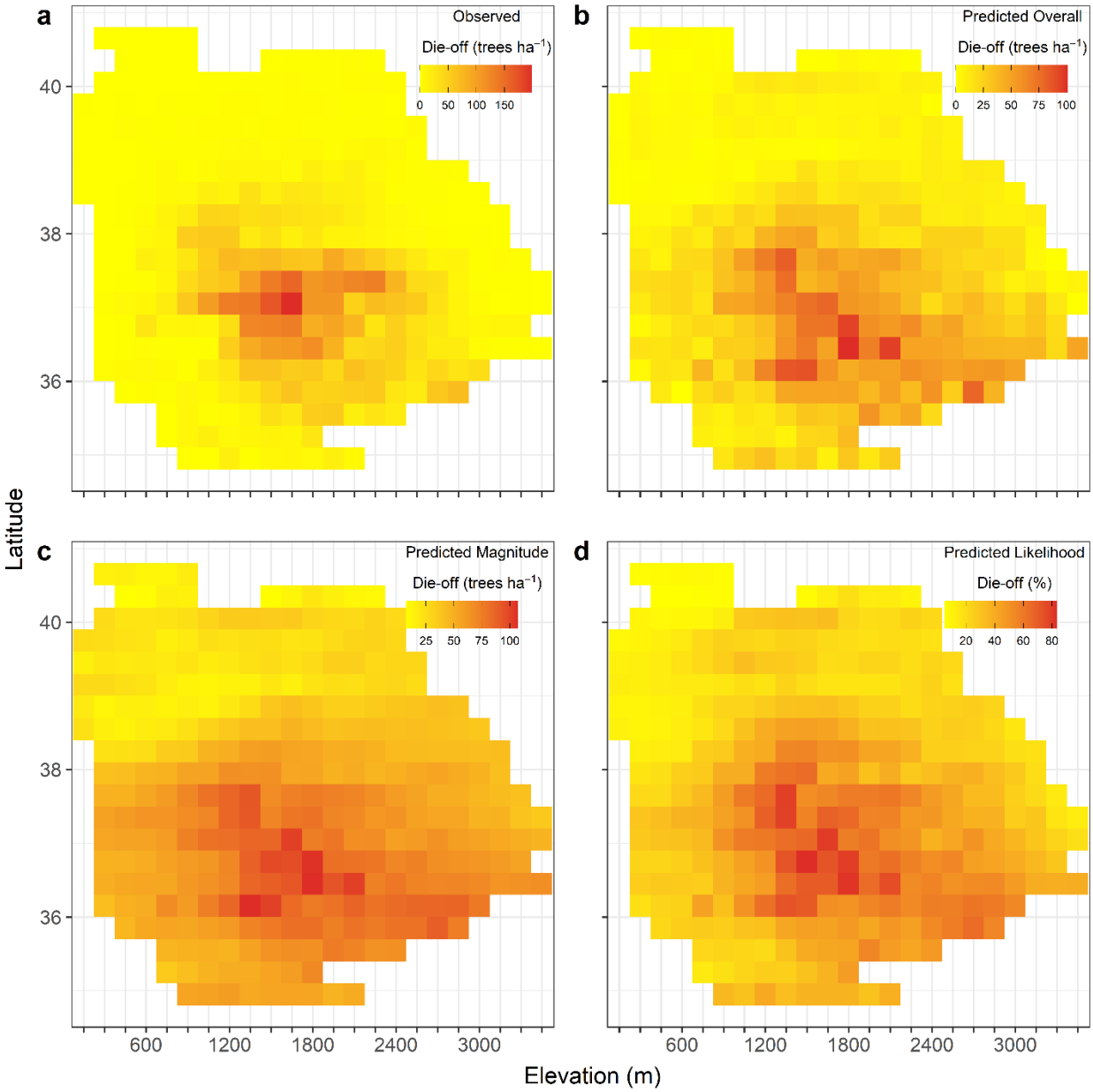

Figure 3.4. Observed and predicted patterns of drought induced die-off overall, probability and magnitude for remote sensing and FIA data sets the Sierra Nevada and foothills. The panels show observed drought induced die-off (a), predicted overall die-off (b), predicted mortality magnitude (c), and predicted mortality probability (d). Each cell represents the mean of pixels in one 0.3° latitude and 150-m elevation bin. We excluded bins with less than 5 pixels. All panels have N = 12,319.

3.3 Spatial Patterns of Predicted Die-off

When using the inputs for the 2012-2015 drought conditions the models predict die-off in the South Sierra (Figure 3.4). The predictions of overall die-off and die-off likelihood have the most spatial agreement with die-off observations for both analyses and highest levels of die-off magnitude or die-off likelihood generally occur where *Corrected ET Fraction* nears the level of climate precipitation (100%) and SPI48 was most negative in the lower elevations of the south Sierra Nevada. The predictions of die-off magnitude are generally higher in the South Sierra Nevada where the 2012-2015 drought exposure was most extended, but do not show as much variation due to the other predictors.

Large areas of the Sierra Nevada continued to have high predicted die-off magnitudes and die-off probabilities when we predicted die-off risk with an SPI48 of -2.5 and other (Figure C.5, Figure C.6). Die-off magnitude was relatively constant across the Sierra Nevada with somewhat higher values in the north Sierra in the 2019 predictions. Die-off likelihood was greatest in locations with high *Corrected ET Fraction* and in the North Sierra in the 2019 predictions.

Corrected ET Fraction decreased in locations where die-off was present, while there was little change in stand height across the Sierra Nevada (Figure 3.5, Figure C.7). In locations where die-off was present, *Corrected ET Fraction* decreased by 6.5 ± 0.1 %, while in places where die-off was absent *Corrected ET Fraction* decreased by 1.1 ± 0.1 % (Figure 3.5a, Figure C.7a). In locations where die-off was present, *Stand Height* decreased by 0.2 ± 0.06 m, while in locations where die-off was absent there was no observed change in *Stand Height* 0.0 ± 0.4 (Figure 3.5b, Figure C.7b).

Both die-off likelihood and die-off magnitude decreased in locations where die-off was present when we held SPI48 constant at -2.5 and updated the other predictors to 2019 values (Figure 3.5, Figure C.7, Figure C.10). In locations where die-off was present Δ Die-off Likelihood decreased by 5.3 ± 0.1 %, while in locations where die-off was absent Δ Die-off Likelihood decreased by 0.9 ± 0.06 % (Figure 3.5c, Figure C.7c). In locations where die-off was present Δ Die-off Magnitude decreased by 5.5 ± 0.1 trees ha^{-1}, while in locations where die-off was absent Δ Die-off Magnitude decreased by 0.9 ± 0.05 trees ha^{-1} (Figure 3.5d, Figure C.7d).

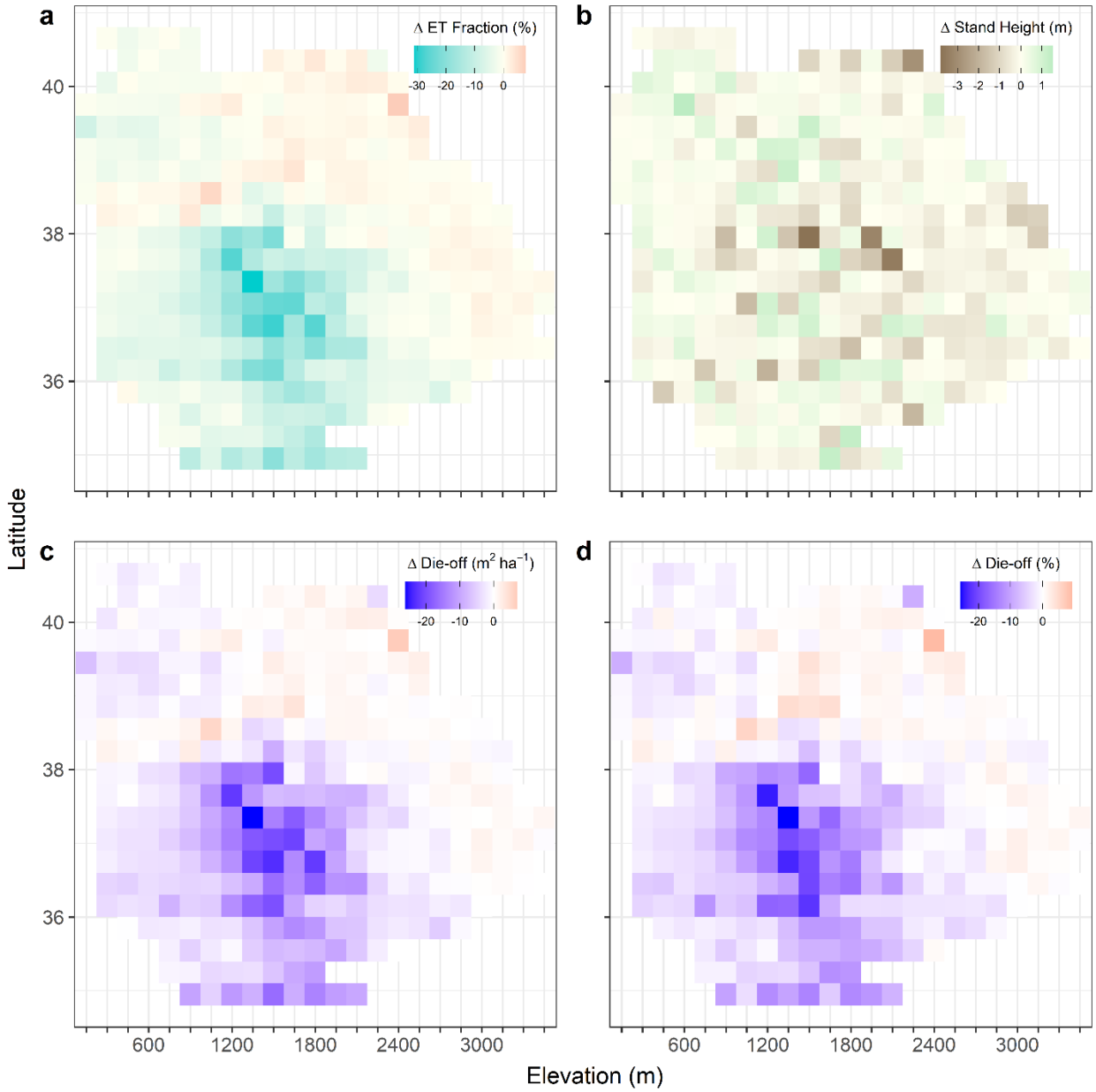

Figure 3.5. Observed changes (Δ) in Corrected ET Fraction, Stand Height, predicted die-off likelihood (%) and predicted die-off magnitude for the remote sensing analysis. The panels show Δ ET Fraction (a), Δ Stand Height (b), Δ Die-off Likelihood (c), and Δ Die-off Magnitude (d). Each cell represents the mean of pixels in one 0.3° latitude and 150-m elevation bin. We excluded bins with less than 5 pixels. All panels have N = 12,319.

3.4 Discussion

3.4.1 Die-off Model Performance and Predictions

All the potential predictors of die-off were correlated at least one other predictor. For our models we selected metrics of water balance (*Corrected ET Fraction*), forest density (*Stand Height*) and drought exposure (*SPI48*) that were relatively independent from each other and correlated with die-off magnitude. The models of die-off likelihood and magnitude we trained with *Corrected ET Fraction*, *Stand Height*, and *SPI48* performed similarly when trained with either remote sensing or FIA data. The remote sensing model of die-off likelihood performed better (R^2 = 0.23, *accuracy* = 0.67; Figure 3.3a) than the FIA model of die-off likelihood than the FIA model (R^2 = 0.13, *accuracy* = 0.59; Figure 3.3c), while the FIA model of die-off magnitude (R^2 = 0.27; Figure 3.3d) performed better than the remote sensing model (R^2 = 0.19; Figure 3.3b). For the models of die-off likelihood *SPI48* x *Corrected ET Fraction* followed by *SPI48* x *Stand Height* were the most important predictors. For the models of die-off magnitude *SPI48* x *Corrected ET Fraction* followed by *Corrected ET Fraction* were the most important predictors. Predicted die-off likelihood and magnitude using an SPI48 set at -2.5 and other predictors updated to 2019 values remained high across the Sierra Nevada. Predicted die-off likelihoods were greatest in locations with *Corrected ET Fraction* near 100% and high values of *Stand Height* which occur at moderate elevations in the south Sierra Nevada and more broadly across the north Sierra Nevada. Predicted die-off magnitudes were relatively high across the Sierra Nevada, with somewhat higher values in the north Sierra Nevada and at moderate elevations in the south Sierra Nevada. In locations where recent die-off occurred, there was a decrease in

Corrected ET Fraction of about 5% which led to predicted decreases of die-off likelihood by about 5% and die-off magnitude by about 5 trees ha^{-1} (Figure 3.5).

3.4.2 Links to Mechanistic Explanations for Die-off

The importance of drought exposure, forest structure and water balance to predicting die-off risk align with theoretical frameworks for forest drought vulnerability. One key predictor is the level of drought exposure according to *SPI48* which appears to an initiating factor required for drought induced die-off to occur but is not sufficient to explain die-off on its own (Goulden & Bales, 2019; Young, Stevens, Earles, Moore, et al., 2017). Another important factor is the *Corrected ET Fraction*, which accounts for the level of pre-drought water use (*ET*) and general water availability ($Pr_{climate}$). It corrects for the overall abundance of trees (*Tree Cover*) in the forest stand. Locations with $ET_{pre\text{-}drought}$ close to $Pr_{climate}$ are more susceptible to die-off, while locations with low *ET* or high *ET* and higher $Pr_{climate}$ are less vulnerable (Goulden & Bales, 2019). Forest stand must also have trees present in order to produce die-off so correcting the ET Fraction for tree cover eliminates sites with ET close to $Pr_{climate}$, but without sufficient trees present to produce die-off (Norlen & Goulden, 2023). Forest structure in general and *Stand Height* specifically have been repeatedly observed as predictors of drought induced die-off. Forest density metrics likely contribute to die-off prediction by ensuring that trees are present to kill, but also that the types of trees present are susceptible by being tall and therefore more exposed to hydraulic or atmospheric stress or densely packed and more susceptible to competition (Breshears et al., 2013; Hemming-Schroeder et al., 2023; Stovall et al., 2019; Young, Stevens, Earles, & Moore, 2017). Other factors that we were not able to capture in our model due to a lack of ecosystem level metrics in the remote sensing record related to

properties important for bark beetle host selection such as the species and size distribution of trees are almost certainly also important (Fettig et al., 2019; Robbins et al., 2022). Continuing climate change impacts provide the opportunity to leverage advances in remote sensing and modeling to better understand the influence of species and size distribution in landscape scale analyses of forest drought vulnerability.

3.4.3 Implications for Research and Modeling

The continuing impact of climate change provides the opportunity to leverage advances in remote sensing and modeling to better understand the influence of species and size distribution in landscape scale analyses of forest drought vulnerability. Advances in predicting the risk of die-off are limited by the relatively low quality of die-off observation and complexity of ecology and physiology underlying the phenomenon (Slaton et al., 2021; Trugman et al., 2021). Part of this problem is due to the relatively heterogeneous and rare nature of forest die-off compared to other forest disturbances such as fires, land use change, and harvest. Current observations of die-off occurrence and magnitude and predictors of die-off allow for dynamic predictions but are not able to capture factors such as the species composition and size structure of forests which are known to be important factors in predicting die-off. Most current research on forest die-off either focuses on a broad landscape level or on granular plot-based analysis of individual trees. Future research using a combination of process-based models, field data sets, and next generation remote sensing that consider the both the characteristics of mortality at the individual tree level and that span across the landscape could allow for improved understanding die-off risk.

3.4.4 Current and Future Die-off Vulnerability

Forest without recent disturbance, especially those at moderate elevations with relatively high tree cover and where water use and annual precipitation are similar in magnitude (*Corrected ET Fraction* near 100%) are currently have the highest probability of die-off. These vulnerability levels are dynamic and vary with changes to forest structure and density. In the future as temperatures continue to increase and precipitation regimes change forests that are not currently vulnerable to die-off will likely become vulnerable (Coffield et al., 2021; Hill et al., 2023). Increases in temperature and therefore ET are essentially inevitable over the next several decades. However, the precipitation regime is much more uncertain (Coffield et al., 2021). Whether California and other regions see increases, decreases, or essentially equivalent precipitation will determine a large portion of the level of die-off in the future. A key next step is a time evolving predictive model that estimates die-off risk at the end of the wet season for the upcoming dry season. This would allow managers to identify forests with die-off risk and prioritize land management actions to reduce risk.

3.4.5 Implications for Ecosystem Services

Forests provide well-known ecosystem service benefits on a global scale through carbon sequestration (Pan et al., 2011) and on a local scale through controls on wildfire risk, habitat, recreation, and production of fresh water (Ninan & Inoue, 2013; Thom & Seidl, 2016). Forest die-off reduces tree cover, leads to lower forest carbon uptake (Swann et al., 2018), and increases in the dead pool of sequestered carbon which will gradually be released into the atmosphere (Walden et al., 2019). Forest die-off also decreases water use which can either increase runoff and water yield (Zimmermann et al., 2000) or decrease

water yield in temperature and snow limited ecosystems (Biederman et al., 2015). An increases in water quantity will likely be linked to decreased water quality (Mikkelson et al., 2012).

3.4.6 Implications for Land Management and Policy

Predicted decreases in die-off likelihood and magnitude in areas that experienced die-off suggest that land management strategies may be able to increase forest resistance to drought. Reducing tree density can be beneficial for decreasing die-off risk as well as fire risk but should be weighed against the cost of reduced carbon sequestration. The ambitious million-acre annual fuel treatment strategy in California in addition to reducing fire risk may produce additional co-benefits of decrease the likelihood and magnitude of predicted die-off (Crowfoot et al., 2021; Norlen et al., 2023). This also means that efforts to increase forest density as a climate mitigation strategy can be counterproductive if the location of those efforts are not carefully considered considering potential threats from increased drought stress and disturbance under climate change. Natural climate solutions focused on improved forest management that reduces tree cover or forest density could decrease the risk of forest die-off, while forest management and restoration that increases forest density or tree cover could increase risk of drought induced die-off. Implementation of natural climate solutions in forests that considers climate change amplified risks from forest die-off as well as self-limiting feedbacks, will improve the likelihood that proposed forest climate mitigation projects provide long-term carbon sequestration benefits despite increased climate stress.

3.5 Acknowledgements.

This research was funded by the Ridge to Reef Graduate Training Program funded in part by the National Science Foundation Research Traineeship award DGE-1735040 and Strategic Growth Council grant number CCR20021 to The Center for Ecosystem Climate Solutions (CECS). CECS is supported by the California Strategic Growth Council's Climate Change Research Program with funds from California Climate Investments, a statewide initiative that puts billions of Cap-and-Trade dollars to work reducing greenhouse gas emissions, strengthening the economy, and improving public health and the environment – particularly in disadvantaged communities. This manuscript was greatly improved by comments from VN Boot. We also acknowledge the indigenous peoples and land of California. UC Irvine, where most of this research took place, is located on the ancestral territories of the Acjachemen and Tongva peoples, many of whom maintain active physical, spiritual, and cultural ties to the region.

3.6 References

Abatzoglou, J. T., McEvoy, D. J., & Redmond, K. T. (2017). The West Wide Drought Tracker: Drought Monitoring at Fine Spatial Scales. *Bulletin of the American Meteorological Society*, *98*(9), 1815–1820.

Allen, C. D., Breshears, D. D., & McDowell, N. G. (2015). On underestimation of global vulnerability to tree mortality and forest die-off from hotter drought in the Anthropocene. *Ecosphere* . https://esajournals.onlinelibrary.wiley.com/doi/abs/10.1890/ES15-00203.1

Allred, B. W., Bestelmeyer, B. T., Boyd, C. S., Brown, C., Davies, K. W., Duniway, M. C., Ellsworth, L. M., Erickson, T. A., Fuhlendorf, S. D., Griffiths, T. V., Jansen, V., Jones, M. O., Karl, J., Knight, A., Maestas, J. D., Maynard, J. J., McCord, S. E., Naugle, D. E., Starns, H. D., … Uden, D. R. (2021). Improving Landsat predictions of rangeland fractional cover with multitask learning and uncertainty. *Methods in Ecology and Evolution / British Ecological Society*, *2041-210X.13564*. https://doi.org/10.1111/2041-210x.13564

Anderegg, W. R. L., Anderegg, L. D. L., & Huang, C.-Y. (2019). Testing early warning metrics for drought-induced tree physiological stress and mortality. *Global Change Biology*, *25*(7), 2459–2469.

Anderegg, W. R. L., Chegwidden, O. S., Badgley, G., Trugman, A. T., Cullenward, D., Abatzoglou, J. T., Hicke, J. A., Freeman, J., & Hamman, J. J. (2022). Future climate risks from stress, insects and fire across US forests. *Ecology Letters*, *25*(6), 1510–1520.

Anderegg, W. R. L., Trugman, A. T., Badgley, G., Anderson, C. M., Bartuska, A., Ciais, P., Cullenward, D., Field, C. B., Freeman, J., Goetz, S. J., Hicke, J. A., Huntzinger, D., Jackson, R. B., Nickerson, J., Pacala, S., & Randerson, J. T. (2020). Climate-driven risks to the climate mitigation potential of forests. *Science*, *368*(6497). https://doi.org/10.1126/science.aaz7005

Anderegg, W. R. L., Trugman, A. T., Badgley, G., Konings, A. G., & Shaw, J. (2020). Divergent forest sensitivity to repeated extreme droughts. *Nature Climate Change*. https://doi.org/10.1038/s41558-020-00919-1

Bechtold, W. A., & Patterson, P. L. (2005). *The Enhanced Forest Inventory and Analysis Program--national Sampling Design and Estimation Procedures*. USDA Forest Service, Southern Research Station.

Biederman, J. A., Somor, A. J., Harpold, A. A., Gutmann, E. D., Breshears, D. D., Troch, P. A., Gochis, D. J., Scott, R. L., Meddens, A. J. H., & Brooks, P. D. (2015). Recent tree die-off has little effect on streamflow in contrast to expected increases from historical studies. *Water Resources Research*, *51*(12), 9775–9789.

Breshears, D. D., Adams, H. D., Eamus, D., McDowell, N. G., Law, D. J., Will, R. E., Williams, A. P., & Zou, C. B. (2013). The critical amplifying role of increasing atmospheric moisture demand on tree mortality and associated regional die-off. *Frontiers in Plant Science*, *4*, 266.

Breshears, D. D., Cobb, N. S., Rich, P. M., Price, K. P., Allen, C. D., Balice, R. G., Romme, W. H., Kastens, J. H., Floyd, M. L., Belnap, J., Anderson, J. J., Myers, O. B., & Meyer, C. W. (2005). Regional vegetation die-off in response to global-change-type drought. *Proceedings of the National Academy of Sciences of the United States of America*, *102*(42), 15144–15148.

Brodrick, P. G., Anderegg, L. D. L., & Asner, G. P. (2019). Forest Drought Resistance at Large Geographic Scales. *Geophysical Research Letters*, *46*(5), 2752–2760.

Brodrick, P. G., & Asner, G. P. (2017). Remotely sensed predictors of conifer tree mortality during severe drought. *Environmental Research Letters: ERL [Web Site]*, *12*(11), 115013.

Burrill, E. A., Wilson, A. M., Turner, J. A., Pugh, S. A., Menlove, J., Christiansen, G., Conkling, B. L., & David, W. (2018). The Forest Inventory and Analysis Database: database description and user guide version 8.0 for Phase 2. *US Department of Agriculture, Forest Service*.

Coffield, S. R., Hemes, K. S., Koven, C. D., Goulden, M. L., & Randerson, J. T. (2021). Climate-Driven Limits to Future Carbon Storage in California's Wildland Ecosystems. *AGU Advances*, *2*(3), e2021AV000384.

Crookston, N. L., & Dixon, G. E. (2005). The forest vegetation simulator: A review of its structure, content, and applications. *Computers and Electronics in Agriculture*, *49*(1), 60–80.

Crowfoot, W., Blumenfeld, J., & Porter, T. (Eds.). (2021). *California's Wildfire and Forest Resilience Action Plan*. California Department of Water Resources.

Daly, C., Halbleib, M., Smith, J. I., Gibson, W. P., Doggett, M. K., Taylor, G. H., Curtis, J., & Pasteris, P. P. (2008). Physiographically sensitive mapping of climatological temperature and precipitation across the conterminous United States. *International Journal of Climatology*, *28*(15), 2031–2064.

Essen, M., McCaffrey, S., Abrams, J., & Paveglio, T. (2023). Improving wildfire management outcomes: shifting the paradigm of wildfire from simple to complex risk. *Journal of Environmental Planning and Management*, *66*(5), 909–927.

Fargione, J. E., Bassett, S., Boucher, T., Bridgham, S. D., Conant, R. T., Cook-Patton, S. C., Ellis, P. W., Falcucci, A., Fourqurean, J. W., Gopalakrishna, T., Gu, H., Henderson, B., Hurteau, M. D., Kroeger, K. D., Kroeger, T., Lark, T. J., Leavitt, S. M., Lomax, G., McDonald, R. I., … Griscom, B. W. (2018). Natural climate solutions for the United States. *Science Advances*, *4*(11), eaat1869.

Fettig, C. J., Mortenson, L. A., Bulaon, B. M., & Foulk, P. B. (2019). Tree mortality following drought in the central and southern Sierra Nevada, California, U.S. *Forest Ecology and Management*, *432*, 164–178.

Field, J. P., Breshears, D. D., Bradford, J. B., Law, D. J., Feng, X., & Allen, C. D. (2020). Forest Management Under Megadrought: Urgent Needs at Finer Scale and Higher Intensity. *Frontiers in Forests and Global Change*, *3*. https://doi.org/10.3389/ffgc.2020.502669

Gorelick, N., Hancher, M., Dixon, M., Ilyushchenko, S., Thau, D., & Moore, R. (2017). Google Earth Engine: Planetary-scale geospatial analysis for everyone. *Remote Sensing of Environment*, *202*, 18–27.

Goulden, M. L., Anderson, R. G., Bales, R. C., Kelly, A. E., Meadows, M., & Winston, G. C. (2012). Evapotranspiration along an elevation gradient in California's Sierra Nevada. *Journal of Geophysical Research: Biogeosciences*, *117*(G3). https://doi.org/10.1029/2012JG002027

Goulden, M. L., & Bales, R. C. (2019). California forest die-off linked to multi-year deep soil drying in 2012–2015 drought. *Nature Geoscience*, *12*(8), 632–637.

Greenwell, B., Boehmke, B., & Gray, B. (2020). Package 'vip.' *Variable Importance Plots*, *12*(1), 343–366.

Griscom, B. W., Adams, J., Ellis, P. W., Houghton, R. A., Lomax, G., Miteva, D. A., Schlesinger, W. H., Shoch, D., Siikamäki, J. V., Smith, P., Woodbury, P., Zganjar, C., Blackman, A., Campari, J., Conant, R. T., Delgado, C., Elias, P., Gopalakrishna, T., Hamsik, M. R., … Fargione, J. (2017). Natural climate solutions. *Proceedings of the National Academy of Sciences of the United States of America*, *114*(44), 11645–11650.

Hemming-Schroeder, N. M., Gutierrez, A. A., Allison, S. D., & Randerson, J. T. (2023). Estimating Individual Tree Mortality in the Sierra Nevada Using Lidar and Multispectral Reflectance Data. *Journal Of*. https://agupubs.onlinelibrary.wiley.com/doi/abs/10.1029/2022JG007234?casa_token=s6NrDvrCRVkAAAAA:dLgm5GNFKGLLp4P4V-YJxQLG9W8VJn4D5xWyLwbaJbmaZye5_SiXQAAHDfjDdw5NXEWd7hsT_RFvdkm5

Hicke, J. A., Xu, B., Meddens, A. J. H., & Egan, J. M. (2020). Characterizing recent bark beetle-caused tree mortality in the western United States from aerial surveys. *Forest Ecology and Management*. https://www.sciencedirect.com/science/article/pii/S0378112720311713

Hill, A. P., Nolan, C. J., Hemes, K. S., Cambron, T. W., & Field, C. B. (2023). Low-elevation conifers in California's Sierra Nevada are out of equilibrium with climate. *PNAS Nexus*, *2*(2), gad004.

Johnson, E. W., & Ross, J. (2008). Quantifying error in aerial survey data. *Australian Forestry*, *71*(3), 216–222.

Jones, M. O., Allred, B. W., Naugle, D. E., Maestas, J. D., Donnelly, P., Metz, L. J., Karl, J., Smith, R., Bestelmeyer, B., Boyd, C., Kerby, J. D., & McIver, J. D. (2018). Innovation in rangeland monitoring: annual, 30 m, plant functional type percent cover maps for U.S. rangelands, 1984–2017. *Ecosphere* , *9*(9), e02430.

Jump, A. S., Ruiz-Benito, P., Greenwood, S., Allen, C. D., Kitzberger, T., Fensham, R., Martínez-Vilalta, J., & Lloret, F. (2017). Structural overshoot of tree growth with climate variability and the global spectrum of drought-induced forest dieback. *Global Change Biology*, *23*(9), 3742–3757.

Kim, H., & Marcouiller, D. W. (2015). Considering disaster vulnerability and resiliency: the case of hurricane effects on tourism-based economies. *The Annals of Regional Science*, *54*(3), 945–971.

Knight, C. A., Tompkins, R. E., Wang, J. A., York, R., Goulden, M. L., & Battles, J. J. (2022). Accurate tracking of forest activity key to multi-jurisdictional management goals: A case study in California. *Journal of Environmental Management*, *302*(Pt B), 114083.

Koltunov, A., Ramirez, C. M., Ustin, S. L., Slaton, M., & Haunreiter, E. (2020). eDaRT: The Ecosystem Disturbance and Recovery Tracker system for monitoring landscape disturbances and their cumulative effects. *Remote Sensing of Environment*, *238*, 111482.

Kuhn, M., Vaughan, D., & Hvitfeldt, E. (2021). yardstick: Tidy characterizations of model performance. *R Package Version 0.0*.

Kuhn, Max, & Silge, J. (2022). *Tidy Modeling with R*. "O'Reilly Media, Inc."

Liu, Y., Kumar, M., Katul, G. G., & Porporato, A. (2019). Reduced resilience as an early warning signal of forest mortality. *Nature Climate Change*, *9*(11), 880–885.

Madakumbura, G. D., Goulden, M. L., Hall, A., Fu, R., Moritz, M. A., Koven, C. D., Kueppers, L. M., Norlen, C. A., & Randerson, J. T. (2020). Recent California tree mortality portends future

increase in drought-driven forest die-off. *Environmental Research Letters: ERL [Web Site]*. http://iopscience.iop.org/article/10.1088/1748-9326/abc719

Mikkelson, K. M., Dickenson, E. R. V., Maxwell, R. M., McCray, J. E., & Sharp, J. O. (2012). Water-quality impacts from climate-induced forest die-off. *Nature Climate Change*, *3*(3), 218–222.

Ninan, K. N., & Inoue, M. (2013). Valuing forest ecosystem services: What we know and what we don't. *Ecological Economics: The Journal of the International Society for Ecological Economics*, *93*, 137–149.

Norlen, C. A., & Goulden, M. L. (2023). Recent tree mortality dampens semi-arid forest die-off during subsequent drought. *AGU Advances*. https://doi.org/10.1029/2022AV000810

Norlen, C. A., Hemes, K. S., Wang, J., Randerson, J. T., & Goulden, M. (2023). *History of fire enhances the drought resilience of semi-arid conifer forests*. *2023*, B064-0001.

Ohmann, J. L., & Gregory, M. J. (2002). Predictive mapping of forest composition and structure with direct gradient analysis and nearest- neighbor imputation in coastal Oregon, U.S.A. *Canadian Journal of Forest Research. Journal Canadien de La Recherche Forestiere*, *32*(4), 725–741.

Ohmann, J. L., Gregory, M. J., & Roberts, H. M. (2014). Scale considerations for integrating forest inventory plot data and satellite image data for regional forest mapping. *Remote Sensing of Environment*, *151*, 3–15.

Pan, Y., Birdsey, R. A., Fang, J., Houghton, R., Kauppi, P. E., Kurz, W. A., Phillips, O. L., Shvidenko, A., Lewis, S. L., Canadell, J. G., Ciais, P., Jackson, R. B., Pacala, S. W., McGuire, A. D., Piao, S., Rautiainen, A., Sitch, S., & Hayes, D. (2011). A large and persistent carbon sink in the world's forests. *Science*, *333*(6045), 988–993.

R Core Team. (2020). *R: A language and environment for statistical computing*. R Foundation for Statistical Computing. https://www.R-project.org/

Robbins, Z. J., Xu, C., Aukema, B. H., Buotte, P. C., Chitra-Tarak, R., Fettig, C. J., Goulden, M. L., Goodsman, D. W., Hall, A. D., Koven, C. D., Kueppers, L. M., Madakumbura, G. D., Mortenson, L. A., Powell, J. A., & Scheller, R. M. (2022). Warming increased bark beetle-induced tree mortality by 30% during an extreme drought in California. *Global Change Biology*, *28*(2), 509–523.

Rogers, B. M., Solvik, K., Hogg, E. H., Ju, J., Masek, J. G., Michaelian, M., Berner, L. T., & Goetz, S. J. (2018). Detecting early warning signals of tree mortality in boreal North America using multiscale satellite data. *Global Change Biology*, *24*(6), 2284–2304.

Slaton, M. R., Warren, K., Koltunov, A., & Smith, S. (2021). Chapter 12 - Accuracy assessment of Insect and Disease Survey and eDaRT for monitoring forest health. *Gen. Tech. Rep. SRS-261*, *261*, 187–195.

Smith, W. B. (2002). Forest inventory and analysis: a national inventory and monitoring program. *Environmental Pollution* , *116 Suppl 1*, S233-42.

Stovall, A. E. L., Shugart, H., & Yang, X. (2019). Tree height explains mortality risk during an intense drought. *Nature Communications*, *10*(1), 1–6.

Swann, A. L. S., Laguë, M. M., Garcia, E. S., Field, J. P., Breshears, D. D., Moore, D. J. P., Saleska, S. R., Stark, S. C., Villegas, J. C., Law, D. J., & Minor, D. M. (2018). Continental-scale consequences of

tree die-offs in North America: identifying where forest loss matters most. *Environmental Research Letters: ERL [Web Site]*, *13*(5), 055014.

Thom, D., & Seidl, R. (2016). Natural disturbance impacts on ecosystem services and biodiversity in temperate and boreal forests. *Biological Reviews of the Cambridge Philosophical Society*, *91*(3), 760–781.

Trugman, A. T., Anderegg, L. D. L., Anderegg, W. R. L., Das, A. J., & Stephenson, N. L. (2021). Why is Tree Drought Mortality so Hard to Predict? *Trends in Ecology & Evolution*. https://doi.org/10.1016/j.tree.2021.02.001

Walden, L. L., Fontaine, J. B., Ruthrof, K. X., Matusick, G., Harper, R. J., & Hardy, G. E. S. J. (2019). Carbon consequences of drought differ in forests that resprout. *Global Change Biology*, *25*(5), 1653–1664.

Wang, J. A., Randerson, J. T., Goulden, M. L., Knight, C. A., & Battles, J. J. (2022). Losses of tree cover in California driven by increasing fire disturbance and climate stress. *AGU Advances*, *3*(4). https://doi.org/10.1029/2021av000654

Young, D. J. N., Stevens, J. T., Earles, J. M., & Moore, J. (2017). Long-term climate and competition explain forest mortality patterns under extreme drought. *Ecology*. https://onlinelibrary.wiley.com/doi/abs/10.1111/ele.12711

Young, D. J. N., Stevens, J. T., Earles, J. M., Moore, J., Ellis, A., Jirka, A. L., & Latimer, A. M. (2017). Long-term climate and competition explain forest mortality patterns under extreme drought. *Ecology Letters*, *20*(1), 78–86.

Zarghami, S. A., & Dumrak, J. (2021). A system dynamics model for social vulnerability to natural disasters: Disaster risk assessment of an Australian city. *International Journal of Disaster Risk Reduction*, *60*, 102258.

Zimmermann, L., Moritz, K., Kennel, M., & Bittersohl, J. (2000). Influence of bark beetle infestation on water quantity and quality in the Grosse Ohe catchment(Bavarian Forest National Park). *Silva Gabreta*, *4*(5), 1–62.

CONCLUSION

Summary of Results

Past disturbance whether they are due to drought (Chapter 1) or wildfire (Chapter 2) can produce feedbacks that dampen or reduce the severity of drought induced forest die-off. Despite limitations on high-quality data to observe tree mortality, empirical modeling of forest drought vulnerability (Chapter 3) can provide guidance to land managers and policy makers on risks to current forests and proposed forest-based climate solutions.

Future Research Directions

Physical risk factors to ecosystems due to water availability and climate stress are important, but without consideration of ecological feedbacks and other biological processes, a large portion of the ability of the biosphere to sequester carbon is missed. Because these processes can be complicated to predict and often occur at relatively fine spatial scales, they are understandably often left out of large scale climate models. Higher quality data sets for tracking tree mortality either based on LiDAR, aerial photos, multispectral remote sensing, or a combination of all of these will be of high value to better evaluating forest drought vulnerability (Hemming-Schroeder, N. M., Gutierrez, A. A., Allison, S. D., & Randerson, J. T., 2023). Process based modeling can likely provide insights for some forest properties that may not be observable from space such as changes to vulnerability at the individual tree level due to changes in species composition, size distribution, or both (Robbins et al., 2022). Forest disturbance phenomena occur over long-time scales which are challenging for quantitative methods dominant in western science. Paleoclimatology

methods based on tree rings, burn scars, etc. (Knight et al., 2022) have been able to recreate some of the past of fire history and tree growth. Methods based on traditional knowledge and oral history may be better able to capture the full scope of these effects.

The Risks and Benefits of Forests for Climate Change Mitigation

The apparent ability of forests to quickly readjust to increased climate stress is both a blessing and a curse for human survival under climate change. Hopefully, forests will continue to provide important ecosystem service and store carbon (Ninan & Inoue, 2013). Fortunately, the ability of ecosystems like forests to readjust to increased stress may provide additional time for humans to mitigate climate change by eliminating reliance on fossil fuels and removing greenhouse gases from the atmosphere. Improved understanding of these forest vulnerability to drought will ideally lead to improved opportunities for forest management and restoration which would contribute to solving climate change through climate mitigation and adaptation (Fargione et al., 2018; Field et al., 2020). Increasing carbon storage in semi-arid forest locations like California may be a risky strategy as the risk of forest losses increases with warming and with increased likelihood of droughts. Land management that strategically links management actions that leverage forests vulnerabilities will provide a higher likelihood of successfully contributing one aspect of efforts to mitigate climate change.

References

Fargione, J. E., Bassett, S., Boucher, T., Bridgham, S. D., Conant, R. T., Cook-Patton, S. C., Ellis, P. W., Falcucci, A., Fourqurean, J. W., Gopalakrishna, T., Gu, H., Henderson, B., Hurteau, M. D., Kroeger, K. D., Kroeger, T., Lark, T. J., Leavitt, S. M., Lomax, G., McDonald, R. I., … Griscom, B. W. (2018). Natural climate solutions for the United States. *Science Advances*, *4*(11), eaat1869.

Field, J. P., Breshears, D. D., Bradford, J. B., Law, D. J., Feng, X., & Allen, C. D. (2020). Forest Management Under Megadrought: Urgent Needs at Finer Scale and Higher Intensity. *Frontiers in Forests and Global Change*, *3*. https://doi.org/10.3389/ffgc.2020.502669

Hemming-Schroeder, N. M., Gutierrez, A. A., Allison, S. D., & Randerson, J. T. (2023). Estimating Individual Tree Mortality in the Sierra Nevada Using Lidar and Multispectral Reflectance Data. *Journal of Geophysical Research: Biogeosciences*, *128*(5). https://agupubs.onlinelibrary.wiley.com/doi/abs/10.1029/2022JG007234?casa_token=s6NrDvrCRVkAAAAA:dLgm5GNFKGLLp4P4V-YJxQLG9W8VJn4D5xWyLwbaJbmaZye5_SiXQAAHDfjDdw5NXEWd7hsT_RFvdkm5

Knight, C. A., Anderson, L., Bunting, M. J., Champagne, M., Clayburn, R. M., Crawford, J. N., Klimaszewski-Patterson, A., Knapp, E. E., Lake, F. K., Mensing, S. A., Wahl, D., Wanket, J., Watts-Tobin, A., Potts, M. D., & Battles, J. J. (2022). Land management explains major trends in forest structure and composition over the last millennium in California's Klamath Mountains. *Proceedings of the National Academy of Sciences of the United States of America*, *119*(12), e2116264119.

Ninan, K. N., & Inoue, M. (2013). Valuing forest ecosystem services: What we know and what we don't. *Ecological Economics: The Journal of the International Society for Ecological Economics*, *93*, 137–149.

Robbins, Z. J., Xu, C., Aukema, B. H., & Buotte, P. C. (2022). Warming increased bark beetle-induced tree mortality by 30% during an extreme drought in California. *Global Change Biology*. https://onlinelibrary.wiley.com/doi/abs/10.1111/gcb.15927

APPENDIX A

Supporting Information for Chapter 1

Recent tree mortality dampens semi-arid forest die-off during subsequent drought

Methods for Supplementary Figures

We calculated hillshade from a Digital Elevation Model (DEM) using Earth Engine to create an elevation map base for supplementary Figures S1, S6, S7, S9, S11, and S13. We retrieved the 2012 version of the 1/3 arc second United States Geological Survey (USGS) DEM from https://developers.google.com/earth-engine/datasets/catalog/USGS_NED.

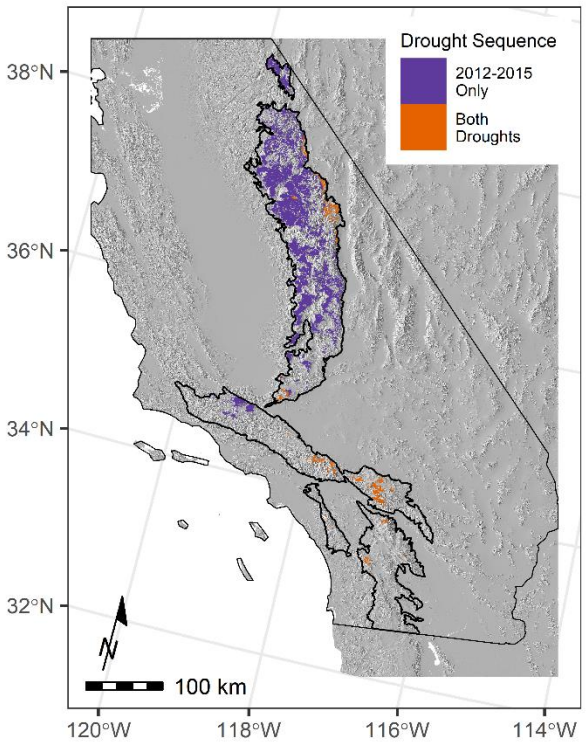

Figure A.1. Masks for sequential drought exposure across California. Purple represents Drought exposure to SPI48 ≤ -1.5 in 2012-2015 only. Orange represents exposure to SPI48 ≤ -1.5 in both 1999-2002 and 2012-2015. Both panels are masked to include only grid cells that are conifer dominated forests and that have no recorded fires since 1980. The sample size is N = 62,887.

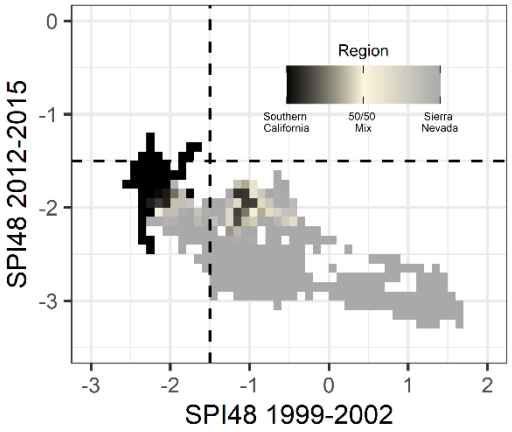

Figure A.2. The distribution of SPI48 in 1999-2002 and 2012-2015 within the Sierra Nevada and Southern California Mountains. The color bar from black to gray represents the proportion of grid cells in the Southern California Mountains versus Sierra Nevada for a particular sequence of SPI48 exposure. The sample size for panel (b) is N = 62,887.

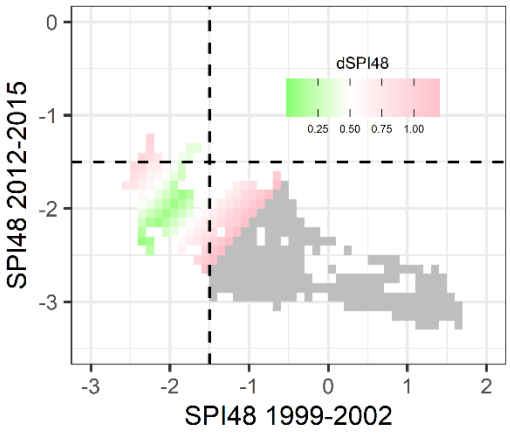

Figure A.3. The distribution of SPI48 in 1999-2002 and 2012-2015 within the Sierra Nevada and Southern California Mountains. The color bar from pink to green represents the difference between 1999-2002 and 2012-2015 drought exposure in units of SPI48 (dSPI48). The gray values represent dSPI48 > 1.2. The sample size for panel (b) is N = 62,887.

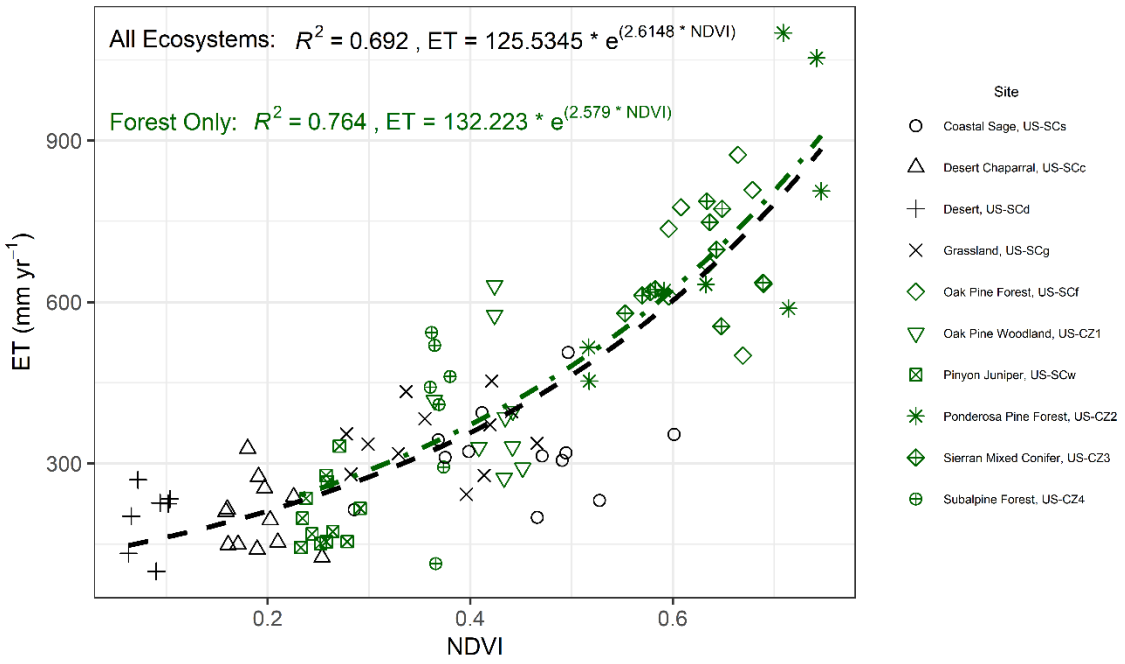

Figure A.4. The empirical relationship between annual mean NDVI from Landsat and total annual ET (mm yr^{-1}) from ten California flux towers. The annual sum of ET and mean NDVI are calculated for each water year (October 1 – September 30). The sample size is N = 97 for All Ecosystems and N = 54 for Forest Only.

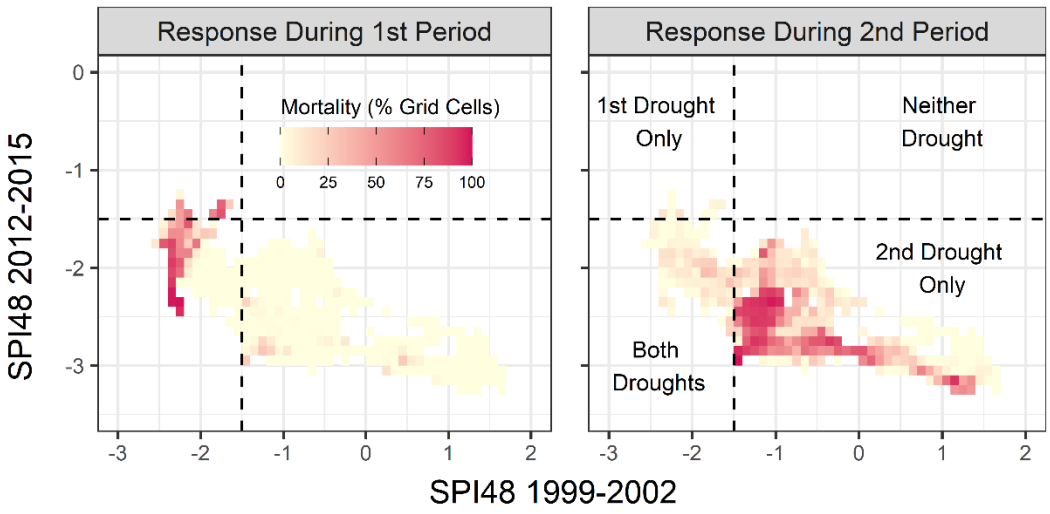

Figure A.5. The proportion of grid cells with forest die-off, observed with aerial detection surveys (ADS), arranged by SPI48 exposure in 1999-2002 and 2012-2015. In the color bar, cream represents 0 % of grid cells with die-off (ADS) and red represents 100 % of grid cells with die-off (ADS). The sample size for both panels is N = 62,887.

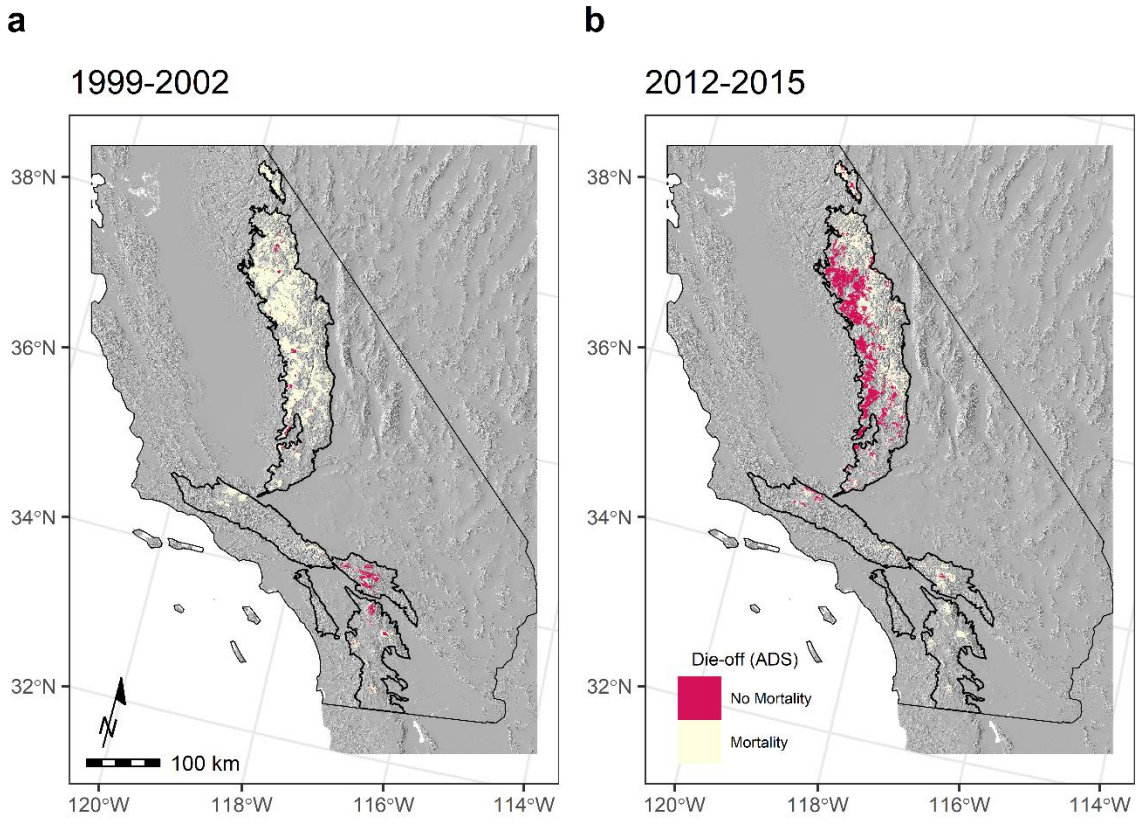

Figure A.6. Presence of forest die-off according to aerial detection surveys (ADS) in 1999-2002 (a) and 2012-2015 (b) in grid cells across the study region. Locations of study region sample pixels have been masked for conifer dominated forests that have no recorded fires since 1980. In the color bar, cream represents no mortality and red represents morality in each grid cell. Mortality is defined as ≥ 5 dead trees acre^{-1}. The sample size for both panels is N = 62,887.

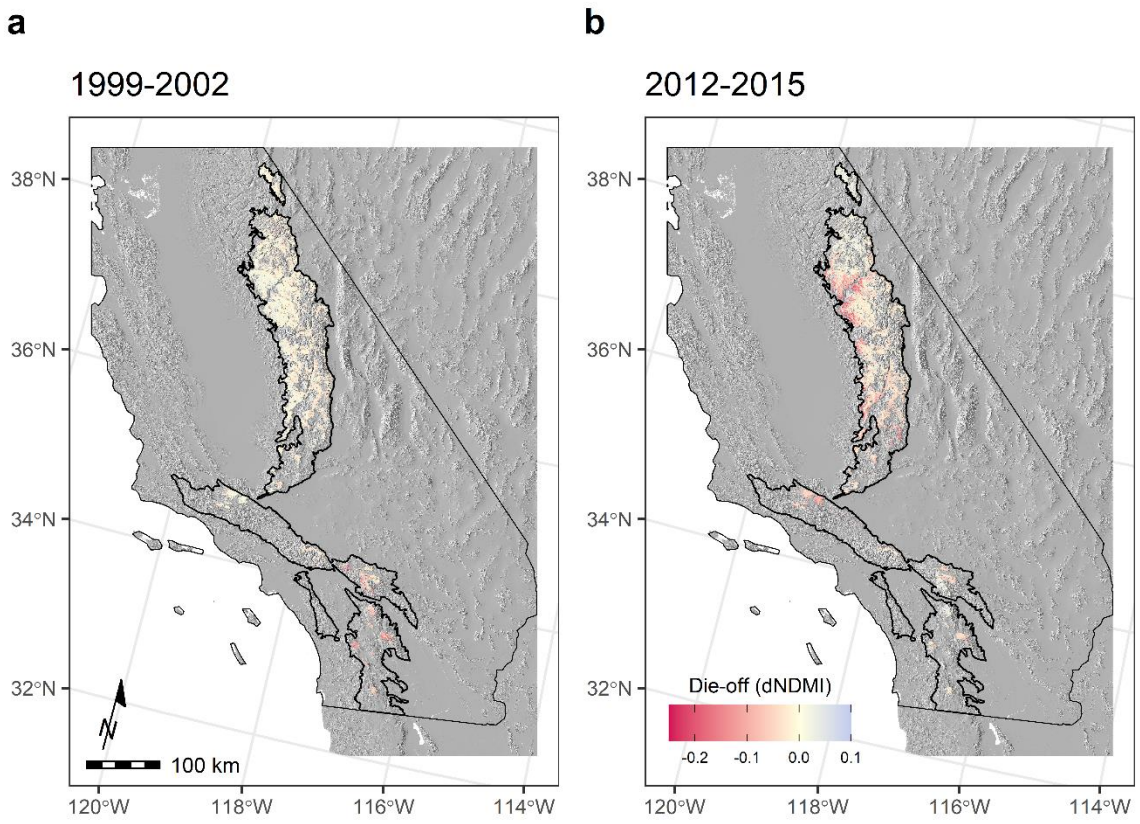

Figure A.7. Forest die-off (dNDMI) for 1999-2002 (a) and 2012-2015 (b) across the study region. Locations of study region sample pixels have been masked to include only conifer dominated forests that have no recorded fires since 1980. In the color bar, red represents negative values of dNDMI or severe forest die-off, cream represents no change in dNDMI or forest condition, and blue represents positive dNDMI or possible forest regrowth. The sample size for both panels is N = 62,887.

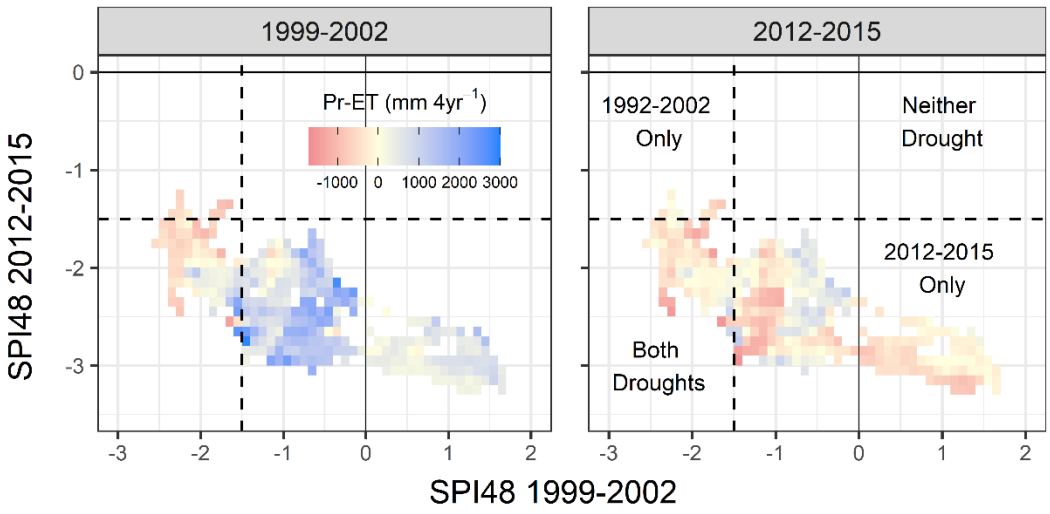

Figure A.8. The distribution of four-year Pr-ET by SPI48 exposure in 1999-2002 and 2012-2015. In the color bar, red represents negative four-year Pr-ET or high drought water deficit, cream represents four-year Pr-ET near zero or moderate to no drought water deficit, and blue represents positive four-year Pr-ET or excess water availability. The sample size for both panels is N = 62,887.

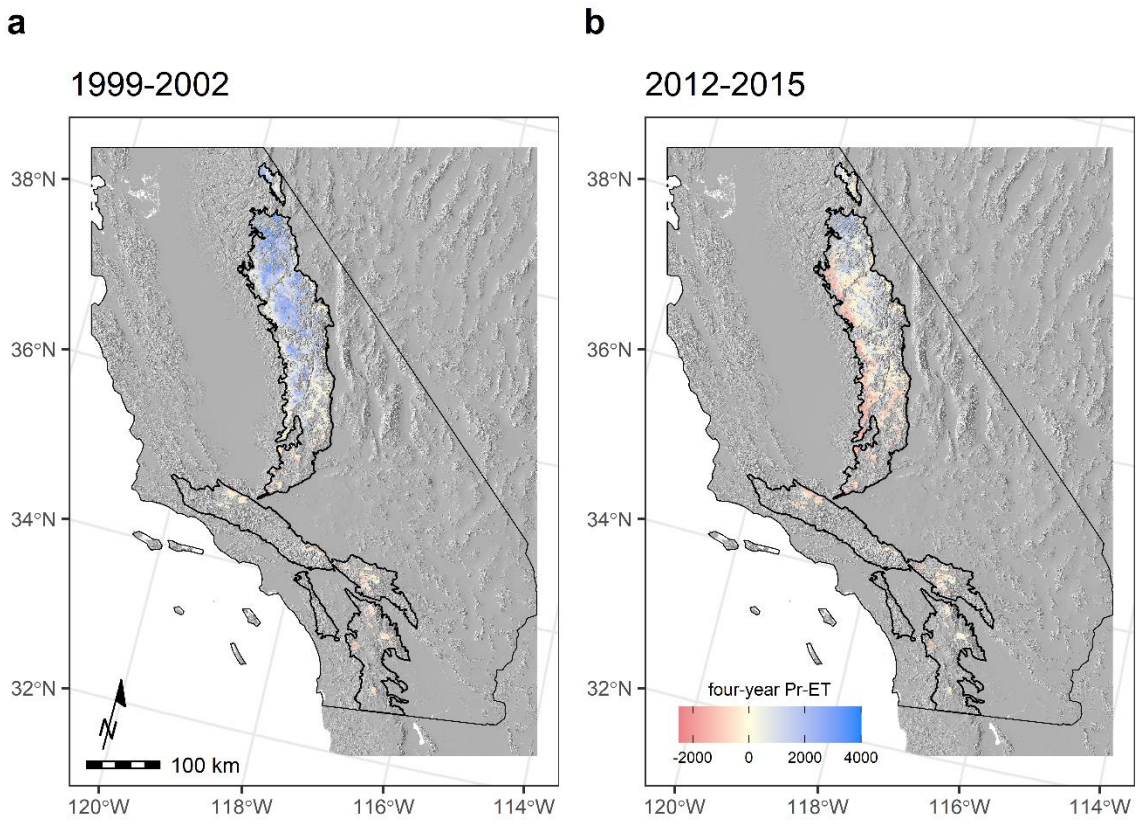

Figure A.9. Cumulative Moisture Deficit (four-year Pr-ET) for 1999-2002 (a) and 2012-2015 (b) across the study region. Locations of study region sample pixels have been masked to include only conifer dominated forests that have no recorded fires since 1980. In the color bar, red represents negative four-year Pr-ET or high Cumulative Moisture Deficit, cream represents four-year Pr-ET near zero or moderate to no Cumulative Moisture Deficit, and blue represents positive four-year Pr-ET or excess water availability. The sample size for both panels is N = 62,887.

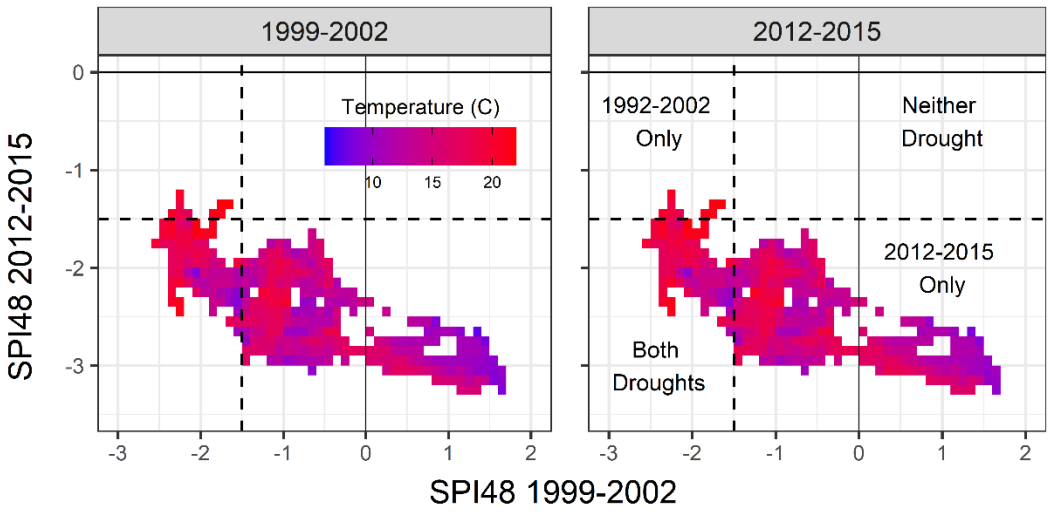

Figure A.10. The distribution of maximum Temperature (T_{max}) by SPI48 exposure in 1999-2002 and 2012-2015. In the color bar, blue represents lower T_{max} and red represents higher T_{max}. The sample size for both panels is N = 62,887.

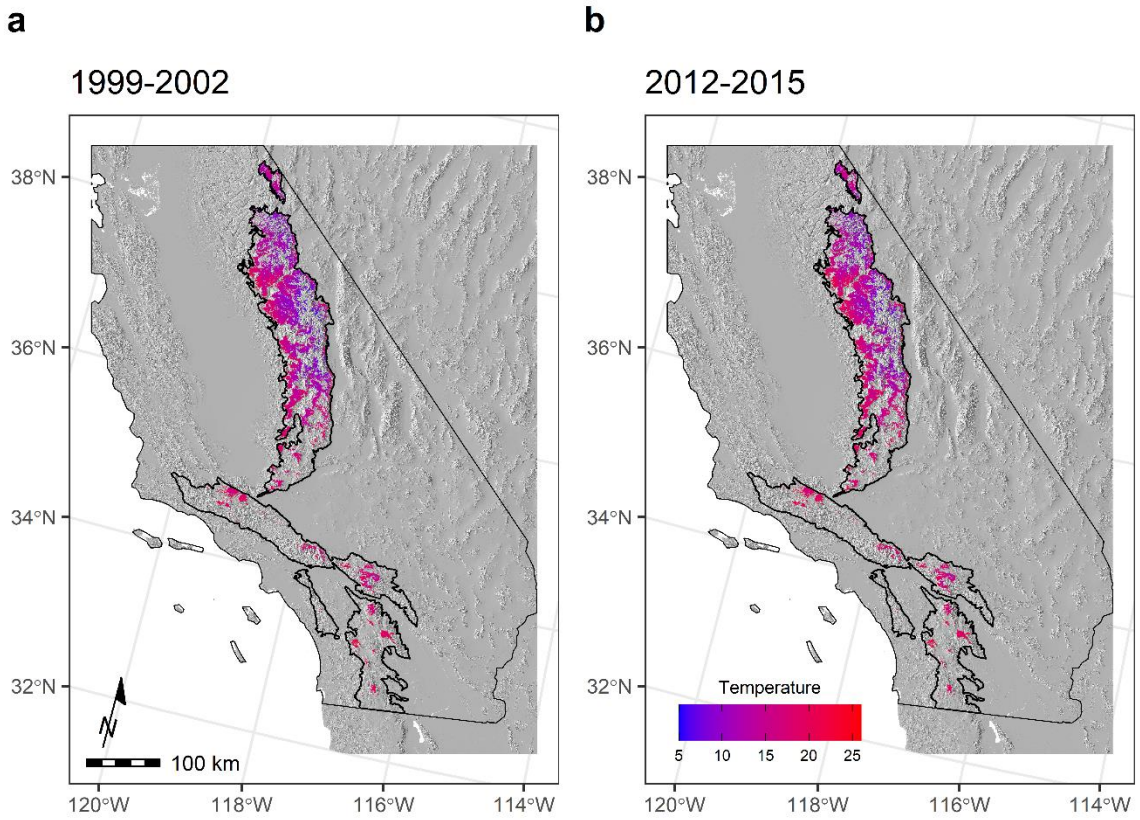

Figure A.11. Maximum temperature (T_{max}) for 1999-2002 (a) and 2012-2015 (b) across the study region. Locations of study region sample pixels have been masked for conifer dominated forests that have no recorded fires since 1980. In the color bar, blue represents lower T_{max} and red represents higher T_{max}. The sample size for both panels is N = 62,887.

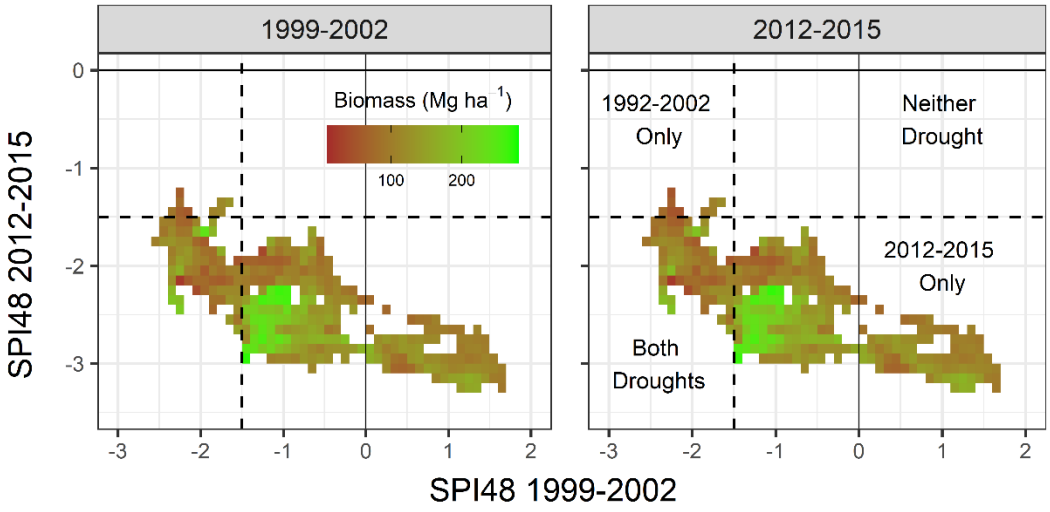

Figure A.12. The distribution of aboveground live biomass (AGB) by SPI48 exposure in 1999-2002 and 2012-2015. In the color bar, brown represents lower AGB and green represents higher AGB. The sample size for both panels is N = 62,887.

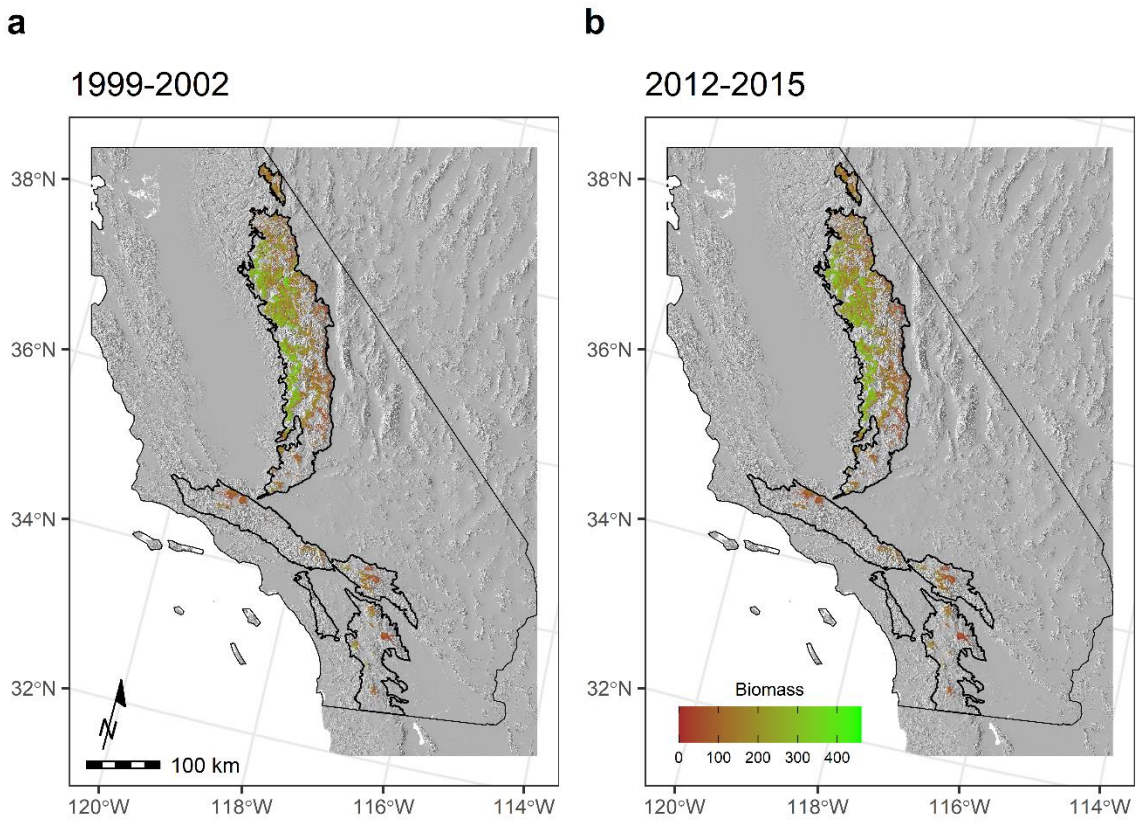

Figure A.13. Aboveground live biomass density (AGB) for 1999-2002 (a) and 2012-2015 (b) across the study region. Locations of study region sample pixels have been masked for conifer dominated forests that have no recorded fires since 1980. In the color bar, brown represents lower AGB and green represents higher AGB. The sample size for both panels is N = 62,887.

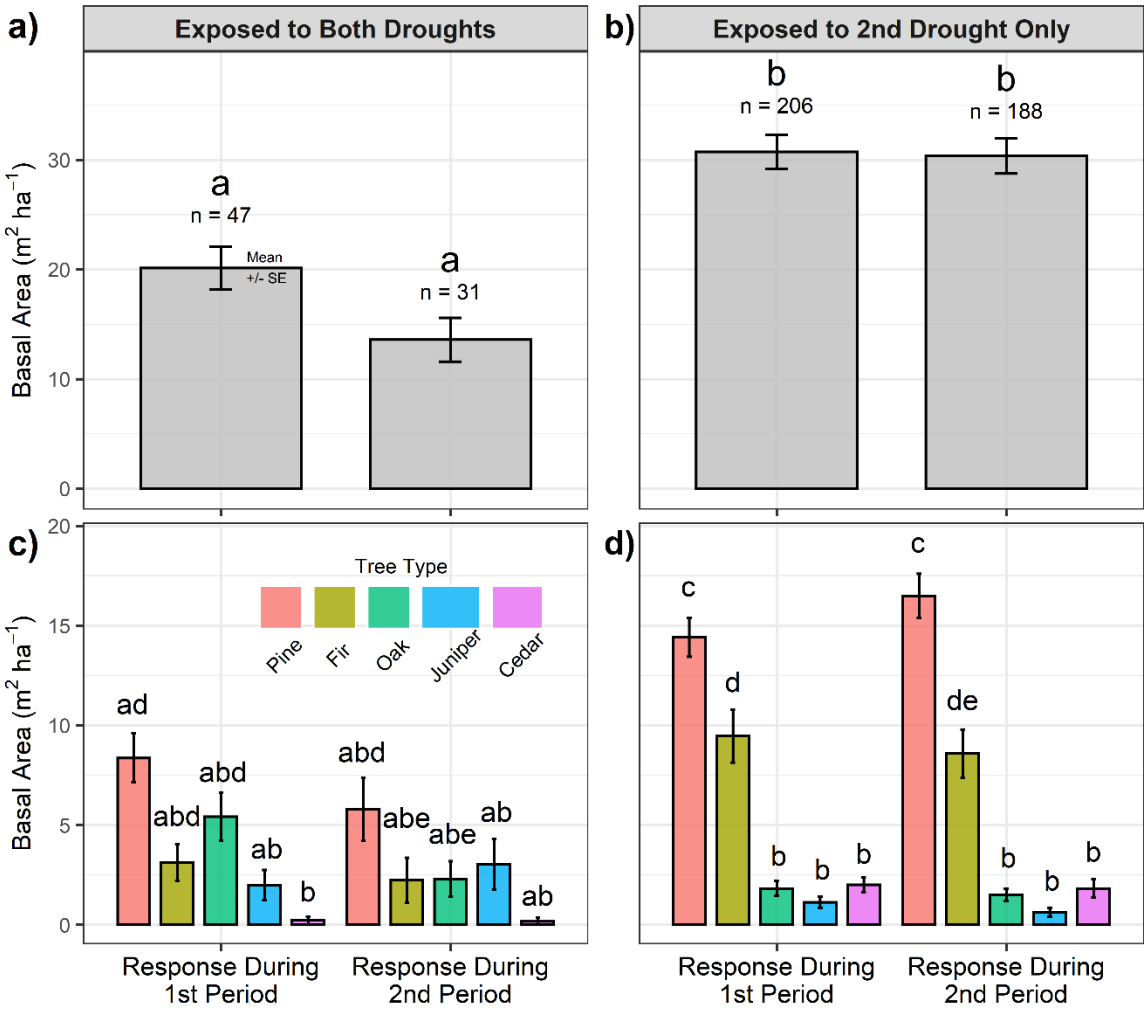

Figure A.14. Comparison of needleleaf conifer basal area (m^2 ha^{-1}) from field observations, in 1999-2002 and 2012-2015 and between locations exposed to Both Droughts and drought in 2nd Drought Only. Panels (a) and (b) represent the basal area of all trees in each plot, while panels (c) and (d) represent the basal area in each plot separated by the most common tree genera. The letters represent comparison with a significant difference ($p<0.05$) using a Tukey Honestly Significant Difference Test.

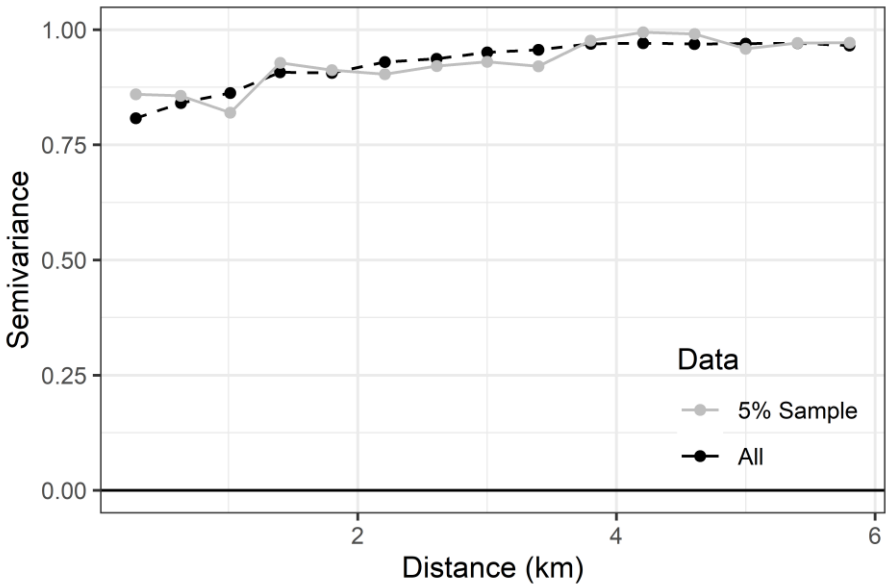

Figure A.15. Comparison of spatial autocorrelation measured with semi-variance by distance between grid cells for the 300-meter resolution data versus a random sub-sample of 5% of the 300-meter data.

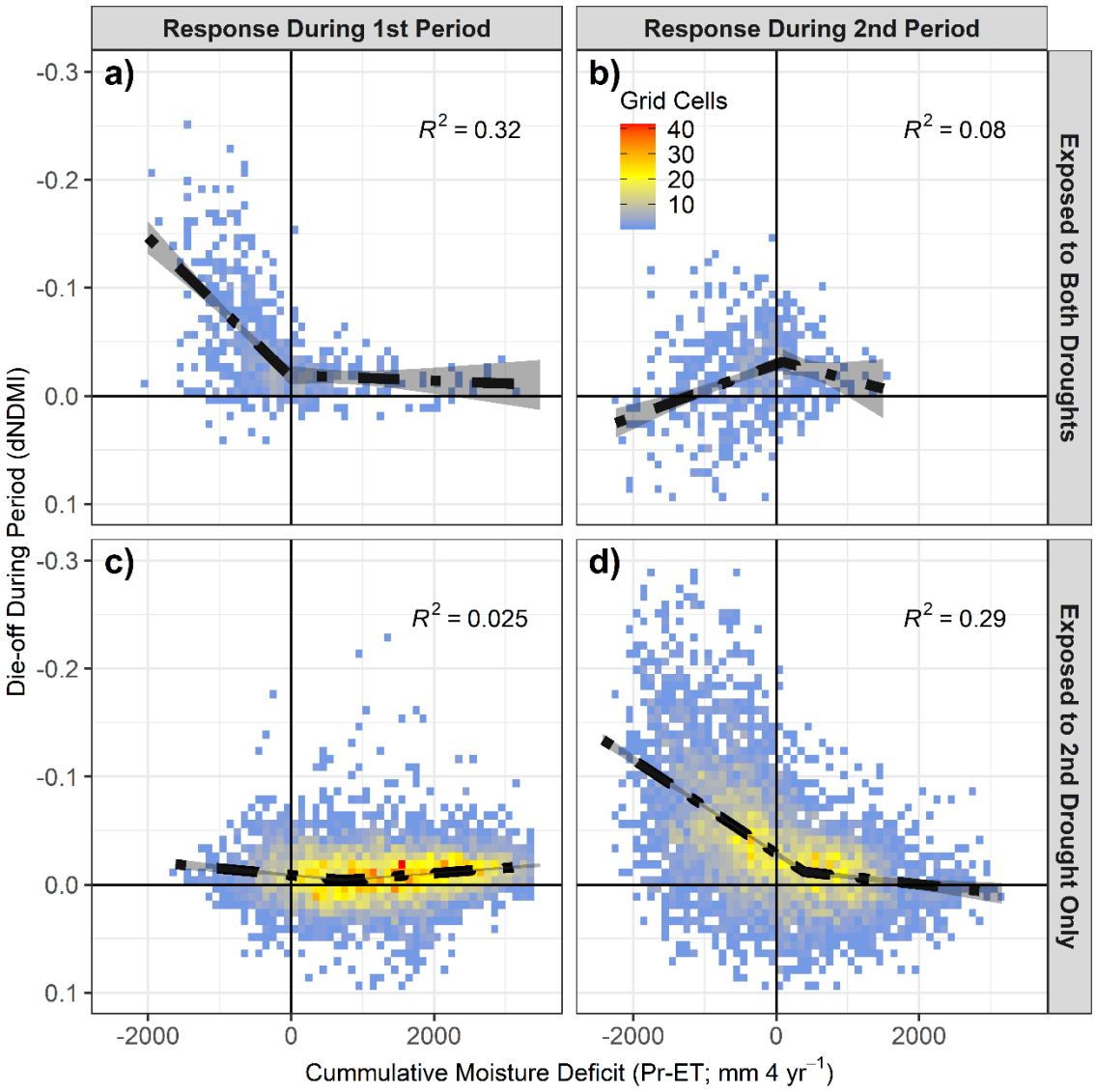

Figure A.16. Comparison of four-year Pr-ET as a predictor of forest die-off severity (dNDMI) in four combinations of drought exposure and time period using a random 5% sub-sample of the Both Droughts and 2nd Drought Only regions. The top two panels show the relationship between four-year Pr-ET and dNDMI for locations exposed to Both Droughts in 1999-2002 (a) and 2012-2015 (b). The bottom two panels show the relationship between four-year Pr-ET and dNDMI in locations exposed to drought in 2nd Drought Only in 1999-2002 (c) and 2012-2015 (d). The solid black line in all panels shows the piecewise linear (top left, bottom right) or linear regression fit (top right, bottom left) for four-year Pr-ET as a predictor of dNDMI. The sample size for the top two panels is N = 447. The sample size the bottom two panels is N = 2,046.

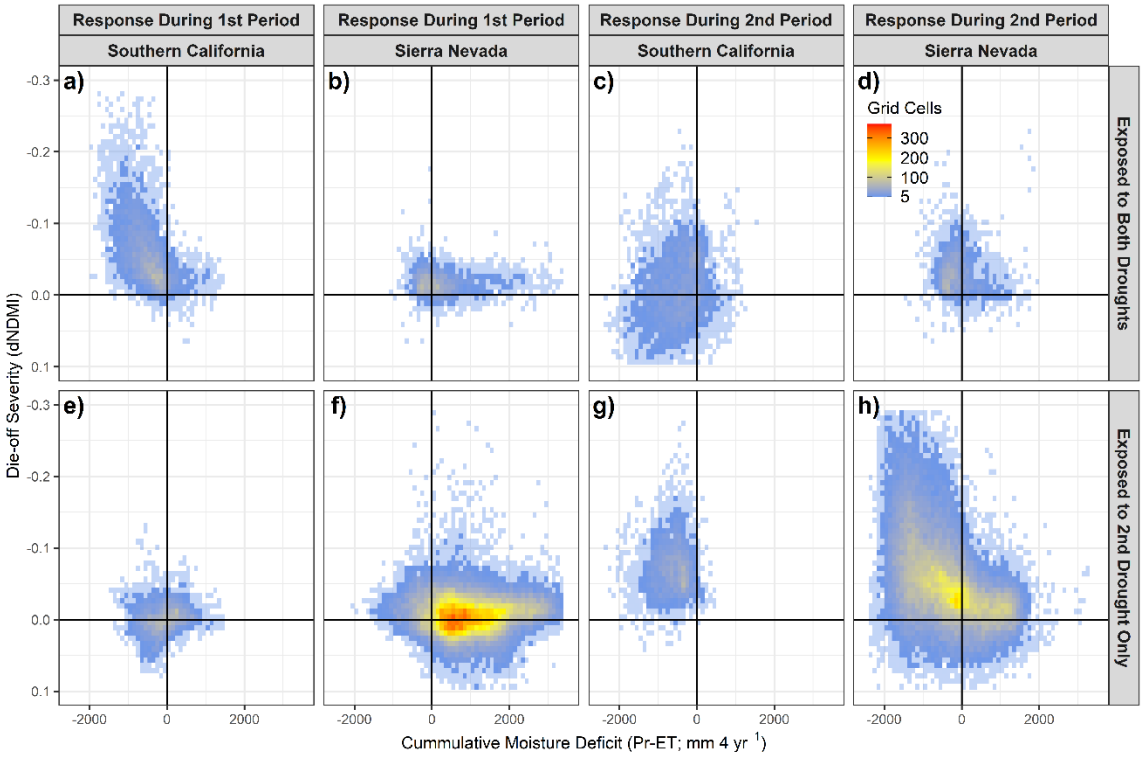

Figure A.17. Comparison of four-year Pr-ET and die-off severity (dNDMI) in eight combinations of drought exposure, time period, and region. The top four panels show the relationship between four-year Pr-ET and dNDMI for locations exposed to Both Droughts in 1999-2002 (a, b) and 2012-2015 (c, d). The bottom four panels show the relationship between four-year Pr-ET and dNDMI in locations exposed to drought in 2nd Drought Only in 1999-2002 (e, f) and 2012-2015 (g, h). The sample size for the panels a) and c) is N = 5,745. The sample for panels b) and d) is N = 3,178. The sample size for panels e) and g) is N = 4,070. The sample size for panels f) and h) is N = 45,152.

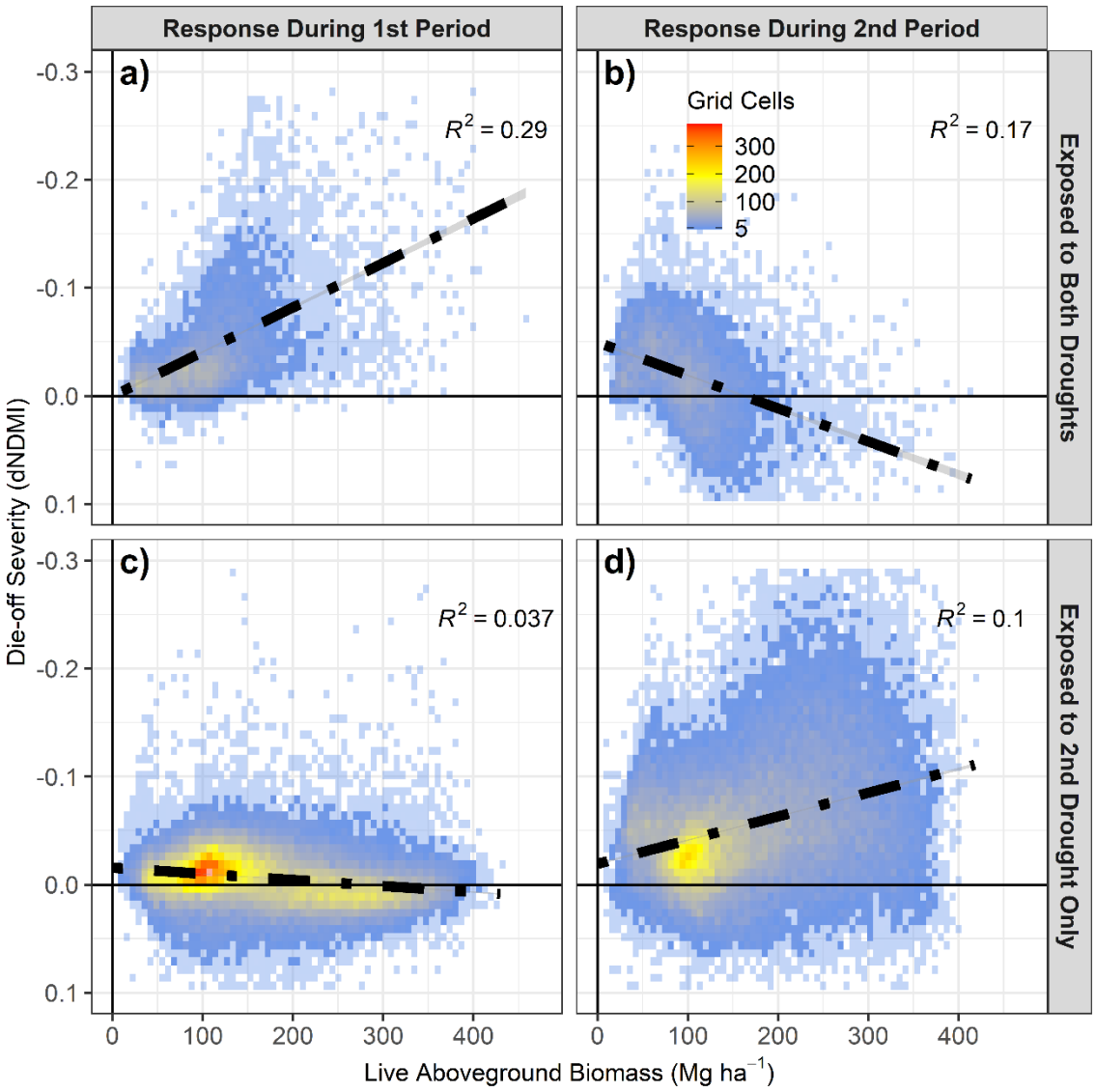

Figure A.18. Comparison of Aboveground Live Biomass (AGB) density as a predictor of forest die-off severity (dNDMI) in four combinations of drought exposure and time period. The top two panels show the relationship between AGB and dNDMI for locations exposed to Both Droughts in 1999-2002 (a) and 2012-2015 (b). The bottom two panels show the relationship between AGB and dNDMI in locations exposed to drought in 2nd Drought Only in 1999-2002 (c) and 2012-2015 (d). The dashed black line in all panels shows the linear regression fit for AGB as a predictor of dNDMI. The partially opaque blue squares represent combinations of dNDMI and four-year Pr-ET with less than 5 grid cell observations. The sample size for the top two panels is N = 8,933. The sample size the bottom two panels is N = 40,922.

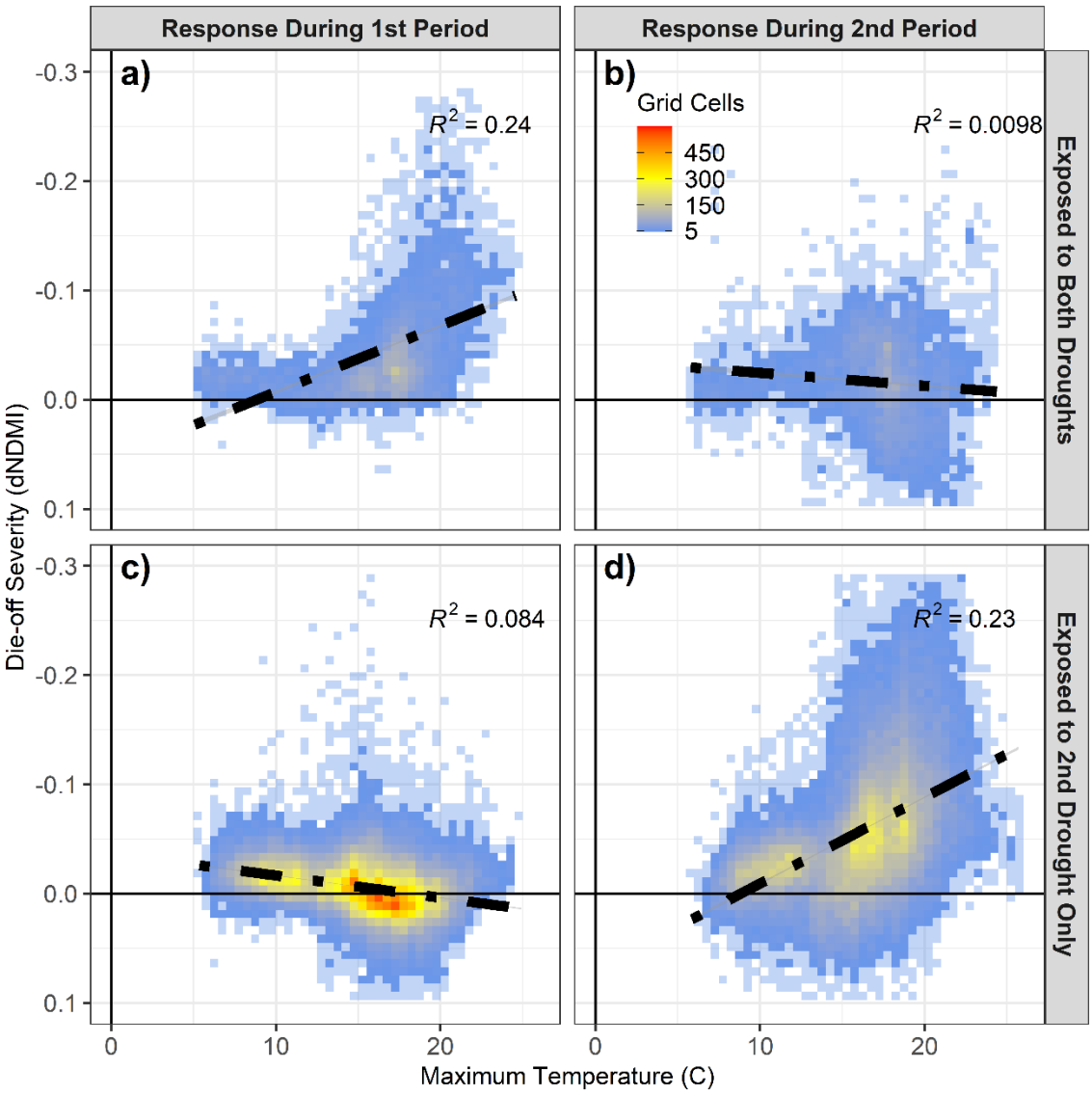

Figure A.19. Comparison of Maximum Temperature (T_{max}) as a predictor of forest die-off severity (dNDMI) in four combinations of drought exposure and time period. The top two panels show the relationship between T_{max} and dNDMI for locations exposed to Both Droughts in 1999-2002 (a) and 2012-2015 (b). The bottom two panels show the relationship between AGB and dNDMI in locations exposed to drought in 2nd Drought Only in 1999-2002 (c) and 2012-2015 (d). The dashed black line in all panels shows the linear fit for Tmax as a predictor of dNDMI. The partially opaque blue squares represent combinations of dNDMI and four-year Pr-ET with less than 5 grid cell observations. The sample size for the top two panels is N = 8,933. The sample size the bottom two panels is N = 40,922.

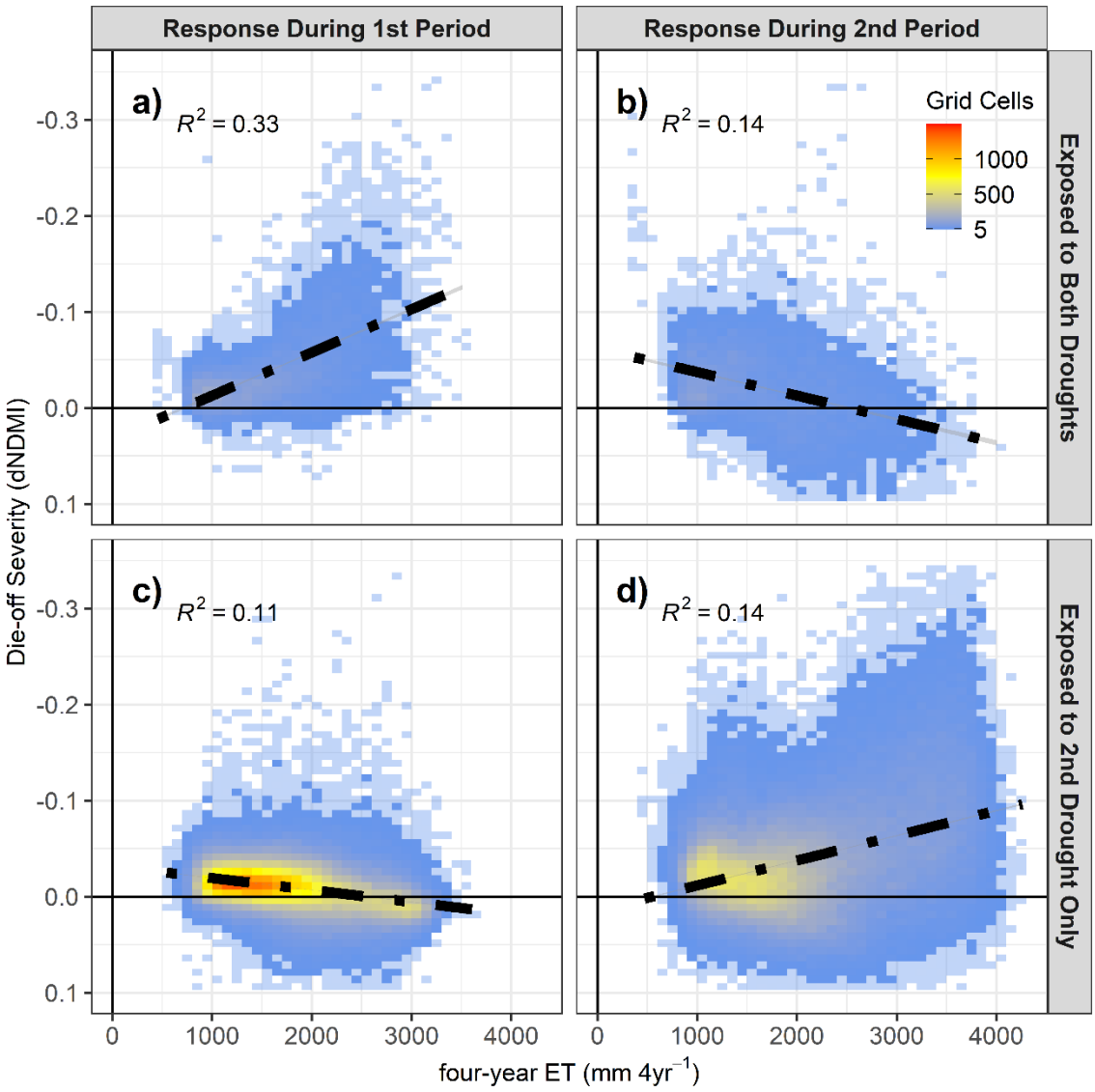

Figure A.20. Comparison of four-year Evapotranspiration (ET) as a predictor of forest die-off severity (dNDMI) in four combinations of drought exposure and time period. The top two panels show the relationship between AGB and dNDMI for locations exposed to Both Droughts in 1999-2002 (a) and 2012-2015 (b). The bottom two panels show the relationship between AGB and dNDMI in locations exposed to drought in 2nd Drought Only in 1999-2002 (c) and 2012-2015 (d). The dashed black line in all panels shows the linear regression fit for AGB as a predictor of dNDMI. The partially opaque blue squares represent combinations of dNDMI and four-year Pr-ET with less than 5 grid cell observations. The sample size for the top two panels is N = 8,933. The sample size the bottom two panels is N = 40,922.

Table S1: Paired two-tailed T-Test Results

Variable	Drought Sequence	Estimate 1	Estimate 2	Difference	Low 95% CI	High 95% CI	t	p-value
Biomass (Mg ha^{-1})	Both Droughts	113.531	109.381	4.150	3.761	4.538	20.949	0.000
Biomass (Mg ha^{-1})	2012-2015 Only	169.560	169.717	-0.157	-0.292	-0.022	-2.282	0.023
dNDMI	Both Droughts	-0.046	-0.016	-0.031	-0.032	-0.029	-38.626	0.000
dNDMI	2012-2015 Only	-0.006	-0.057	0.051	0.050	0.052	161.143	0.000
Pr-ET (mm $4yr^{-1}$)	Both Droughts	-213.429	-348.617	135.188	128.364	142.013	38.830	0.000
Pr-ET (mm $4yr^{-1}$)	2012-2015 Only	872.284	-421.463	1293.747	1288.667	1298.828	499.139	0.000
Temperature (C)	Both Droughts	16.473	16.943	-0.470	-0.479	-0.461	-102.991	0.000
Temperature (C)	2012-2015 Only	15.155	15.986	-0.832	-0.834	-0.829	-641.900	0.000

Table A.1. Comparison of various geospatial observations of ecosystem and climate properties between two time periods (1999-2002 and 2012-2015) for two drought sequences using paired t-tests.

Table S2: ANOVA and Tukey HSD Results

Variable	Comparison	Estimate 1	Estimate 2	Difference	Low 95% CI	High 95% CI	p-value
Biomass (Mg ha^{-1})	2012-2015-1999-2002	140.965	143.368	-2.403	-3.900	-0.906	0.002
Biomass (Mg ha^{-1})	Both Droughts-2012-2015 Only	111.456	170.002	-58.547	-60.046	-57.049	0.000
Biomass (Mg ha^{-1})	2012-2015:2012-2015 Only-1999-2002:2012-2015 Only	169.577	170.428	-0.851	-3.560	1.858	0.851
Biomass (Mg ha^{-1})	1999-2002:Both Droughts-1999-2002:2012-2015 Only	113.531	170.428	-56.897	-59.675	-54.119	0.000
Biomass (Mg ha^{-1})	2012-2015:Both Droughts-1999-2002:2012-2015 Only	109.381	170.428	-61.047	-63.825	-58.269	0.000
Biomass (Mg ha^{-1})	1999-2002:Both Droughts-2012-2015:2012-2015 Only	113.531	169.577	-56.046	-58.824	-53.269	0.000
Biomass (Mg ha^{-1})	2012-2015:Both Droughts-2012-2015:2012-2015 Only	109.381	169.577	-60.196	-62.974	-57.419	0.000
Biomass (Mg ha^{-1})	2012-2015:Both Droughts-1999-2002:Both Droughts	109.381	113.531	-4.150	-6.995	-1.305	0.001
dNDMI	2012-2015-1999-2002	-0.038	-0.025	-0.013	-0.014	-0.012	0.000
dNDMI	Both Droughts-2012-2015 Only	-0.031	-0.032	0.001	0.000	0.002	0.112
dNDMI	2012-2015:2012-2015 Only-1999-2002:2012-2015 Only	-0.058	-0.006	-0.052	-0.054	-0.051	0.000
dNDMI	1999-2002:Both Droughts-1999-2002:2012-2015 Only	-0.046	-0.006	-0.041	-0.043	-0.039	0.000
dNDMI	2012-2015:Both Droughts-1999-2002:2012-2015 Only	-0.016	-0.006	-0.010	-0.012	-0.008	0.000
dNDMI	1999-2002:Both Droughts-2012-2015:2012-2015 Only	-0.046	-0.058	0.011	0.010	0.013	0.000
dNDMI	2012-2015:Both Droughts-2012-2015:2012-2015 Only	-0.016	-0.058	0.042	0.041	0.044	0.000
dNDMI	2012-2015:Both Droughts-1999-2002:Both Droughts	-0.016	-0.046	0.031	0.029	0.033	0.000
Pr-ET (mm $4yr^{-1}$)	2012-2015-1999-2002	-387.599	351.527	-739.126	-754.596	-723.656	0.000
Pr-ET (mm $4yr^{-1}$)	Both Droughts-2012-2015 Only	-281.023	220.127	-501.357	-516.845	-485.868	0.000
Pr-ET (mm $4yr^{-1}$)	2012-2015:2012-2015 Only-1999-2002:2012-2015 Only	-422.913	863.886	-1286.798	-1314.795	-1258.801	0.000
Pr-ET (mm $4yr^{-1}$)	1999-2002:Both Droughts-1999-2002:2012-2015 Only	-213.429	863.886	-1077.315	-1106.029	-1048.600	0.000
Pr-ET (mm $4yr^{-1}$)	2012-2015:Both Droughts-1999-2002:2012-2015 Only	-348.617	863.886	-1212.503	-1241.217	-1183.788	0.000
Pr-ET (mm $4yr^{-1}$)	1999-2002:Both Droughts-2012-2015:2012-2015 Only	-213.429	-422.913	209.484	180.777	238.190	0.000
Pr-ET (mm $4yr^{-1}$)	2012-2015:Both Droughts-2012-2015:2012-2015 Only	-348.617	-422.913	74.295	45.589	103.002	0.000
Pr-ET (mm $4yr^{-1}$)	2012-2015:Both Droughts-1999-2002:Both Droughts	-348.617	-213.429	-135.188	-164.595	-105.781	0.000
Temperature (C)	2012-2015-1999-2002	16.460	15.806	0.654	0.581	0.727	0.000
Temperature (C)	Both Droughts-2012-2015 Only	16.708	15.612	1.096	1.023	1.170	0.000
Temperature (C)	2012-2015:2012-2015 Only-1999-2002:2012-2015 Only	16.023	15.201	0.822	0.689	0.954	0.000
Temperature (C)	1999-2002:Both Droughts-1999-2002:2012-2015 Only	16.473	15.201	1.272	1.136	1.408	0.000
Temperature (C)	2012-2015:Both Droughts-1999-2002:2012-2015 Only	16.943	15.201	1.742	1.606	1.878	0.000
Temperature (C)	1999-2002:Both Droughts-2012-2015:2012-2015 Only	16.473	16.023	0.451	0.315	0.587	0.000
Temperature (C)	2012-2015:Both Droughts-2012-2015:2012-2015 Only	16.943	16.023	0.920	0.785	1.056	0.000
Temperature (C)	2012-2015:Both Droughts-1999-2002:Both Droughts	16.943	16.473	0.470	0.331	0.609	0.000

Table A.2. Comparison of various geospatial observations of ecosystem and climate properties in locations exposed to two drought sequence (Both Droughts and 2012-2015 Only) and two time periods (1999-2002 and 2012-2015) using two-way Analysis of Variance and Tukey Honestly Significant Different tests.

Table S3: FIA ANOVA and Tukey HSD Results

Variable	Comparison	Estimate 1	Estimate 2	Difference	Low 95% CI	High 95% CI	p-value
Mortality (m^2 ha^{-1})	2012-2015-1999-2002	2.331	0.686	1.645	0.985	2.305	0.000
Mortality (m^2 ha^{-1})	Both Droughts-2nd Drought Only	2.098	1.321	0.909	0.022	1.795	0.045
Mortality (m^2 ha^{-1})	2012-2015:2nd Drought Only-1999-2002:2nd Drought Only	2.640	0.117	2.523	1.577	3.470	0.000
Mortality (m^2 ha^{-1})	1999-2002:Both Droughts-1999-2002:2nd Drought Only	3.181	0.117	3.064	1.547	4.582	0.000
Mortality (m^2 ha^{-1})	2012-2015:Both Droughts-1999-2002:2nd Drought Only	0.457	0.117	0.340	-1.468	2.148	0.963
Mortality (m^2 ha^{-1})	1999-2002:Both Droughts-2012-2015:2nd Drought Only	3.181	2.640	0.541	-0.989	2.072	0.799
Mortality (m^2 ha^{-1})	2012-2015:Both Droughts-2012-2015:2nd Drought Only	0.457	2.640	-2.183	-4.003	-0.364	0.011
Mortality (m^2 ha^{-1})	2012-2015:Both Droughts-1999-2002:Both Droughts	0.457	3.181	-2.725	-4.896	-0.553	0.007
Basal Area (m^2 ha^{-1})	2012-2015-1999-2002	28.004	28.762	-0.758	-4.577	3.061	0.697
Basal Area (m^2 ha^{-1})	Both Droughts-2nd Drought Only	17.537	30.562	-13.086	-18.213	-7.958	0.000
Basal Area (m^2 ha^{-1})	2012-2015:2nd Drought Only-1999-2002:2nd Drought Only	30.379	30.730	-0.351	-5.827	5.125	0.998
Basal Area (m^2 ha^{-1})	1999-2002:Both Droughts-1999-2002:2nd Drought Only	20.135	30.730	-10.595	-19.371	-1.820	0.011
Basal Area (m^2 ha^{-1})	2012-2015:Both Droughts-1999-2002:2nd Drought Only	13.599	30.730	-17.131	-27.589	-6.672	0.000
Basal Area (m^2 ha^{-1})	1999-2002:Both Droughts-2012-2015:2nd Drought Only	20.135	30.379	-10.244	-19.098	-1.391	0.016
Basal Area (m^2 ha^{-1})	2012-2015:Both Droughts-2012-2015:2nd Drought Only	13.599	30.379	-16.780	-27.303	-6.256	0.000
Basal Area (m^2 ha^{-1})	2012-2015:Both Droughts-1999-2002:Both Droughts	13.599	20.135	-6.535	-19.096	6.026	0.537

Table A.3. Comparison of field observations of mortality and basal area in locations exposed to two drought sequence (Both Droughts and 2nd Drought Only) and two time periods (1999-2002 and 2012-2015) using two-way Analysis of Variance and Tukey Honestly Significant Different tests.

Table S4: Pine Tree FIA ANOVA and Tukey HSD Results

Variable	Comparison	Estimate 1	Estimate 2	Difference	Low 95% CI	High 95% CI	p-value
Mortality (m^2 ha^{-1})	2012-2015-1999-2002	1.045	0.429	0.617	0.224	1.009	0.002
Mortality (m^2 ha^{-1})	Both Droughts-2nd Drought Only	1.317	0.595	0.771	0.244	1.299	0.004
Mortality (m^2 ha^{-1})	2012-2015:2nd Drought Only-1999-2002:2nd Drought Only	1.176	0.066	1.110	0.547	1.673	0.000
Mortality (m^2 ha^{-1})	1999-2002:Both Droughts-1999-2002:2nd Drought Only	2.019	0.066	1.953	1.051	2.856	0.000
Mortality (m^2 ha^{-1})	2012-2015:Both Droughts-1999-2002:2nd Drought Only	0.253	0.066	0.187	-0.889	1.263	0.970
Mortality (m^2 ha^{-1})	1999-2002:Both Droughts-2012-2015:2nd Drought Only	2.019	1.176	0.843	-0.067	1.754	0.081
Mortality (m^2 ha^{-1})	2012-2015:Both Droughts-2012-2015:2nd Drought Only	0.253	1.176	-0.923	-2.005	0.160	0.126
Mortality (m^2 ha^{-1})	2012-2015:Both Droughts-1999-2002:Both Droughts	0.253	2.019	-1.766	-3.058	-0.474	0.003
Basal Area (m^2 ha^{-1})	2012-2015-1999-2002	14.983	13.298	1.685	-0.816	4.186	0.186
Basal Area (m^2 ha^{-1})	Both Droughts-2nd Drought Only	7.350	15.412	-7.927	-11.285	-4.569	0.000
Basal Area (m^2 ha^{-1})	2012-2015:2nd Drought Only-1999-2002:2nd Drought Only	16.497	14.423	2.074	-1.512	5.660	0.444
Basal Area (m^2 ha^{-1})	1999-2002:Both Droughts-1999-2002:2nd Drought Only	8.369	14.423	-6.053	-11.801	-0.306	0.035
Basal Area (m^2 ha^{-1})	2012-2015:Both Droughts-1999-2002:2nd Drought Only	5.806	14.423	-8.616	-15.466	-1.767	0.007
Basal Area (m^2 ha^{-1})	1999-2002:Both Droughts-2012-2015:2nd Drought Only	8.369	16.497	-8.127	-13.926	-2.329	0.002
Basal Area (m^2 ha^{-1})	2012-2015:Both Droughts-2012-2015:2nd Drought Only	5.806	16.497	-10.690	-17.582	-3.798	0.000
Basal Area (m^2 ha^{-1})	2012-2015:Both Droughts-1999-2002:Both Droughts	5.806	8.369	-2.563	-10.789	5.663	0.853

Table A.4. Comparison of field observations of pine mortality and basal area in locations exposed to two drought sequence (*Both Droughts* and *2nd Drought Only*) and two time periods (*1999-2002* and *2012-2015*) using two-way Analysis of Variance and Tukey Honestly Significant Different tests.

Table S5: Fir Tree FIA ANOVA and Tukey HSD Results

Variable	Comparison	Estimate 1	Estimate 2	Difference	Low 95% CI	High 95% CI	p-value
Mortality (m^2 ha^{-1})	2012-2015-1999-2002	0.994	0.149	0.845	0.366	1.325	0.001
Mortality (m^2 ha^{-1})	Both Droughts-2nd Drought Only	0.417	0.565	-0.080	-0.724	0.563	0.806
Mortality (m^2 ha^{-1})	2012-2015:2nd Drought Only-1999-2002:2nd Drought Only	1.144	0.037	1.107	0.419	1.794	0.000
Mortality (m^2 ha^{-1})	1999-2002:Both Droughts-1999-2002:2nd Drought Only	0.637	0.037	0.599	-0.502	1.701	0.498
Mortality (m^2 ha^{-1})	2012-2015:Both Droughts-1999-2002:2nd Drought Only	0.085	0.037	0.048	-1.264	1.360	1.000
Mortality (m^2 ha^{-1})	1999-2002:Both Droughts-2012-2015:2nd Drought Only	0.637	1.144	-0.507	-1.618	0.604	0.642
Mortality (m^2 ha^{-1})	2012-2015:Both Droughts-2012-2015:2nd Drought Only	0.085	1.144	-1.059	-2.379	0.262	0.165
Mortality (m^2 ha^{-1})	2012-2015:Both Droughts-1999-2002:Both Droughts	0.085	0.637	-0.552	-2.128	1.024	0.804
Basal Area (m^2 ha^{-1})	2012-2015-1999-2002	7.690	8.285	-0.595	-3.598	2.407	0.697
Basal Area (m^2 ha^{-1})	Both Droughts-2nd Drought Only	2.774	9.046	-6.320	-10.351	-2.288	0.002
Basal Area (m^2 ha^{-1})	2012-2015:2nd Drought Only-1999-2002:2nd Drought Only	8.589	9.462	-0.873	-5.178	3.432	0.954
Basal Area (m^2 ha^{-1})	1999-2002:Both Droughts-1999-2002:2nd Drought Only	3.128	9.462	-6.335	-13.235	0.565	0.085
Basal Area (m^2 ha^{-1})	2012-2015:Both Droughts-1999-2002:2nd Drought Only	2.237	9.462	-7.225	-15.448	0.998	0.108
Basal Area (m^2 ha^{-1})	1999-2002:Both Droughts-2012-2015:2nd Drought Only	3.128	8.589	-5.462	-12.423	1.499	0.181
Basal Area (m^2 ha^{-1})	2012-2015:Both Droughts-2012-2015:2nd Drought Only	2.237	8.589	-6.352	-14.627	1.922	0.197
Basal Area (m^2 ha^{-1})	2012-2015:Both Droughts-1999-2002:Both Droughts	2.237	3.128	-0.891	-10.767	8.986	0.996

Table A.5. Comparison of field observations of fir mortality and basal area in locations exposed to two drought sequence (*Both Droughts* and *2nd Drought Only*) and two time periods (*1999-2002* and *2012-2015*) using two-way Analysis of Variance and Tukey Honestly Significant Different tests.

Table S6: Die-off (dNDMI) Multiple Linear Regression

Variable	Coefficient	Standard Error	T-Statistic	p-value	Relative Importance (%)
Intercept	-0.021	0.002	-13.875	0	0.000
Time Period	0.033	0.001	48.675	0	3.706
Drought Sequence	0.029	0.001	34.855	0	1.952
four-year Pr-ET	0.000	0.000	23.958	0	36.577
four-year Temperature	-0.001	0.000	-13.958	0	9.262
Biomass	0.000	0.000	-7.587	0	2.743
Time Period:Drought Sequence	-0.070	0.001	-66.820	0	45.759

Table A.6. Parameters to predict die-off severity (dNDMI) using multiple linear regression and relative weight analysis of predictor variable contribution to explain variance in dNDMI.

APPENDIX B

Supporting Information for Chapter 2

Recent fire history enhances semi-arid conifer forest drought resistance

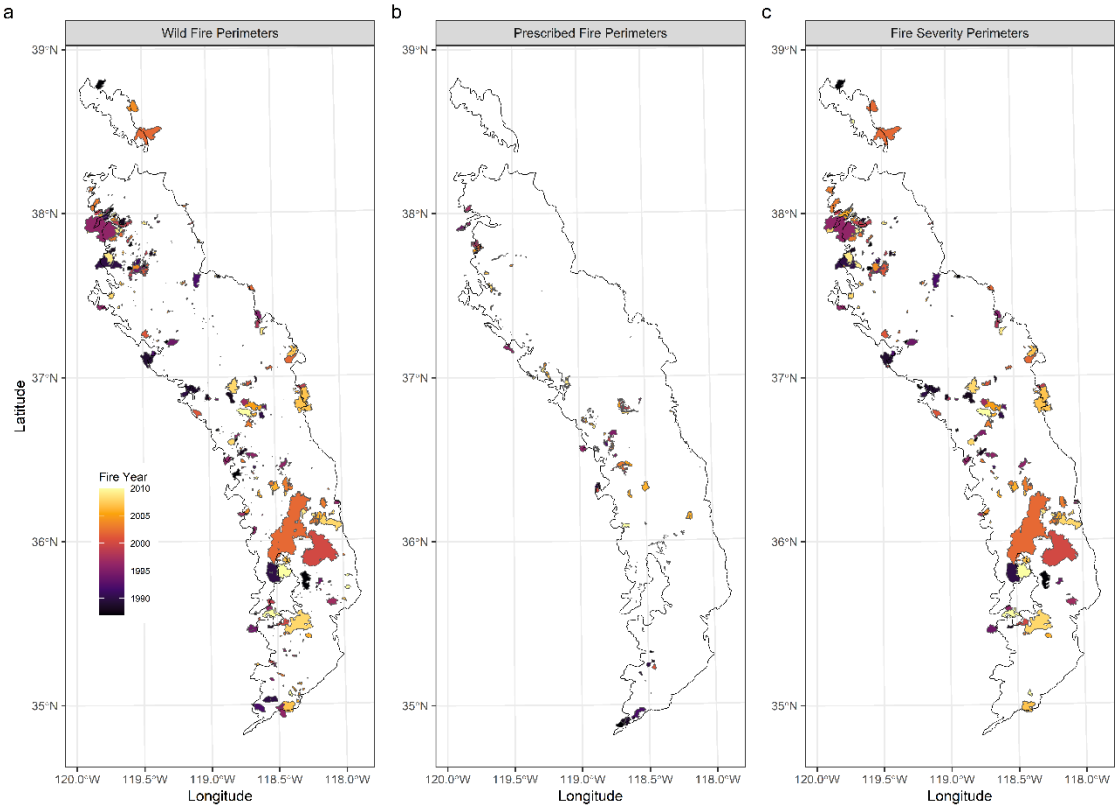

Figure B.1. Fire perimeters in the South Sierra from 1987-2010. Fire perimeters for wildfire are in (a), perimeters for prescribed fires are in (b), and perimeters for wildfires with additional fires severity information are in (c).

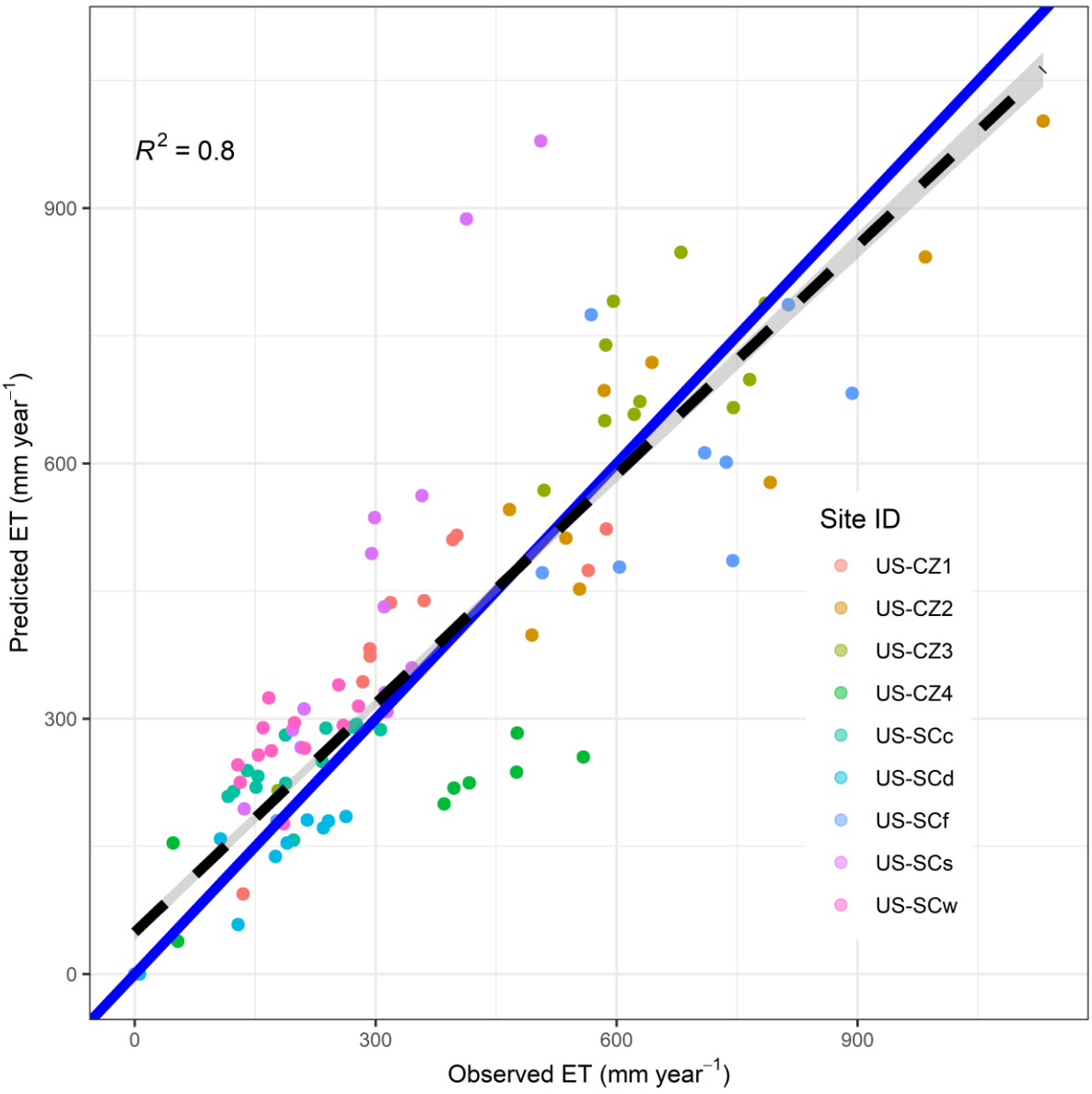

Figure B.2. Relationship between observed ET (measured with flux towers) and predicted ET (scaled from NDVI).

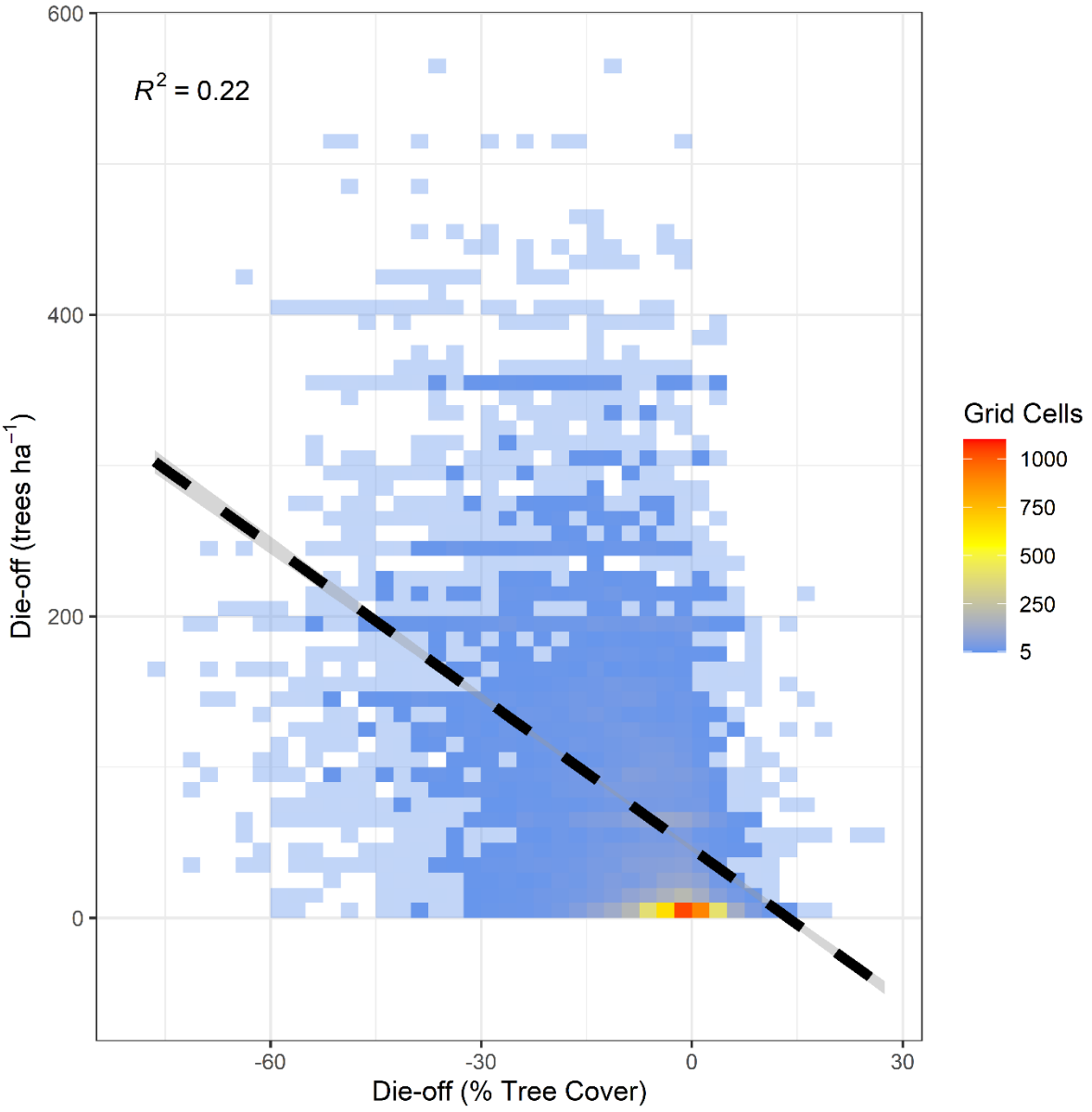

Figure B.3. Comparison between die-off measured as change in tree cover (x-axis) and as with aerial detection surveys (ADS) from wildfire and prescribed fire samples and spatially matched controls.

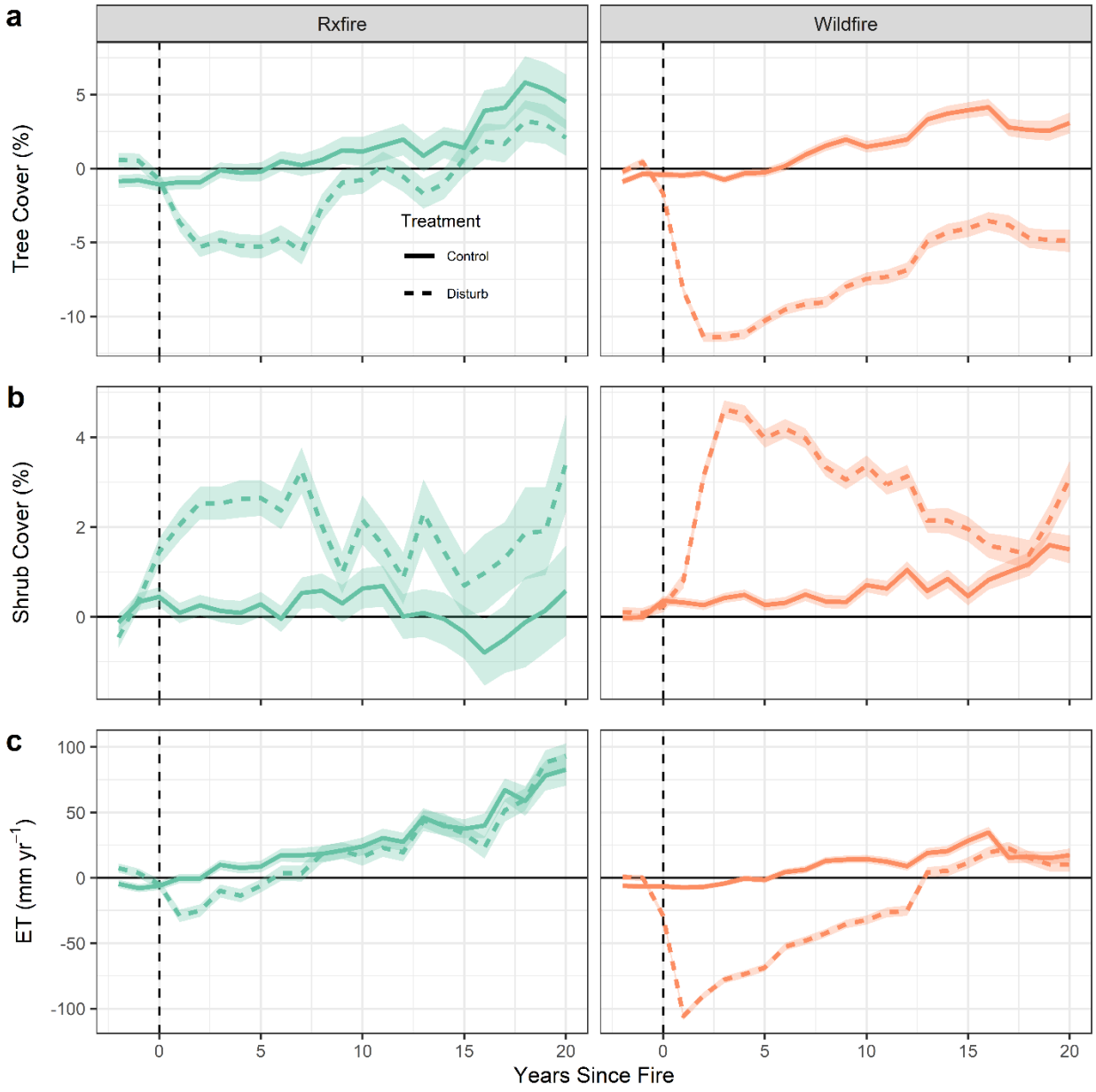

Figure B.4. The impact of wildfire and prescribed (Rx) fire on tree cover (a), shrub cover (b), and ET (c) following exposure to wildfire or prescribed fire paired with spatially matched controls. Values are for each grid well were subtracted by the mean of the values immediately before the fire (stand age -1 and -2). The error bars show the 95% confidence intervals.

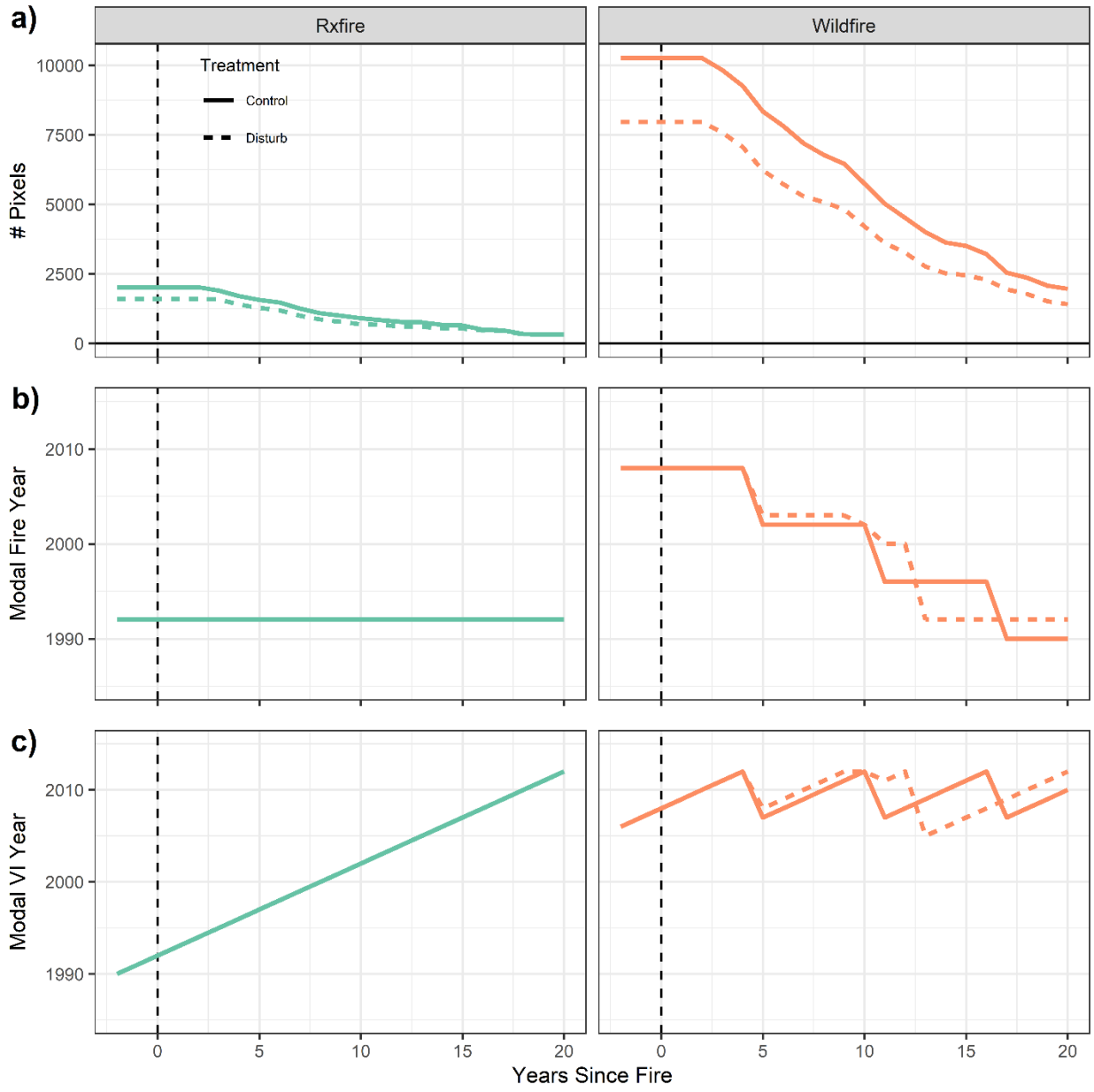

Figure B.5. The number of pixels, modal fire year, and modal vegetation index (VI) year for prescribed fires (Rxfire) and wildfire samples and their spatially matched controls.

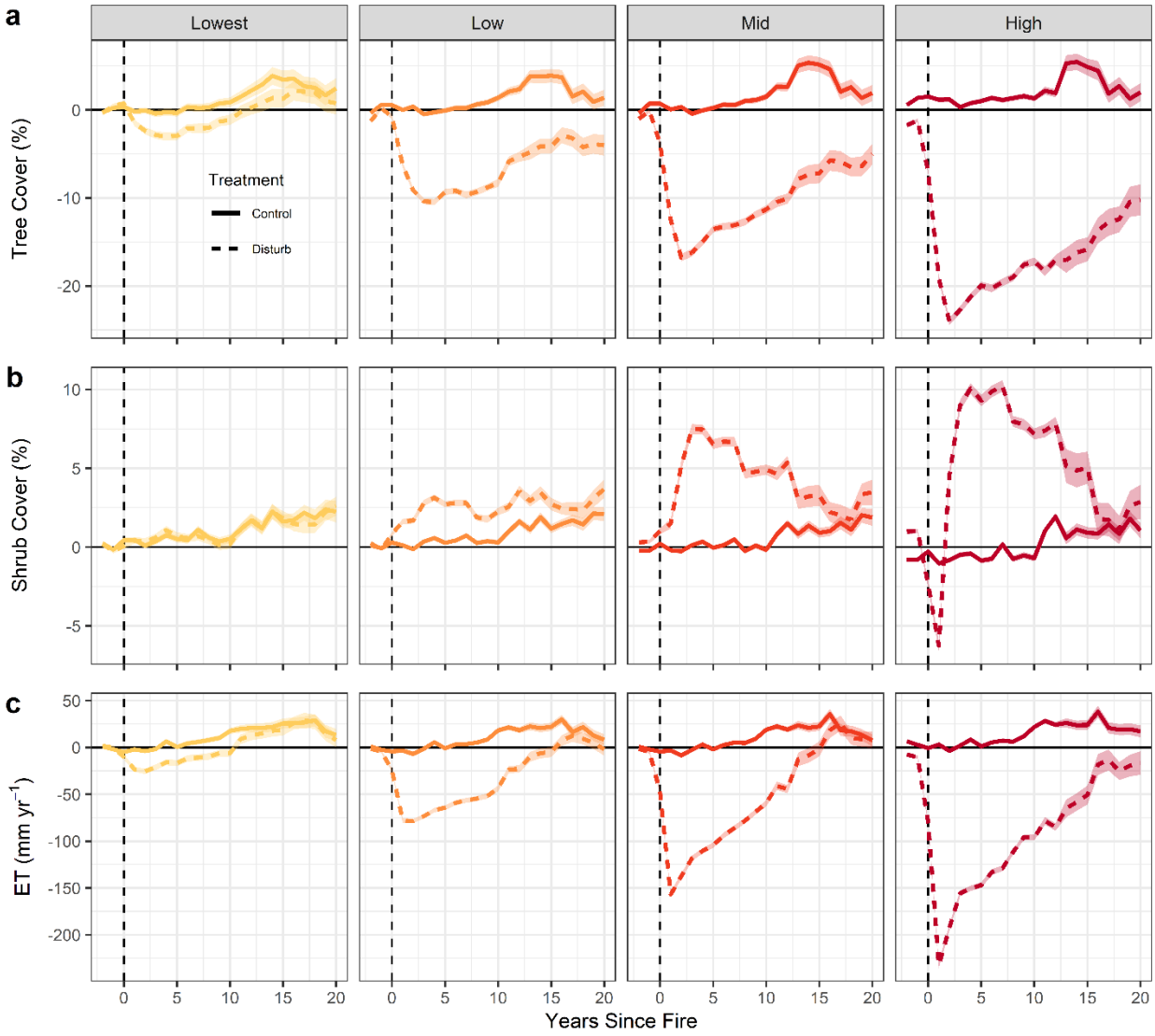

Figure B.6. The impact of fire severity on tree cover (a), shrub cover (b), and ET (c) following exposure to fire with spatially matched controls. Values are for each grid well were subtracted by the mean of the values immediately before the fire (stand age -1 and -2). The error bars show the 95% confidence intervals.

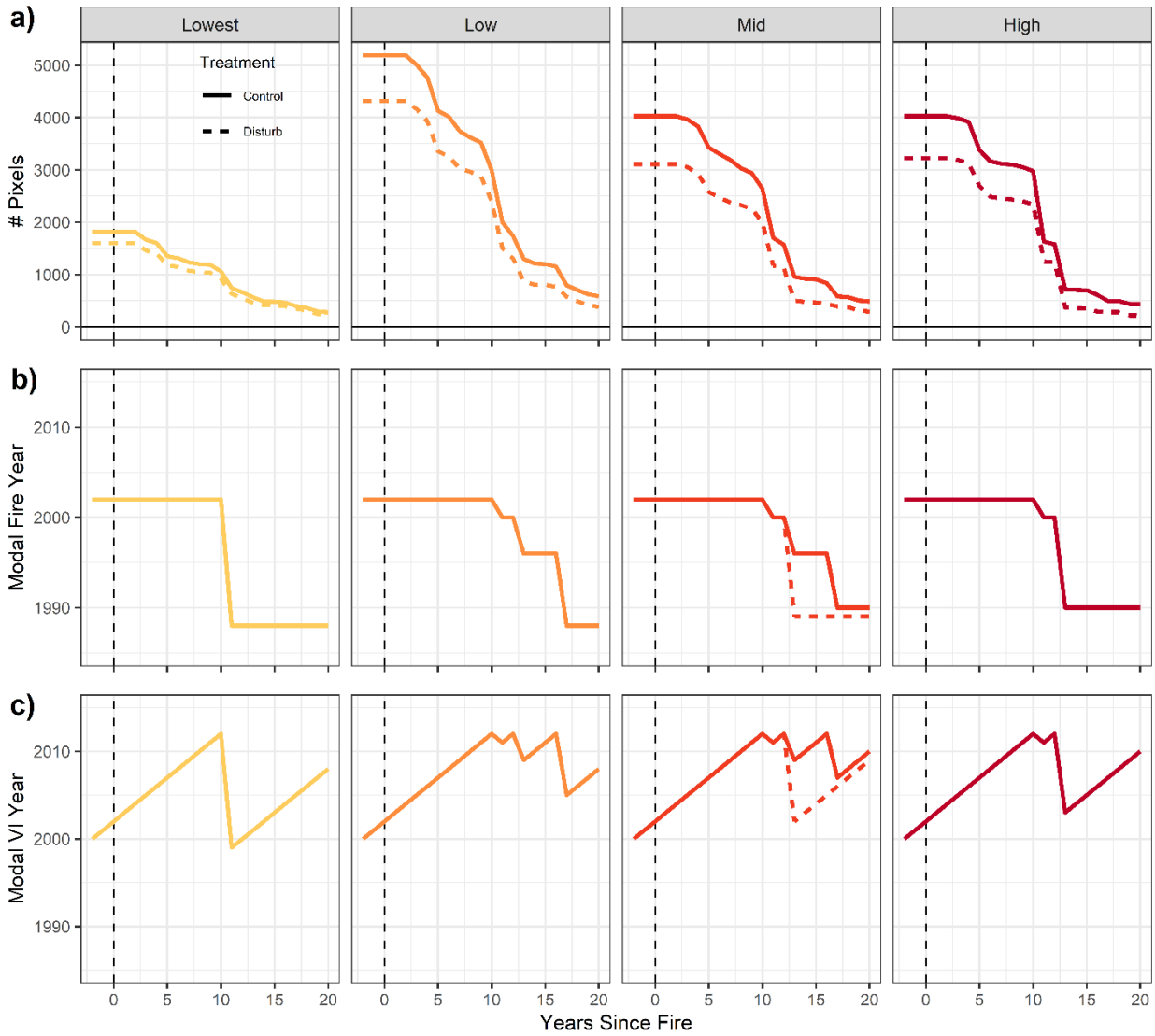

Figure B.7. The number of pixels, modal fire year, and modal vegetation index (VI) year for fire severity samples and their spatially matched controls.

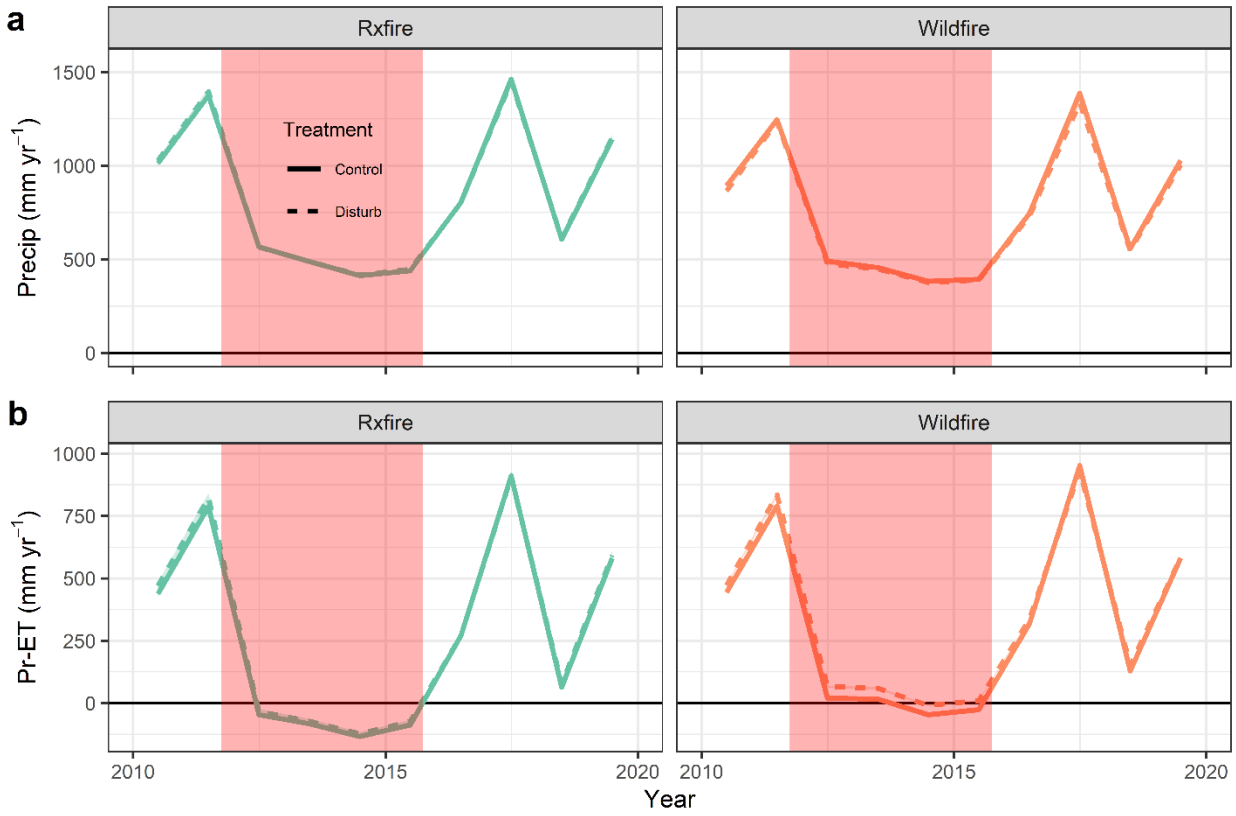

Figure B.8. Precipitation (Pr) and Pr-ET over time in locations exposed to prescribed fire (Rxfire) and wildfire and their spatially matched controls.

Table B.1. Summary of comparisons die-off (ADS), die-off (% tree cover), pre-drought tree cover, pre-drought ET, and four-year Pr-ET between forest stands in exposed to wildfire and prescribed fire and matched to unburned control pixels included absolute and relative (%) differences using a Tukey Honestly Significant Difference test.

Tukey HSD Comparisons between Fire Type Groups

Variable	Fire Severity	Disturb Estimate	Control Estimate	Difference	Low 95% CI	High 95% CI	Difference (%)	Low (%)	High (%)	p-value
Die-off (trees ha^{-1})	Prescribed Fire	94.3	118.5	-24.2	-34.0	-14.4	-20.4	-12.1	-28.7	0.000
Die-off (trees ha^{-1})	Wild Fire	50.6	85.0	-34.5	-39.0	-29.9	-40.5	-35.2	-45.9	0.000
Die-off (% Tree Cover)	Prescribed Fire	-10.0	-14.7	4.6	3.6	5.6	-31.6	-38.3	-24.9	0.000
Die-off (% Tree Cover)	Wild Fire	-4.2	-8.6	4.4	3.9	4.8	-50.8	-55.9	-45.7	0.000
Pre-Drought Tree Cover (%)	Prescribed Fire	39.3	48.3	-9.0	-10.8	-7.2	-18.6	-14.8	-22.3	0.000
Pre-Drought Tree Cover (%)	Wild Fire	25.8	35.8	-10.0	-10.8	-9.2	-27.9	-25.6	-30.1	0.000
Pre-Drought ET (mm yr^{-1})	Prescribed Fire	565.7	581.0	-15.3	-30.4	-0.2	-2.6	0.0	-5.2	0.045
Pre-Drought ET (mm yr^{-1})	Wild Fire	397.2	452.5	-55.4	-62.1	-48.6	-12.2	-10.7	-13.7	0.000
Pr-ET (mm $4yr^{-1}$)	Prescribed Fire	-301.5	-350.8	49.2	-12.0	110.5	-14.0	-31.5	3.4	0.165
Pr-ET (mm $4yr^{-1}$)	Wild Fire	126.2	-37.4	163.7	136.4	190.9	-437.2	-510.0	-364.4	0.000

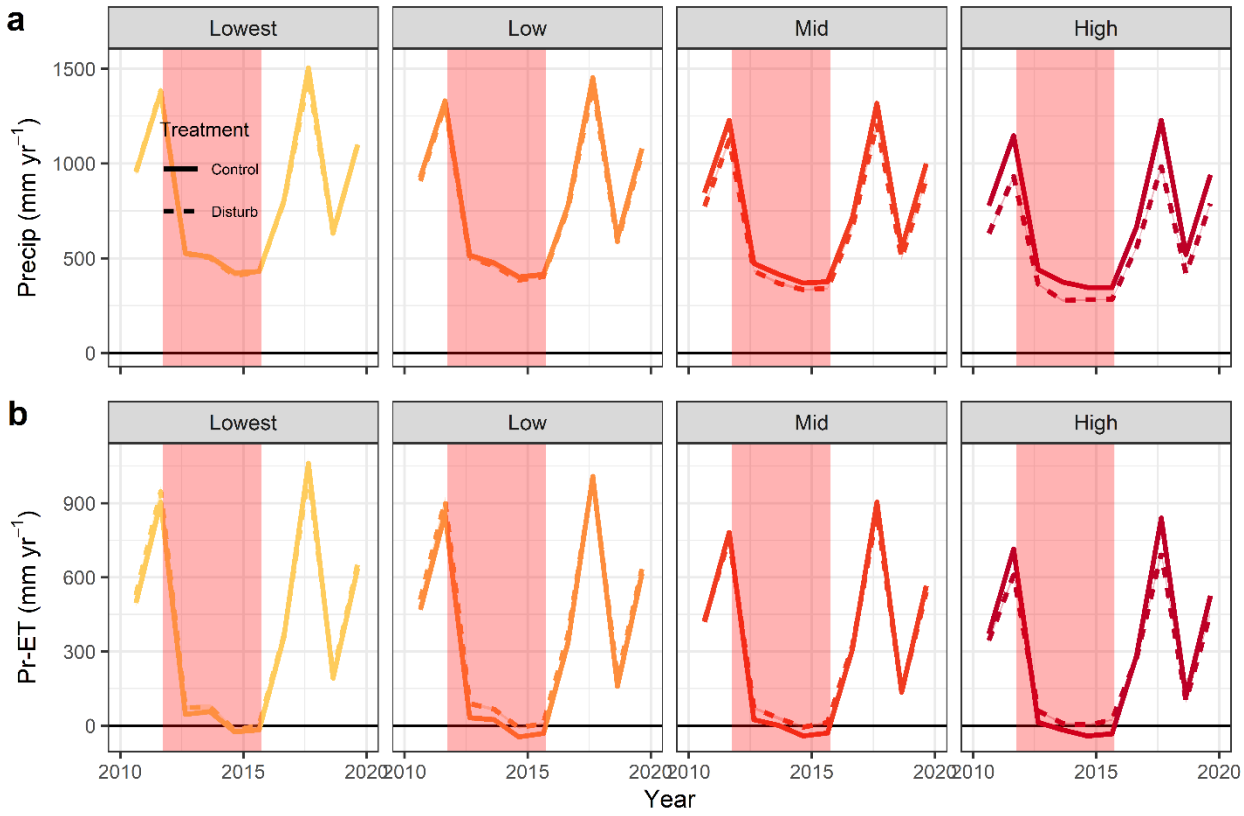

Figure B.9. Precipitation (Pr) and Pr-ET over time in locations exposed to different fire severity levels and their spatially matched controls.

Table B.2. Summary of comparisons die-off (ADS), die-off (% tree cover), pre-drought tree cover, pre-drought ET, and four-year Pr-ET between forest stands in exposed to different fire severity levels and matched to unburned control pixels included absolute and relative (%) differences using a Tukey Honestly Significant Difference test.

Tukey HSD Comparisons between Fire Severity Groups

Variable	Fire Severity	Disturb Estimate	Control Estimate	Difference	Low 95% CI	High 95% CI	Difference (%)	Low (%)	High (%)	p-value
Die-off (trees ha^{-1})	Lowest	60.0	78.4	-18.4	-28.7	-8.2	-23.5	-10.5	-36.6	0.000
Die-off (trees ha^{-1})	Low	47.2	78.1	-30.9	-37.0	-24.8	-39.6	-31.8	-47.4	0.000
Die-off (trees ha^{-1})	Moderate	31.7	64.3	-32.6	-40.1	-25.1	-50.7	-39.1	-62.4	0.000
Die-off (trees ha^{-1})	High	16.2	60.4	-44.2	-52.0	-36.4	-73.2	-60.3	-86.1	0.000
Die-off (% Tree Cover)	Lowest	-7.3	-8.0	0.7	-0.2	1.6	-8.9	-20.6	2.7	0.279
Die-off (% Tree Cover)	Low	-4.5	-8.0	3.6	3.0	4.1	-44.4	-51.4	-37.4	0.000
Die-off (% Tree Cover)	Moderate	-1.4	-6.3	4.9	4.3	5.6	-77.9	-88.1	-67.6	0.000
Die-off (% Tree Cover)	High	0.3	-5.4	5.8	5.1	6.4	-106.0	-117.8	-94.2	0.000
Pre-Drought Tree Cover (%)	Lowest	35.2	37.7	-2.6	-4.3	-0.8	-6.8	-2.1	-11.4	0.000
Pre-Drought Tree Cover (%)	Low	27.9	37.6	-9.7	-10.8	-8.7	-25.8	-23.0	-28.6	0.000
Pre-Drought Tree Cover (%)	Moderate	18.2	32.7	-14.4	-15.7	-13.2	-44.2	-40.5	-48.0	0.000
Pre-Drought Tree Cover (%)	High	10.9	29.8	-18.9	-20.1	-17.7	-63.4	-59.3	-67.4	0.000
Pre-Drought ET (mm yr^{-1})	Lowest	431.0	452.6	-21.7	-37.8	-5.5	-4.8	-1.2	-8.3	0.001
Pre-Drought ET (mm yr^{-1})	Low	394.8	455.7	-60.9	-70.6	-51.2	-13.4	-11.2	-15.5	0.000
Pre-Drought ET (mm yr^{-1})	Moderate	346.4	423.2	-76.8	-88.1	-65.6	-18.2	-15.5	-20.8	0.000
Pre-Drought ET (mm yr^{-1})	High	289.9	403.3	-113.4	-124.5	-102.3	-28.1	-25.4	-30.9	0.000
Pr-ET (mm $4yr^{-1}$)	Lowest	134.6	63.5	71.1	4.5	137.7	111.9	216.8	7.1	0.027
Pr-ET (mm $4yr^{-1}$)	Low	157.2	-14.7	171.9	131.8	211.9	-1172.8	-1446.2	-899.4	0.000
Pr-ET (mm $4yr^{-1}$)	Moderate	113.0	-40.2	153.2	106.8	199.6	-380.8	-496.2	-265.3	0.000
Pr-ET (mm $4yr^{-1}$)	High	104.5	-75.2	179.7	133.7	225.6	-239.1	-300.2	-177.9	0.000

APPENDIX C

Supporting Information for Chapter 3

Where are forests most vulnerable to drought induced die-off?

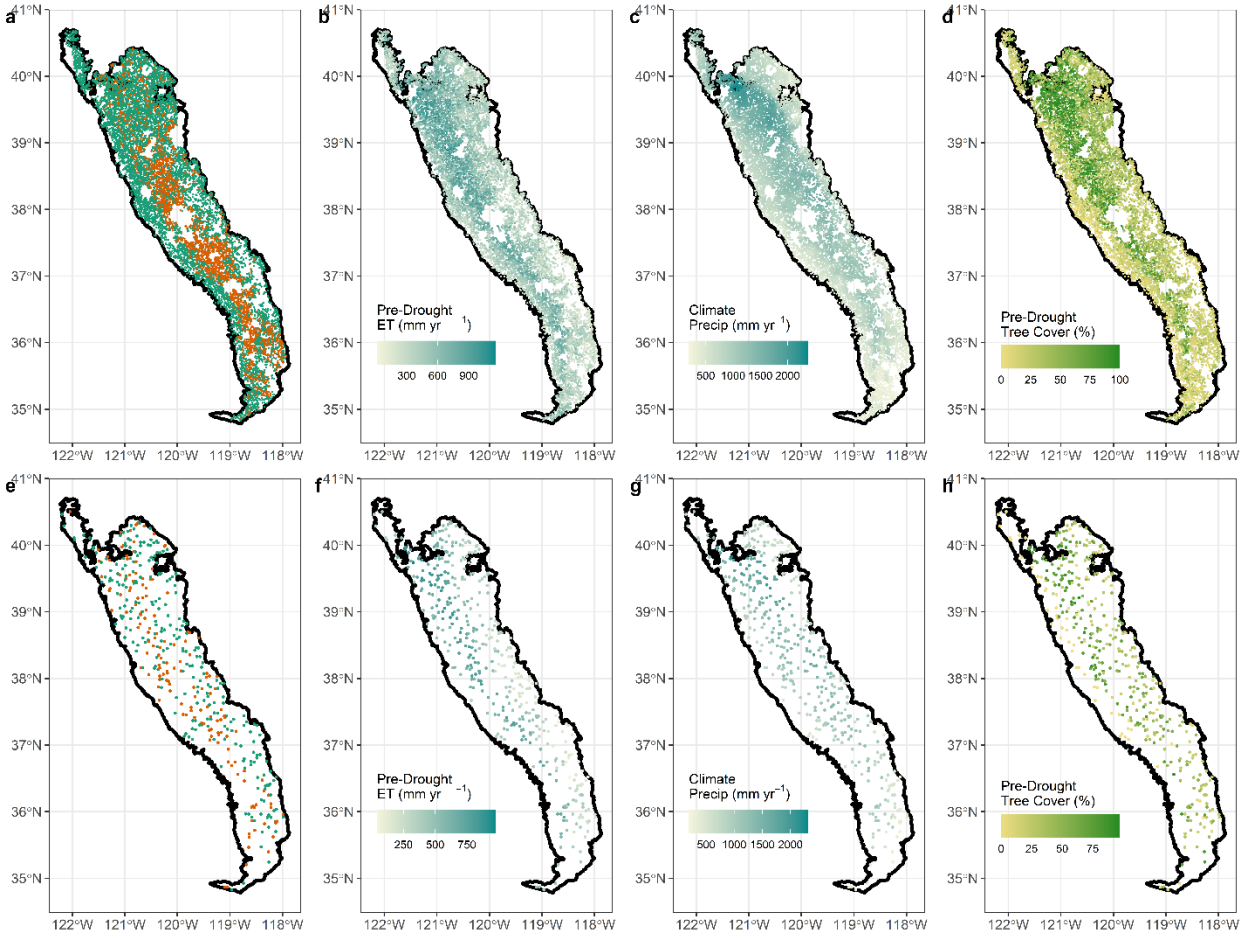

Figure C.1. Spatial patterns of drought induced die-off presence and risk factors for remote sensing and FIA data sets in the Sierra Nevada and foothills. Panels a, b, c, and d show remote sensing data with N = 12,319 randomly selected pixels in each. Panels e, f, g, and h show FIA data with 4 = 409 plots from inventory years 2016-2019. The panels show above background forest die-off (a, e), pre-drought ET (b, f), 1981-2010 annual climate precipitation (c, h), and pre-drought tree cover (d, h).

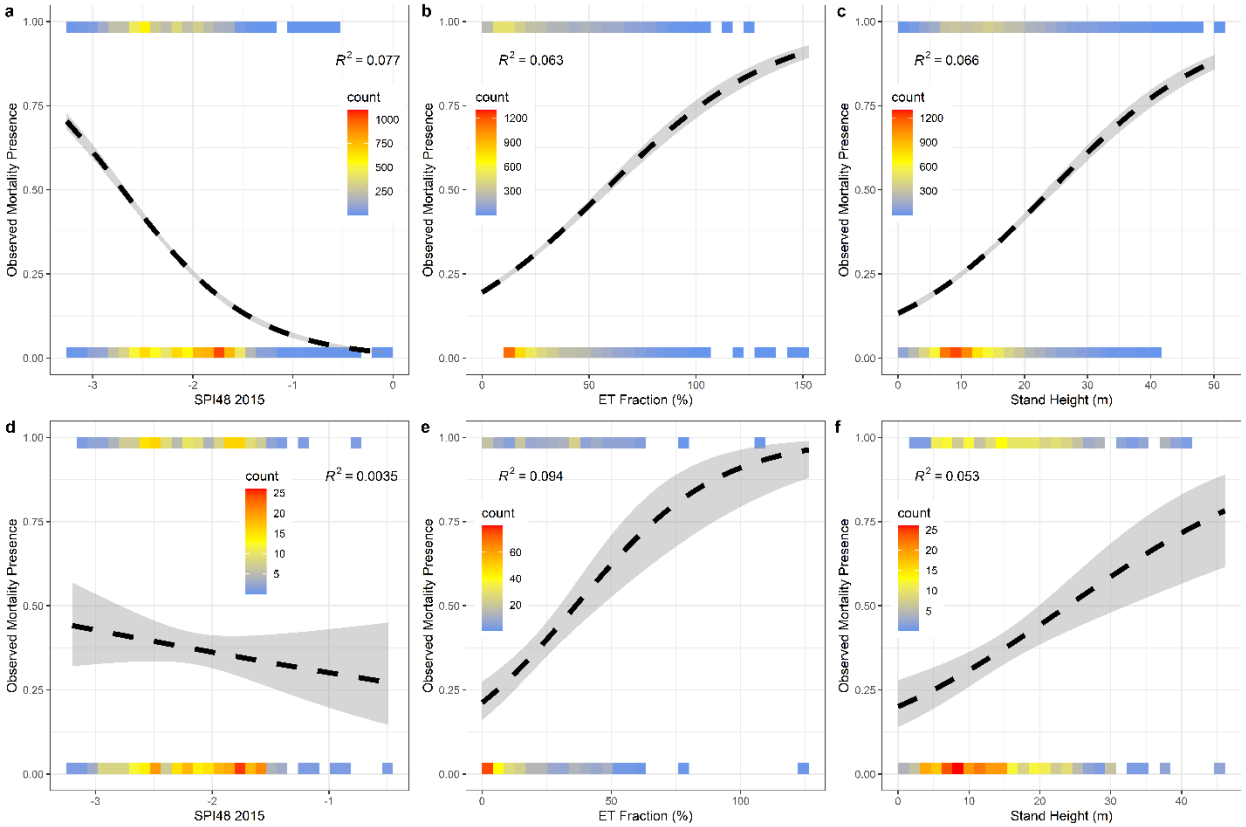

Figure C.2. Predictions of die-off probability from logistic models trained with remote sensing and FIA data. Each panel displays 40% of the original sample held out for model testing. The shading represents 95% confidence intervals. The first through third panels (a, b, c) shows the fit of logistic models to predict the probability of die-off occurrence using three different predictors with remote sensing data with a sample size of N = 4,822. The fourth through sixth panels (d, e, f) shows the fit of logistic models to predict the probability of die-off occurrence with FIA data using three different predictors with a sample size of N = 164.

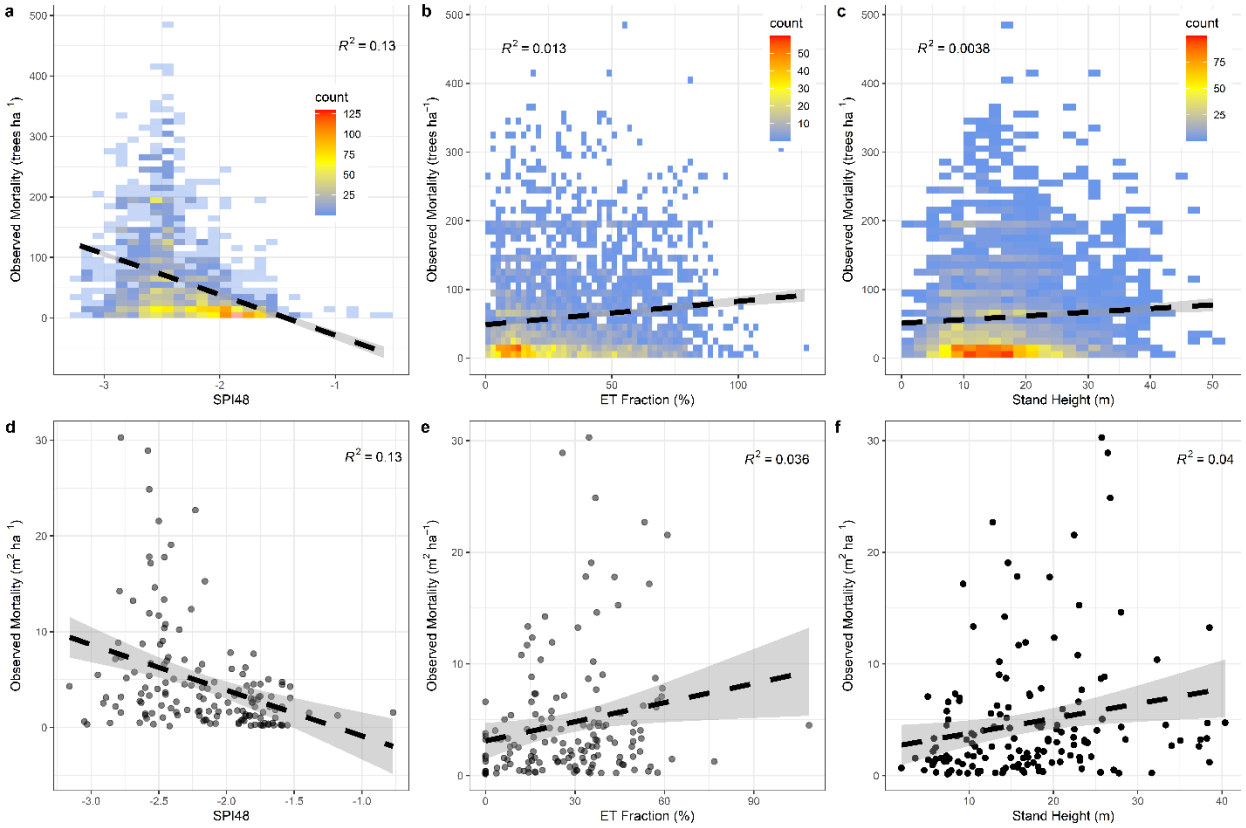

Figure C.3. Predictions of die-off magnitude for linear regression models trained with remote sensing and FIA data. Each panel displays 40% of the original sample held out for model testing. The shading represents 95% confidence intervals. The first through third panels (a, b, c) show the fit of a linear regression model to predict the magnitude of die-off trained with locations with mortality present using three different predictors with remote sensing data with a sample size of N = 1,498. The fourth through sixth panels (e, f, g) shows the fit of a linear regression model to predict the magnitude of die-off from locations where die-off occurred using three different predictors using FIA data with a sample size of N = 61.

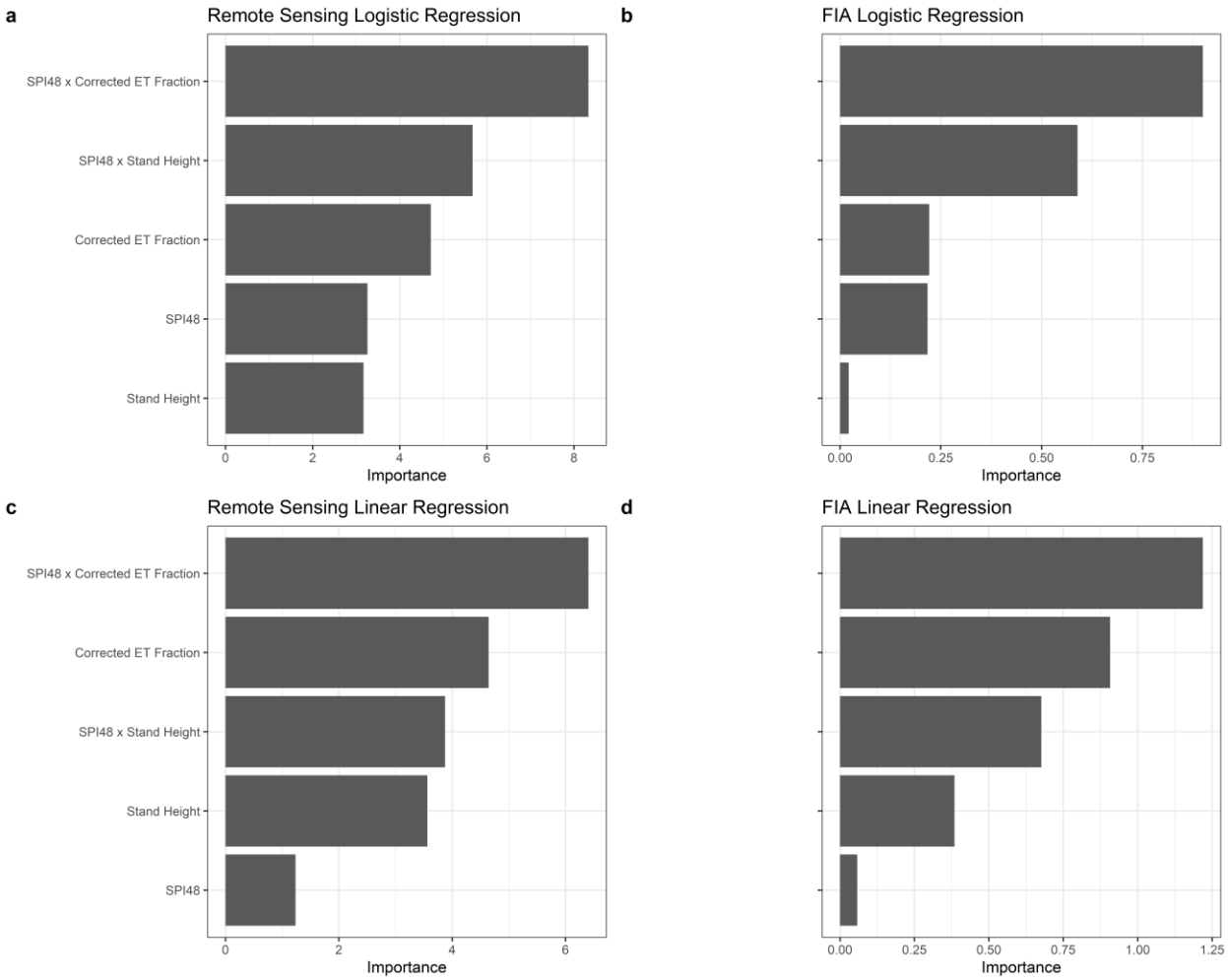

Figure C.4. Comparison of the importance of predictor variables in linear regression and logistic regression models trained with remote sensing and FIA data. The first two panels (a, b) show the relative importance of the predictors for logistic regression models. The third and fourth panels (c, d) show the relative importance of predictors for the linear regression models.

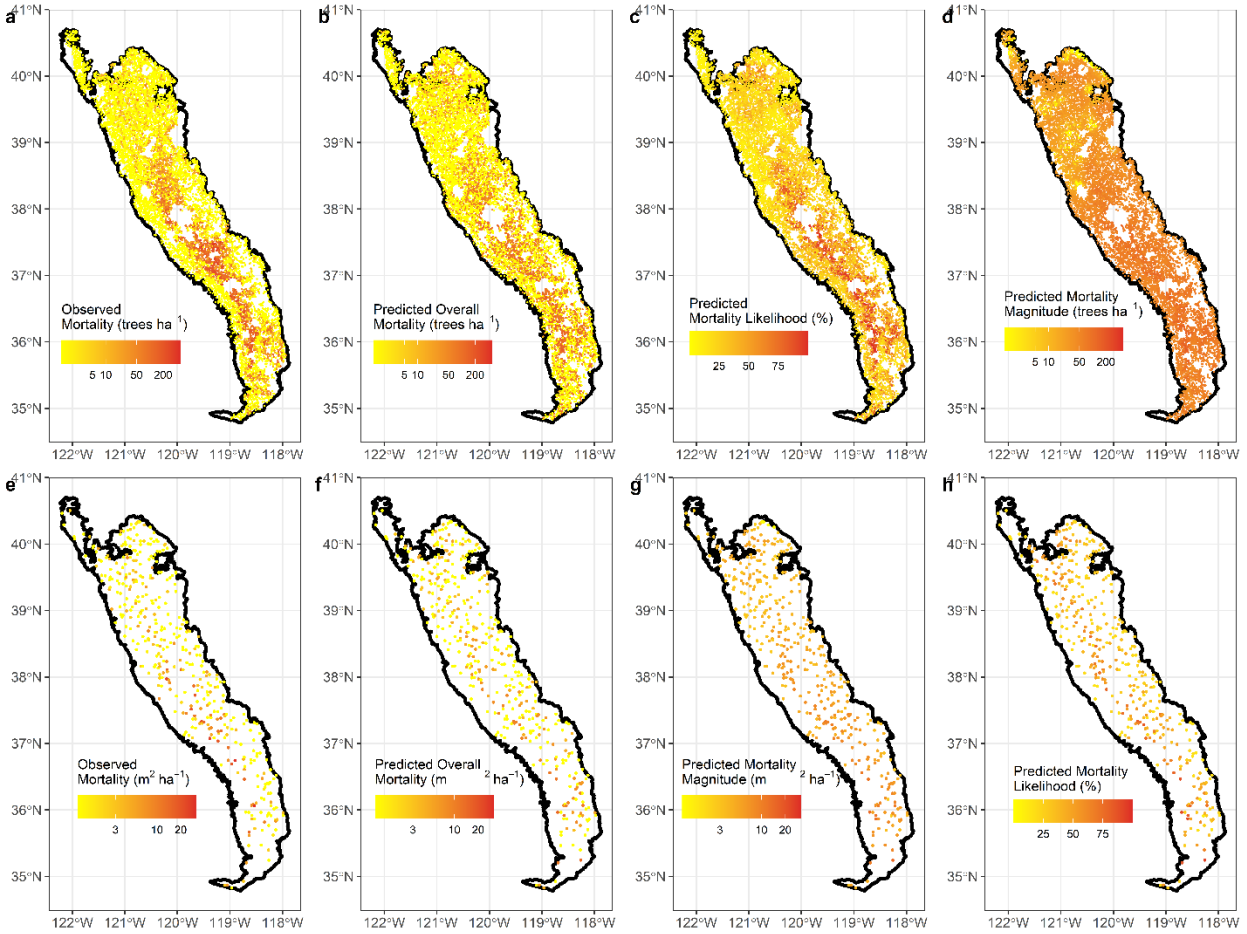

Figure C.5. Spatial patterns of observed die-off, overall predicted die-off, predicted die-off magnitude, and predicted die-off likelihood for remote sensing and FIA data sets in the Sierra Nevada and foothills. Predicted values are based on observed conditions for the 2012-2015 drought. Panels a, b, c, and d show remote sensing data with N = 12,319 randomly selected pixels in each. Panels e, f, g, and h show FIA data with 4 = 409 plots from inventory years 2016-2019. The panels show observed die-off (a, e), predicted overall die-off (b, f), predicted die-off magnitude (c, h), and predicted die-off likelihood (d, h).

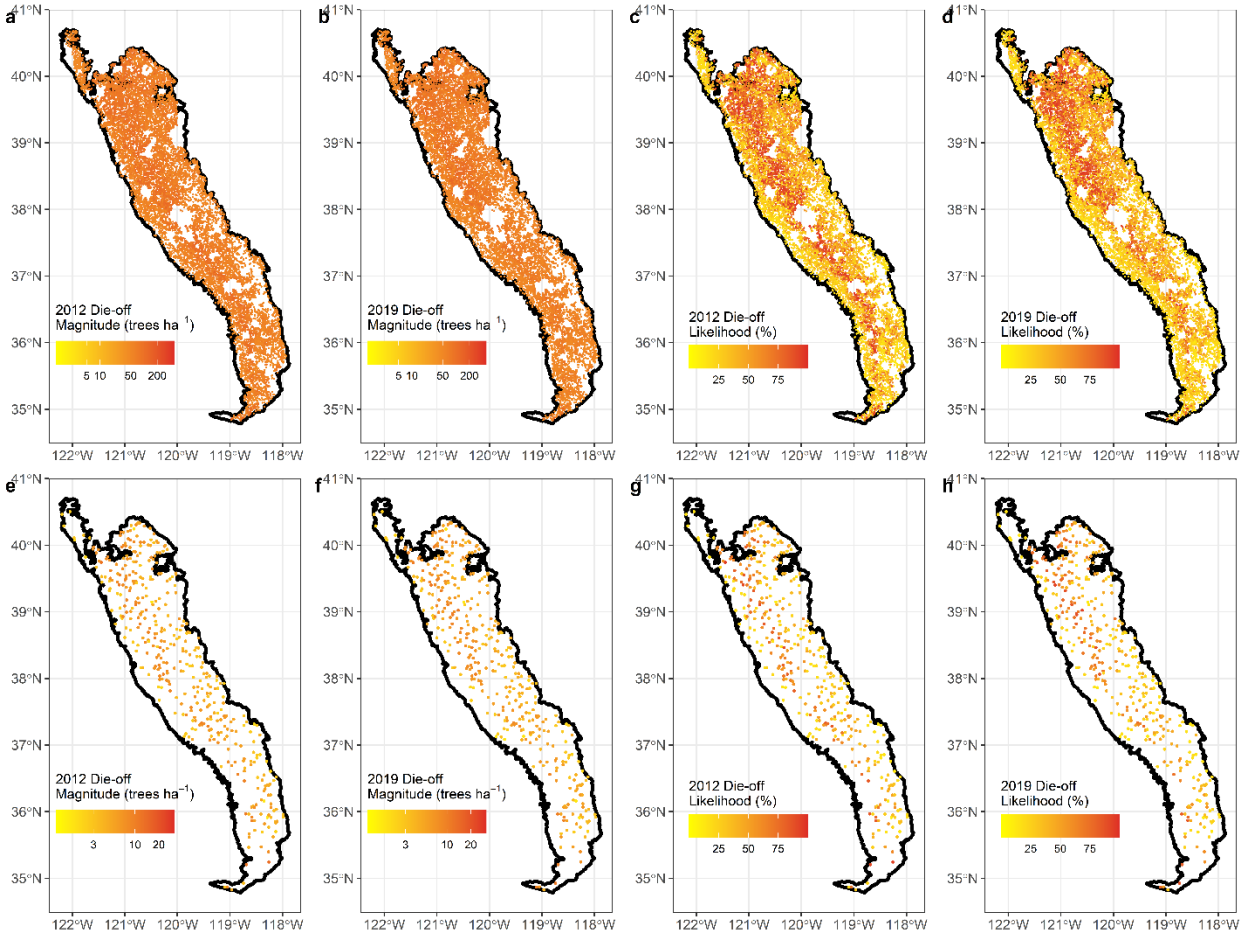

Figure C.6. Spatial patterns of predicted die-off magnitude, and predicted die-off likelihood with SPI48 held constant at -2.5 and other conditions varying between 2012 and 2019 conditions for remote sensing and FIA data sets in the Sierra Nevada and foothills. Panels a, b, c, and d show remote sensing data with N = 12,319 randomly selected pixels in each. Panels e, f, g, and h show FIA data with 4 = 409 plots from inventory years 2016-2019. The panels show predicted die-off magnitude for 2012 (a, e), predicted die-off magnitude for 2019 (b, f), predicted die-off likelihood for 2012 (c, h), and predicted die-off likelihood for 2019 (d, h).

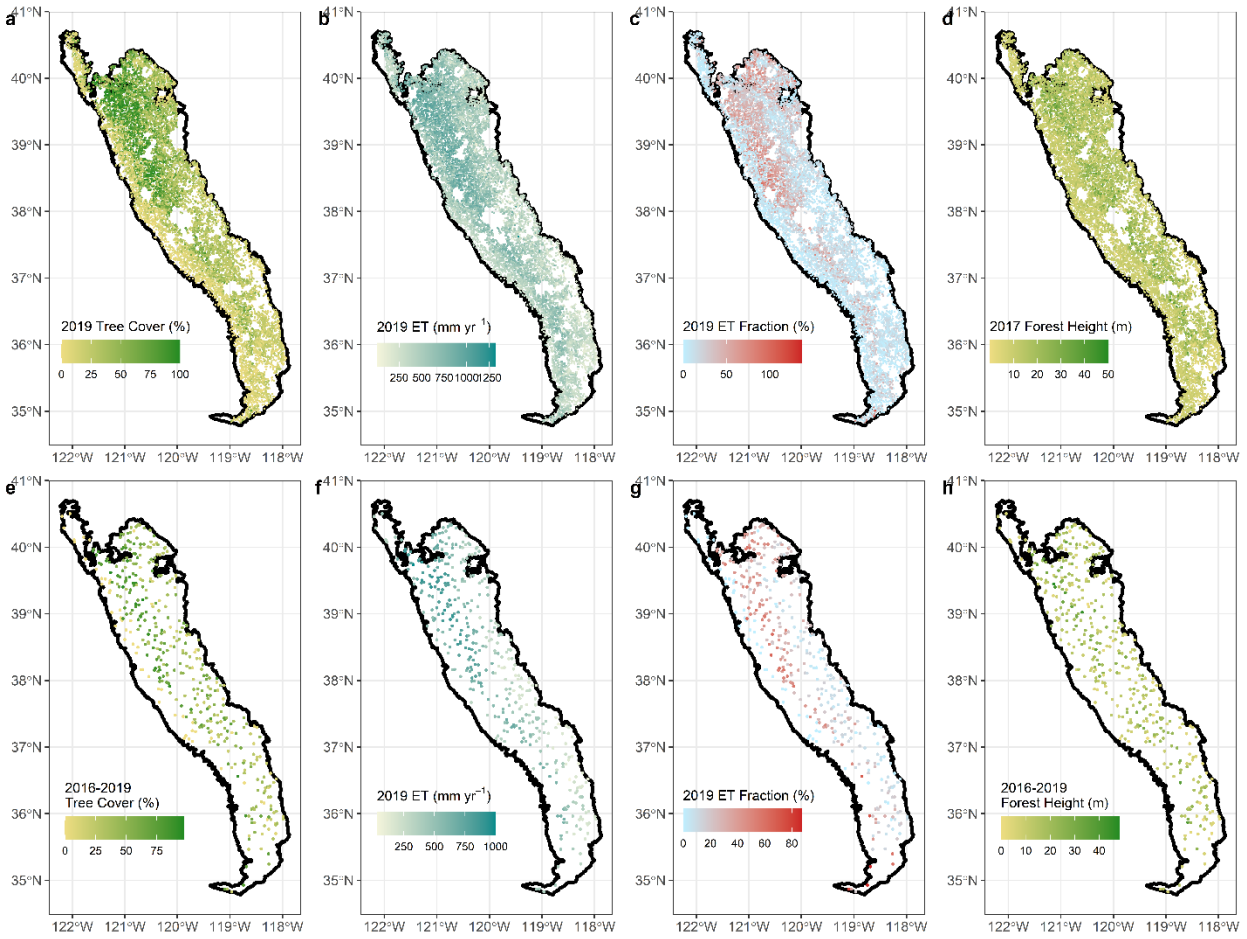

Figure C.7. Spatial patterns of drought induced risk factors under 2019 conditions for remote sensing and FIA data sets in the Sierra Nevada and foothills. Panels a, b, c, and d show 2019 remote sensing data with N = 12,319 randomly selected pixels in each. Panels e, f, g, and h show FIA data with 4 = 409 plots from inventory years 2016-2019. The panels show Tree Cover (a, e), ET (b), Corrected ET Fraction (c), and Tree Height (d). Each panel displays N = 12,419 randomly sampled 30-meter grid cells.

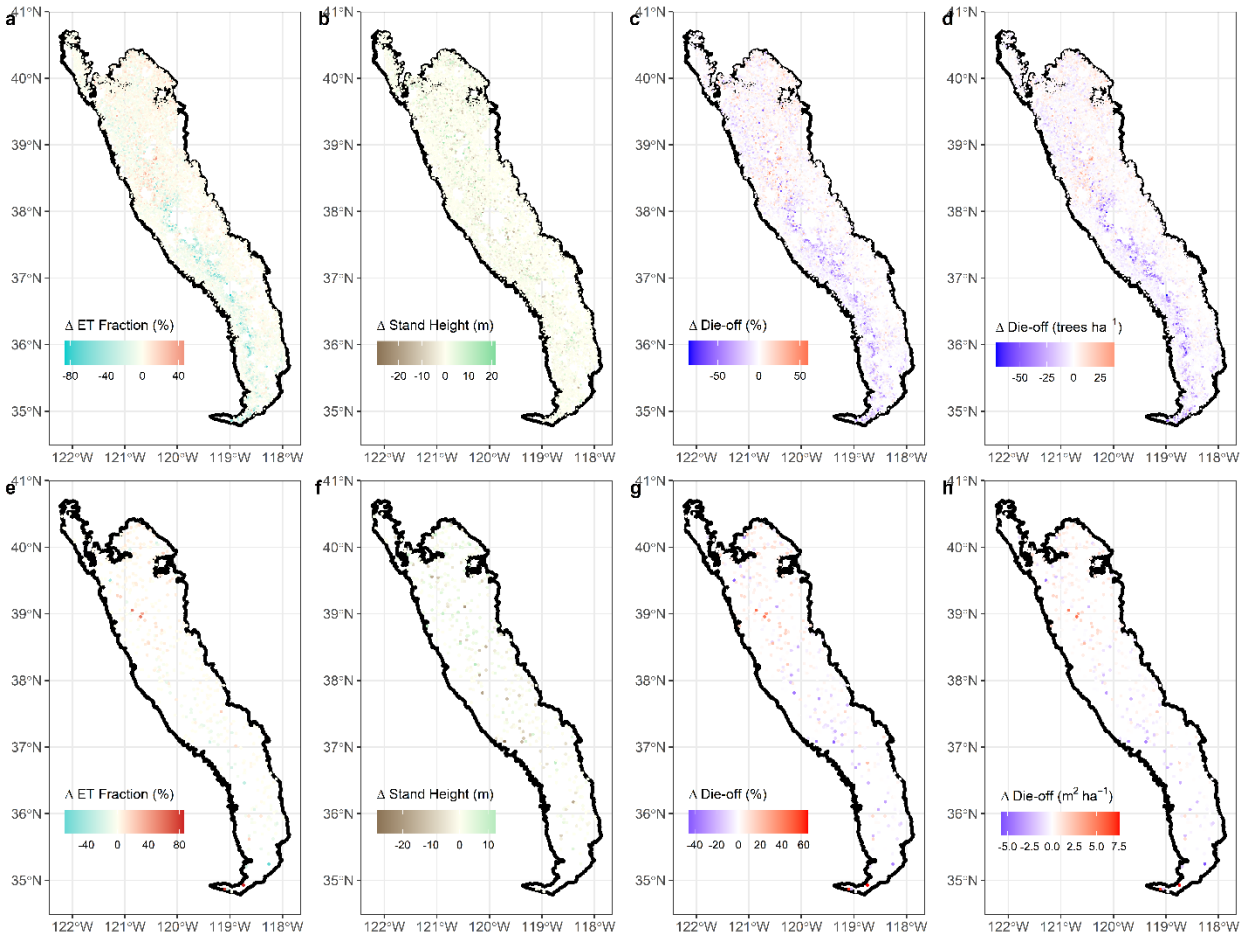

Figure C.8. Spatial patterns of changes in die-off factors and die-off predictions between 2012 and 2019 for remote sensing and FIA data sets in the Sierra Nevada and foothills. Panels a, b, c, and d show remote sensing data with N = 12,319 randomly selected pixels in each. Panels e, f, g, and h show FIA data with N = 409 plots. The panels show Δ Corrected ET Fraction (a, e), Δ Stand Height (b, f), Δ Die-off Likelihood (c, g), and Δ Die-off Magnitude (d, h).

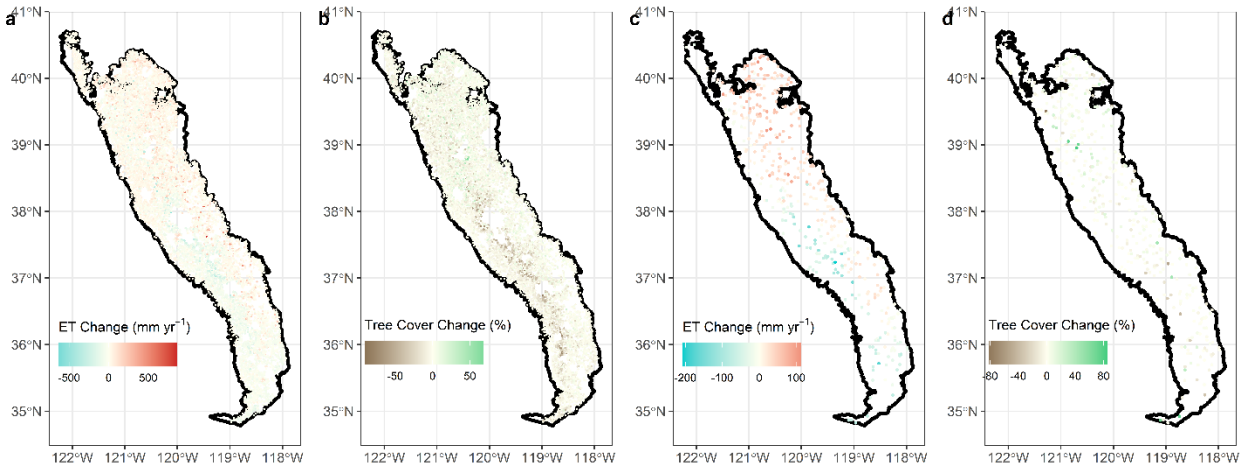

Figure C.9. Spatial patterns of changes in die-off factors between 2012 and 2019 for remote sensing and FIA data sets in the Sierra Nevada and foothills. Panels a and b how remote sensing data with N = 12,319 randomly selected pixels in each. Panels c and d show FIA data with N = 409 plots. The panels show ET Change (a, c), and Tree Cover Change (b, d).

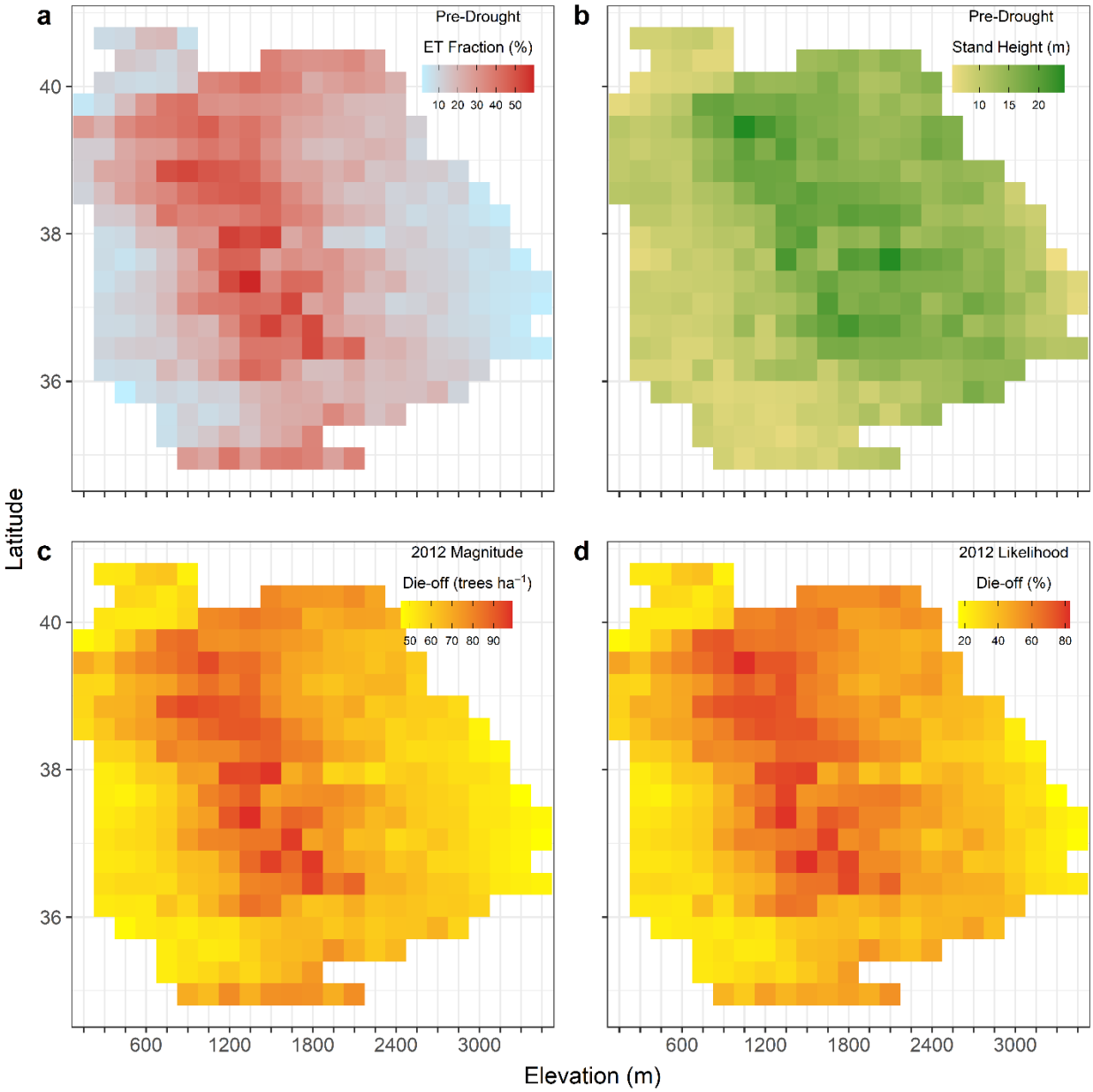

Figure C.10. Observed die-off risk factor conditions and die-off predictions in 2012 for the remote sensing analysis. Die-off predictions were made with SPI48 held constant at -2.5. The panels show ET Fraction (a), Stand Height (b), Die-off Magnitude (c), and Die-off Likelihood (d). Each cell represents the mean of pixels in one 0.3° latitude and 150-m elevation bin. We excluded bins with less than 5 pixels. All panels have N = 12,319.